Article

Cell Chemical Biology

Development of MAP4 Kinase Inhibitors as Motor Neuron-Protecting Agents

Graphical Abstract

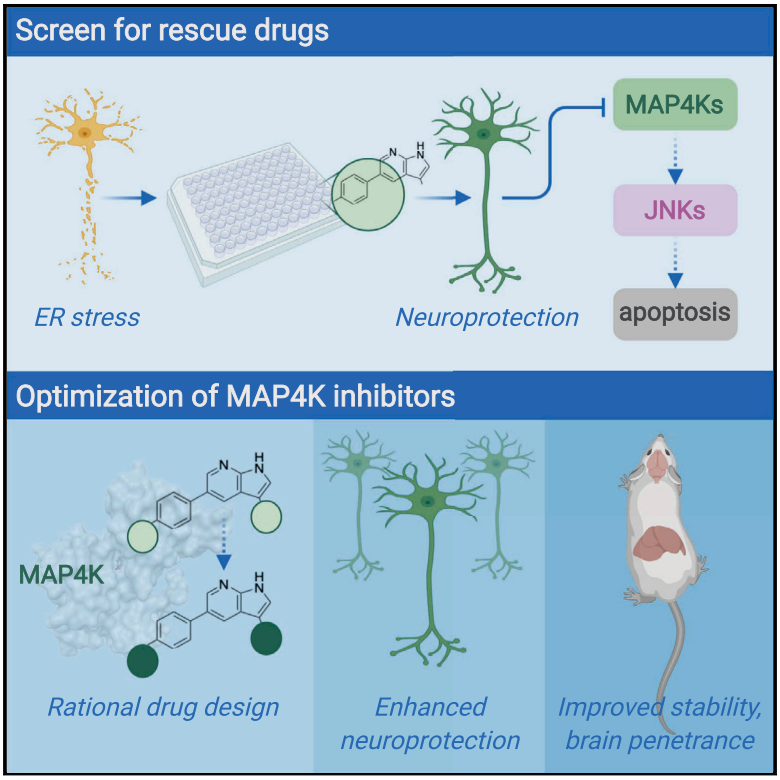

Authors

Pieter H. Bos, Emily R. Lowry, Jonathon Costa, ..., Arie Zask, Hynek Wichterle, Brent R. Stockwell

Correspondence

hw350@columbia.edu (H.W.), bstockwell@columbia.edu (B.R.S.)

In Brief

Using an *in vitro* screening platform to identify compounds that protect neurons from ER stress, a common feature of many neurodegenerative disorders, Bos et al. identified MAP4Ks as important shared targets of neuroprotective compounds. They then developed a series of potent, stable, and brain-penetrant MAP4K inhibitors, including Prostetin/12k.

Highlights

- MAP4K inhibitors protect motor neurons from ER stress-induced apoptosis
- We synthesized URMC-099 analogs to optimize selectivity and pharmacokinetics
- Prostetin/12k is an analog with enhanced MAP4K inhibition and neuroprotection
- Prostetin/12k shows improved stability, CNS penetrance, and oral bioavailability

Bos et al., 2019, Cell Chemical Biology *26*, 1–13
November 21, 2019
https://doi.org/10.1016/j.chembiol.2019.10.005

CellPress

Please cite this article in press as: Bos et al., Development of MAP4 Kinase Inhibitors as Motor Neuron-Protecting Agents, Cell Chemical Biology (2019), https://doi.org/10.1016/j.chembiol.2019.10.005

Cell Chemical Biology
Article

Development of MAP4 Kinase Inhibitors as Motor Neuron-Protecting Agents

Pieter H. Bos,[1,10] Emily R. Lowry,[3,10] Jonathon Costa,[3] Sebastian Thams,[3,9] Alejandro Garcia-Diaz,[3,8] Arie Zask,[1] Hynek Wichterle,[3,4,5,6,7,8,*] and Brent R. Stockwell[1,2,11,*]

[1]Department of Biological Sciences, Columbia University, New York, NY 10027, USA
[2]Department of Chemistry, Columbia University, New York, NY 10027, USA
[3]Department of Pathology and Cell Biology, Columbia University Irving Medical Center, New York, NY 10032, USA
[4]Department of Neurology, Columbia University Irving Medical Center, New York, NY 10032, USA
[5]Department of Neuroscience, Columbia University Irving Medical Center, New York, NY 10032, USA
[6]Department of Rehabilitation and Regenerative Medicine, Columbia University Irving Medical Center, New York, NY 10032, USA
[7]Center for Motor Neuron Biology and Disease, Columbia University Irving Medical Center, New York, NY 10032, USA
[8]Columbia Stem Cell Initiative, Columbia University Irving Medical Center, New York, NY 10032, USA
[9]Present address: Department of Clinical Neuroscience, Division of Neurology, Karolinska Universitetssjukhuset, Stockholm 171 76, Sweden
[10]These authors contributed equally
[11]Lead Contact
*Correspondence: hw350@columbia.edu (H.W.), bstockwell@columbia.edu (B.R.S.)
https://doi.org/10.1016/j.chembiol.2019.10.005

SUMMARY

Disease-causing mutations in many neurodegenerative disorders lead to proteinopathies that trigger endoplasmic reticulum (ER) stress. However, few therapeutic options exist for patients with these diseases. Using an *in vitro* screening platform to identify compounds that protect human motor neurons from ER stress-mediated degeneration, we discovered that compounds targeting the mitogen-activated protein kinase kinase kinase kinase (MAP4K) family are neuroprotective. The kinase inhibitor URMC-099 (compound 1) stood out as a promising lead compound for further optimization. We coupled structure-based compound design with functional activity testing in neurons subjected to ER stress to develop a series of analogs with improved MAP4K inhibition and concomitant increases in potency and efficacy. Further structural modifications were performed to enhance the pharmacokinetic profiles of the compound 1 derivatives. Prostetin/12k emerged as an exceptionally potent, metabolically stable, and blood-brain barrier-penetrant compound that is well suited for future testing in animal models of neurodegeneration.

INTRODUCTION

Many neurodegenerative disorders, including amyotrophic lateral sclerosis (ALS), Alzheimer disease, and Parkinson disease, are characterized by the accumulation of misfolded proteins in the affected neuronal subtypes and the subsequent induction of endoplasmic reticulum (ER) stress pathways (Roussel et al., 2013). These pathways initially engage protective mechanisms that slow protein synthesis and promote refolding or clearance of misfolded proteins. If these efforts are unsuccessful, the unfolded protein response (UPR) activates cell death pathways.

ER stress and the UPR have been implicated in both familial and sporadic forms of ALS, a neurodegenerative disorder that selectively targets motor neurons and progresses rapidly once patients have been diagnosed, with a mean survival time of <5 years (Medinas et al., 2019). Markers of ER stress also are among the earliest pathological features to appear in *in vitro* and *in vivo* models of ALS (Kiskinis et al., 2014; Saxena et al., 2009). Furthermore, while the expression of ALS-causing mutant proteins is not restricted to motor neurons, we have found that motor neurons are significantly more sensitive than other spinal neuronal subtypes to ER stress-inducing compounds (Thams et al., 2019), which may explain their selective vulnerability in ALS.

We harnessed these findings to build a screening platform to identify compounds that could protect against ER stress-mediated neurodegeneration. In this model, stem-cell-derived motor neurons are treated with cyclopiazonic acid (CPA), a mycotoxin that inhibits the transport of calcium from the cytoplasm into the ER by blocking sarcoendoplasmic reticulum calcium transport ATPase pumps (Thams et al., 2019). Because many protein folding chaperones in the ER require calcium as a co-factor, CPA treatment leads to the accumulation of misfolded proteins, the induction of ER stress pathways, and apoptosis in spinal motor neurons *in vitro* (Thams et al., 2019).

Using this platform, we identified broad-spectrum kinase inhibitors, including Gö6976, sunitinib, K252a, and kenpaullone, as compounds that protect motor neurons from ER stress (Thams et al., 2019). These compounds were largely unsuitable for clinical development, either because of poor pharmacokinetic properties or a lack of target specificity.

Here, we identified mitogen-activated protein kinase kinase kinase kinase (MAP4Ks, also known as the STE20 family of kinases) as the shared functional targets of these kinase inhibitors and performed a secondary screen for MAP4K inhibitors that could be tested in *in vivo* models of neurodegeneration. URMC-099 (compound **1**), a MAP3K inhibitor that also strongly inhibits MAP4Ks (Goodfellow et al., 2013), emerged as a

promising hit, but required further optimization to increase its potency and efficacy in motor neurons subjected to ER stress, and to overcome its relatively poor metabolic stability, oral bioavailability, and blood-brain barrier penetration.

By combining structure-based small-molecule design using computational chemistry tools with rapid feedback on the activity of newly synthesized compounds *in vitro* in motor neurons subjected to ER stress, we generated a series of potent compound **1** analogs. Compound **12k** (termed Prostetin for promoting neuronal viability via Ste20 inhibition), which inhibits MAP4Ks at subnanomolar concentrations, was the most promising based on its neuroprotective and pharmacokinetic profiles. Furthermore, we found that **Prostetin/12k** retains the anti-inflammatory properties of **1**, which may provide additional therapeutic benefit in neurodegenerative disorders such as ALS where inflammation may exacerbate disease progression (Boillée et al., 2006; Trias et al., 2016). **Prostetin/12k** is therefore primed for future testing in diverse animal models of neurodegenerative disease.

RESULTS

HGK (MAP4K4) and NUAK1 Are Common Targets of Neuroprotective Kinase Inhibitors

In our original screen for compounds that protect against ER stress-mediated neurodegeneration, libraries of small molecules were combined with the ER-stress-inducing agent CPA and added to mouse stem-cell-derived motor neurons (Figure 1A) (Thams et al., 2019). Four kinase inhibitors emerged as neuroprotective hits—Gö6976, sunitinib, K252a, and kenpaullone—but none were viable therapeutic agents for neurodegeneration: Gö6976 and K252a are insufficiently selective (Anastassiadis et al., 2011); sunitinib does not readily cross the blood-brain barrier (Tang et al., 2012); and paullone derivatives are highly insoluble in aqueous biofluids (Greenwald et al., 2004).

Nevertheless, we reasoned that identifying their shared functional targets could guide the selection of new compounds that would be suitable for *in vivo* use. We mined a publicly available database (Anastassiadis et al., 2011) to compare the catalytic activity of >300 kinases in the presence of the four hit compounds. We also included alsterpaullone in this analysis, because it is a structural analog of kenpaullone that we found to be more potent than kenpaullone in rescuing CPA-treated motor neurons (Figure 1C). We then performed two-way hierarchical clustering analysis to rank the shared targets of these compounds (Figure 1B). Kinases whose activity was strongly inhibited by all five compounds included the AMPK-related kinase NUAK1 and the MAP4K/STE20 kinase HGK (MAP4K4; Figure 1B).

HGK Inhibitors, but Not NUAK1 Inhibitors, Are Strongly Neuroprotective

To evaluate the relative contributions of NUAK1 and HGK to ER-stress-mediated neurodegeneration, and to identify compounds that would be better suited than the original hits for *in vivo* administration, we asked whether known NUAK1 and HGK inhibitors could counteract the effects of the ER-stress-inducing compound CPA. We humanized our screening platform (Figure 1A) by incorporating motor neurons differentiated from human induced pluripotent stem cells derived from a healthy patient. Cells were treated with CPA ± NUAK1 and HGK inhibitors under conditions where motor neuron survival in CPA-treated cells drops to ~40% compared with vehicle-treated controls.

We found that the NUAK1 inhibitors WZ4003 (Banerjee et al., 2014) and HTH 01-015 (Banerjee et al., 2014) did not rescue CPA toxicity at any of the concentrations tested (Figures 1C and S1A). At concentrations above 2 μM, both WZ4003 and HTH 01-015 were toxic to motor neurons even in the absence of CPA (Figure S1A). NUAK1 inhibitors were therefore not suitable for the treatment of ER-stress-mediated neurodegeneration.

We also tested three compounds that had previously been shown to inhibit HGK activity: PF-6260933 (Ammirati et al., 2015), GNE-495 (Ndubaku et al., 2015), and URMC-099 (Goodfellow et al., 2013). All three of the HGK inhibitors tested were neuroprotective, with URMC-099 as the most potent and effective in this assay, restoring survival to 90% at 0.6 μM (Figures 1C and S1B). These findings pointed to a role for HGK in ER stress-mediated neurodegeneration, and suggested that URMC-099 warranted further study.

URMC-099 Inhibits ER Stress-Mediated Apoptosis via the JNK Pathway

Unlike PF-6260933 and GNE-495, URMC-099 is not a selective HGK inhibitor, and its mode of action in stressed neurons was not established. Using published data (Ndubaku et al., 2015), we calculated that GNE-495 was exceptionally selective, with a selectivity score of 0.01 out of 1 (ratio of the number of kinases with less than 20% of activity remaining in the presence of 1 μM GNE-495 to the total number of kinases assayed in cell-free conditions). Meanwhile, URMC-099 was originally optimized to inhibit the MAP3K kinase MLK3 but was shown to bind HGK and inhibit >99% of its activity at 1 μM (Goodfellow et al., 2013). Accordingly, URMC-099 had a weaker selectivity score (0.36) than GNE-495 under similar conditions, based on data from Goodfellow et al. (2013).

To assess whether URMC-099 was acting through the same pathways as HGK-selective compounds in stressed neurons, we evaluated its effects on the c-Jun N-terminal kinase (JNK) signaling pathway. HGK is a well-established regulator of the JNK pathway (Yao et al., 1999), and selective HGK inhibitors have been shown to inhibit JNK pathway activation in the context of neurodegeneration. Yang et al. (2013) showed that kenpaullone, one of the hit compounds from our original screen that strongly and selectively inhibits HGK, prevents motor neuron degeneration in the context of neurotrophic factor withdrawal by inhibiting the TAK1 (MAP3K7)/MKK7/JNK axis of the JNK pathway. Meanwhile, URMC-099 has been shown to prevent MLK3-mediated activation of JNK in microglia in *in vitro* and *in vivo* models of neuroinflammation (Goodfellow et al., 2013).

Through a series of western blots, we observed that URMC-099 prevented the activation of the JNK pathway in CPA-treated motor neurons. We found that URMC-099 attenuated the phosphorylation of the MAP2K MKK4 at Ser257, a site that is associated with cell stress and is essential to the regulation of downstream kinases such as JNK1-3 (mitogen-activated protein kinase [MAPK 8–10]; Figures 1D and 1E) (Deacon and Blank, 1997). Using an antibody that recognizes JNK1, 2, and 3 when phosphorylated at sites known to regulate stress responses (Thr183/Tyr185), we found that URMC-099 significantly

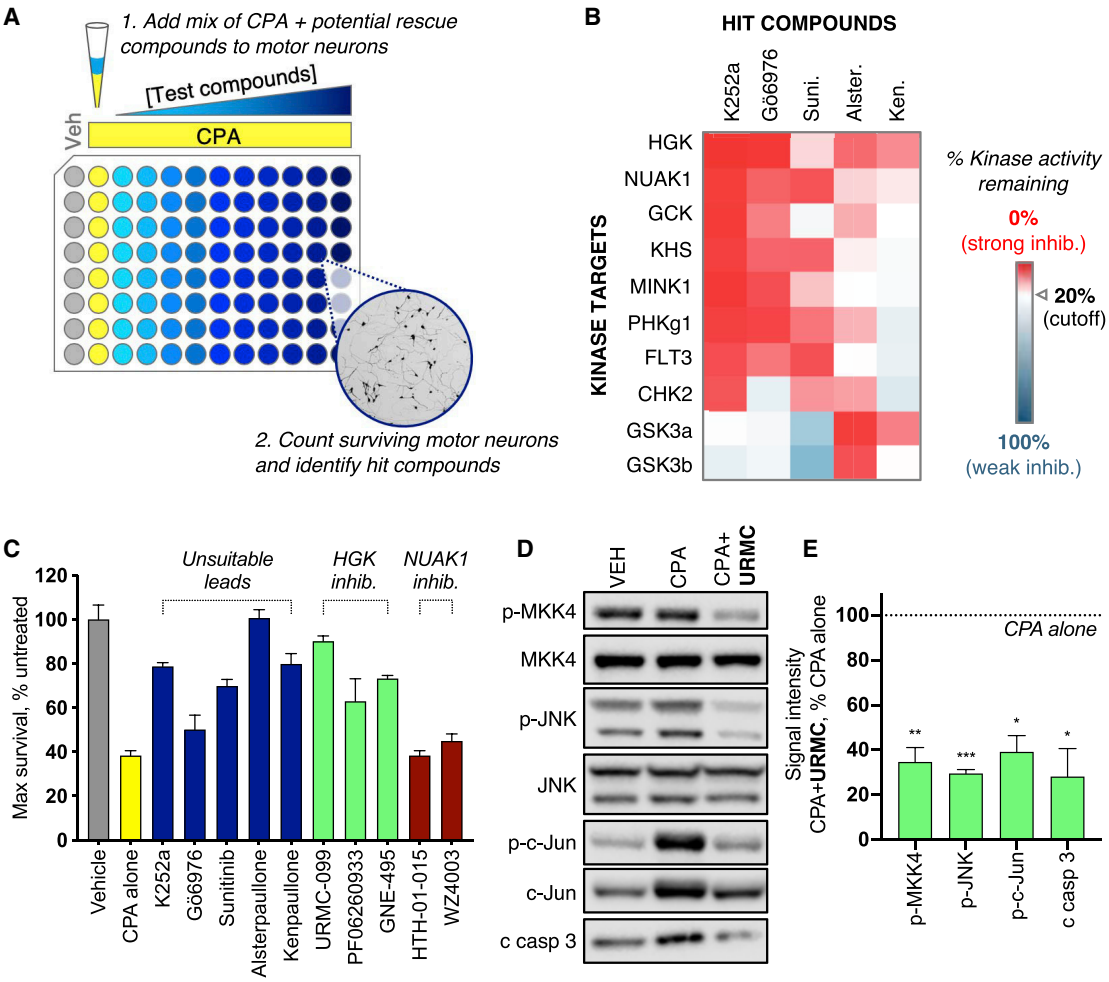

Figure 1. HGK Inhibitors Are Neuroprotective and Act through the JNK Pathway

(A) Schematic of motor neuron CPA survival assay.

(B) Hierarchical clustering of the kinase targets of neuroprotective hits from previous survival screens. HGK and NUAK1 are shared targets of these compounds. Red indicates that a given kinase is strongly inhibited by a hit compound (0%–20% activity remaining); blue indicates that a kinase is poorly inhibited (>20% activity remaining).

(C) Maximum efficacy of compounds that rescue motor neurons from ER stress-induced neurodegeneration (expressed as the maximum motor neuron survival recorded across all concentrations tested, percentage of untreated controls). Hits from the initial screen are in blue; HGK and NUAK1 inhibitors are in green and maroon, respectively. Compounds were tested in motor neurons derived from the stem cells of a healthy patient. Bars represent means ± SEM of wild-type motor neurons treated with CPA + test compound normalized to vehicle controls. n = 3 replicate wells from a 96-well plate. See also Figure S1.

(D) Western blots of motor neuron cultures treated with vehicle, CPA, or CPA + URMC-099. n = 2 separate motor neuron differentiations.

(E) Quantification of western blots. Band intensities for all phospho-isoforms were normalized to their respective total protein, and are represented as a percentage of CPA band intensities. Bars represent means ± SEM; *p < 0.05, **p < 0.01, ***p < 0.001.

decreased JNK activation compared with CPA treatment alone (Figures 1D and 1E). Neither CPA nor URMC-099 treatment influenced basal levels of MKK4 or JNK expression (Figure 1D), indicating that CPA and URMC-099 were acting in a post-translational, kinase-dependent manner to activate or suppress phosphorylation, respectively.

JNKs phosphorylate and activate transcription factors such as c-Jun to regulate the transcription of apoptosis-related genes (Pulverer et al., 1991), and we have shown that CPA treatment induces rapid c-Jun phosphorylation at Ser63 in motor neurons (Thams et al., 2019). Interestingly, URMC-099 treatment not only suppressed c-Jun phosphorylation (Figure 1E), but also decreased c-Jun expression (Figure 1D), perhaps because activated c-Jun perpetuates its own expression under conditions of stress (Hayakawa et al., 2005).

Finally, we investigated the effects of URMC-099 on the cleavage and activation of caspase-3, a critical step in apoptotic cell death pathways (Robertson et al., 2000). We have previously shown that CPA treatment induces caspase-3 cleavage in motor neurons (Thams et al., 2019), and we found here that URMC-099 attenuated CPA-mediated caspase-3 cleavage (Figures 1D and 1E), suggesting that it acts on apoptotic pathways to promote motor neuron survival. Taken together, these findings suggest that the neuroprotective effects of URMC-099 stem from the inhibition of JNK-mediated apoptotic pathways, and are in line with previous studies that have linked HGK inhibitors with JNK

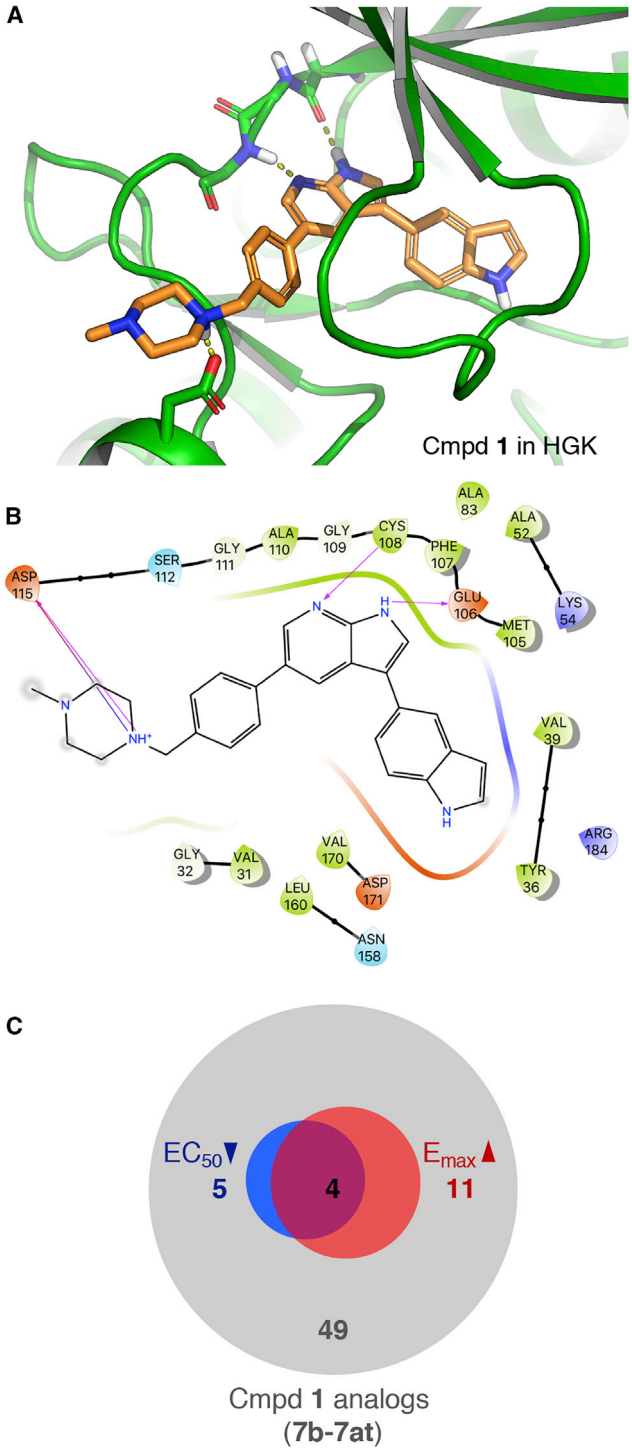

Figure 2. Docking Pose of Compound 1 in HGK and Summary of Analog Properties

(A) Docking pose of compound **1** in a crystal structure of HGK. Dashed lines indicate hydrogen bonds with the hinge region (Cys108, Glu106) and Asp115.

(B) Ligand interaction diagram of compound **1** with HGK corresponding to the docking pose shown in (A) (arrows indicating hydrogen bonds).

(C) Summary of improvements in efficacy (red) and potency (blue) in the CPA survival assay among the first 49 compound **1** analogs that were generated (**7b–7at**).

pathway attenuation, although they do not exclude the involvement of MLK3, a MAP3K that can directly phosphorylate MKK4 (Deacon and Blank, 1997).

Structure-Based Compound Design Yields Potent and Efficacious Derivatives of URMC-099

Considering that URMC-099 (compound **1**) was originally optimized for MLK3 inhibition, but that HGK inhibition was the likely driving force behind the neuroprotective effects of the kinase inhibitors identified in our previous screen (Figure 1B), we speculated that more potent and efficacious derivatives might be obtained by optimizing their capacity to inhibit HGK. Furthermore, we reasoned that increasing the potency of compound **1** analogs could lower their effective dose and thereby mitigate the potential for off-target effects *in vivo* given the low selectivity score calculated for compound **1**.

To aid in the design of analogs, we docked compound **1** in a crystal structure of HGK (PDB: 5DI1) using Glide (Schrödinger Maestro Suite 2017-1) (Figure 2A). From the docking pose and the binding site interaction (Figure 2B), it appeared that: (1) the 7-azaindole moiety binds to the hinge region of the kinase and is essential for activity, (2) the piperazine moiety extends into the solvent-exposed region and could be modified to improve the stability and the physicochemical properties of the molecule, and (3) the indole side chain could be modified to optimize interactions in the binding pocket and increase kinase specificity.

Based on these observations, we set out to generate a series of compound **1** analogs that had a high docking score in HGK and at the same time represented a diverse set of structures. However, the published synthetic route was not easily scalable: the side chain (Scheme 1, R-group) is introduced in the first step, and has to be carried through the entire synthesis, which is not efficient for the generation of side-chain analogs (Goodfellow et al., 2013). Therefore, we developed an improved synthetic route with increased flexibility (Scheme 1). In the first step, a Suzuki coupling of 5-bromo-7-azaindole (**2**) with 4-formylphenylboronic acid in a pressure tube provided aldehyde **3**. Reductive amination with 1-methylpiperazine at room temperature in dichloromethane yielded compound **4**. In the next two steps, compound **4** was iodinated at the 3-position to form compound **5**, followed by the introduction of a Boc-group on the azaindole to yield compound **6**. Initial attempts to forego this protecting group led to significantly decreased yields in the subsequent Suzuki coupling. Compound **6** was used as the substrate for the final Suzuki coupling with a number of boronic acids and boronic pinacol esters. Conveniently, the Boc-group was deprotected under these reaction conditions, obviating an additional deprotection step. Compound **1** and the desired analogs, **7a–7az**, were isolated in reasonable yields (40%–88%) after purification by preparatory high-performance liquid chromatography.

Once this synthetic route was established, we set out to generate a series of structurally diverse compound **1** analogs that met basic HGK docking criteria. We evaluated the analogs for their ability to rescue CPA-mediated toxicity in motor neurons on a rolling basis, providing us with real-time feedback on analog design and allowing us to circumvent structural modifications that decreased the efficacy of the compounds or were overtly

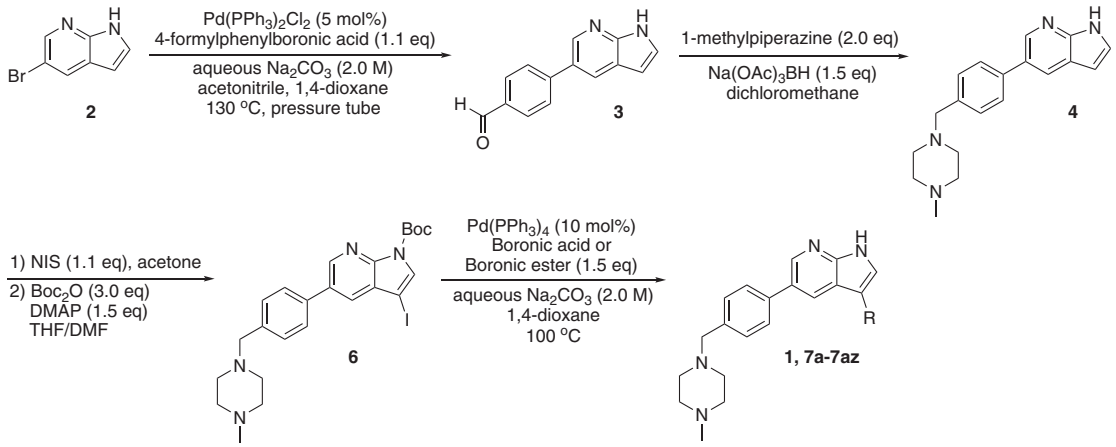

Scheme 1. Flexible Synthesis Route for the Synthesis of Compound 1 and Analogs 7a–7az

toxic. Through this iterative process, we initially developed and tested 49 analogs of compound **1** (**7b–7at**, Figure 2C; Table S1).

For these and all subsequent survival experiments, we used human stem-cell-derived motor neurons carrying the ALS-causing $SOD1^{A4V}$ mutation to maximize the translational potential of these analogs (Thams et al., 2019). Survival in this ALS line dropped to ~10% of untreated controls after CPA treatment (compared with ~40% in the healthy human motor neuron line used in Figures 1C and S1), consistent with our previous findings that CPA exacerbates basal levels of ER stress in ALS motor neurons (Thams et al., 2019). Under these conditions, compound **1** achieved maximum efficacy at 1 μM and completely prevented motor neuron death (102% motor neuron survival compared with untreated controls; Table S1). Out of the 49 analogs, 11 analogs (**7e**, **7h**, **7l**, **7p**, **7v**, **7y**, **7aa**, **7ac**, **7ak**, **7al**, and **7am**) demonstrated greater maximum efficacy than compound **1** (Figure 2C; Table S1), indicating that some analogs were also counteracting the basal levels of cell death that occurred across the 72 h assay independently of CPA. Furthermore, five analogs (**7h**, **7l**, **7m**, **7v**, and **7aa**) were more potent than compound **1** (half maximal effective concentration [EC_{50}] < 0.22 μM), and four analogs (**7h**, **7l**, **7v**, and **7aa**) were both more efficacious and more potent than compound **1** (Figure 2C; Table S1). Only two analogs (**7c** and **7ay**) were completely ineffective (survival ≤ CPA alone; Tables S1 and S2).

HGK Inhibition Correlates Strongly with Motor Neuron Survival

The battery of compound **1** analogs generated and tested here offered a unique opportunity to investigate whether improved potency in the motor neuron survival assays correlated with increased inhibition of HGK or MLK3, given that compound **1** was originally optimized to inhibit MLK3. The neuroprotective effects of compound **1** and 53 analogs (**7b–7at** and **12b–12e**, which are further described below) were assessed concurrently in CPA-treated human ALS motor neuron cultures (Table S2). Meanwhile, the same analogs were analyzed in a cell-free radiolabeled ATP assay (Reaction Biology) to compare the extent to which they could inhibit the activity of HGK, MLK3, or MLK1, a homolog of MLK3 that has also been shown to activate the JNK pathway (Gallo and Johnson, 2002) (Tables S3 and S4).

We then used regression analysis to compare the ability of a given analog to inhibit HGK, MLK1, or MLK3 with its ability to rescue human ALS motor neurons in the CPA survival assay. Overall, we observed a significant correlation between the inhibition of MLK3 activity and neuroprotection ($R^2 = 0.52$; $p < 0.0001$; Figure 3A). We performed the same analysis for MLK1 and found the correlation to be weaker than that for MLK3 ($R^2 = 0.39$; $p < 0.0001$; Figure 3B). Meanwhile, we observed a more robust correlation between the inhibition of HGK activity and neuroprotection than for either MLK ($R^2 = 0.84$; $p < 0.0001$; Figure 3C). These findings point to HGK as an important biological target of compound **1** and its analogs. The fact that some of the analogs tested were highly neuroprotective despite their inability to inhibit MLK3 and MLK1 (e.g., compound **12e** [Tables S1 and S3]) indicates that direct MLK inhibition is not a requirement for motor neuron protection.

The Inhibition of Related MAP4Ks Correlates with Motor Neuron Survival

To further explore the biologically relevant targets of compound **1** and its analogs, we selected 10 analogs ranging from weakly to very strongly protective in CPA-treated motor neurons and evaluated their ability to inhibit a panel of 60 human kinases in the radiolabeled ATP assay (Table S5). The kinases in the expanded panel were selected from known targets of compound **1** (Goodfellow et al., 2013), known targets of other kinase inhibitors that were protective in the CPA survival assay (Thams et al., 2019), and relevant targets from the literature. RNA sequencing data were used to confirm the expression of each kinase in embryonic stem motor neurons (Thams et al., 2019).

We found that the inhibition of HGK, TNIK, MINK1 (MAP4K6), GCK (MAP4K2), and KHS (MAP4K5) all correlated strongly with motor neuron survival (Figure 3D). These findings were also consistent with our analyses of the shared targets of the hit compounds from our preliminary screen (Figure 1B), where HGK, MINK1, GCK, and KHS were all among the most highly ranked targets (TNIK did not appear in our initial analysis of shared targets because its activity was not assessed in the existing publicly

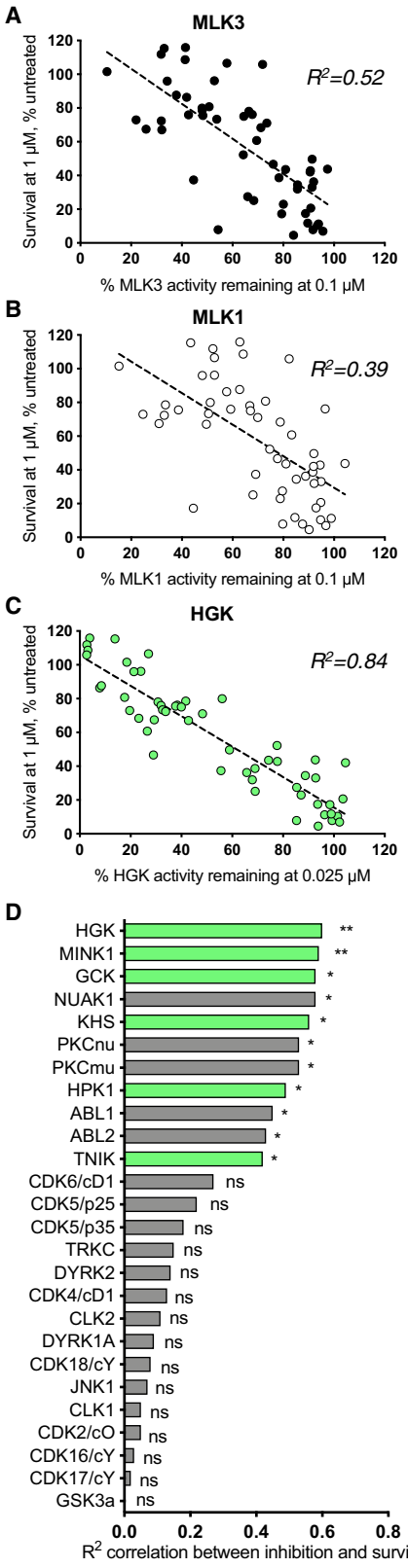

Figure 3. Inhibition of HGK and Related MAP4Ks Correlates Strongly with Motor Neuron Rescue

(A–C) Plots of the associations between motor neuron survival and the inhibition of MLK3 (A), MLK1 (B), or HGK (C) for 53 compound **1** analogs (Table S2). Each data point represents one compound; dashed lines indicate linear regression. HGK inhibition correlates more strongly with motor neuron survival than MLK inhibition.

(D) Ranked R2 values (from Pearson's r) describing the correlation between kinase inhibition and motor neuron survival for ten compound **1** analogs across 60 different kinases. MAP4Ks (highlighted in green) are among the most highly ranked kinases. *$p < 0.05$; **$p < 0.01$.

available database; Anastassiadis et al., 2011.) Because the catalytic domains of all MAP4K kinases are highly conserved (Read et al., 2019), it is possible that neuroprotection by compound **1** and its analogs hinges on the inhibition of several MAP4K family members simultaneously (Larhammar et al., 2017).

Compound 12k Exhibits Increased Metabolic Stability

Among the HGK inhibitors that we tested in CPA-treated motor neurons *in vitro*, compound **1** is unique in that it exhibits CNS penetrance *in vivo* without any overt toxicity. Both PF-6260933 and GNE-495 had been modified to prevent CNS penetrance because previous brain-penetrant iterations had been poorly tolerated in multi-dose assays in mice (Dow et al., 2018; Ndubaku et al., 2015). By contrast, compound **1** has previously been shown to be well-tolerated over long-term dosing regimens and to modulate CNS phenotypes in mice: in a study by Marker et al. (2013), compound **1** was administered intraperitoneally (i.p.) at 10 mg/kg twice a day for 28 days, and was found to attenuate HIV-mediated microgliosis in the brain.

Although the study by Marker et al. (2013) highlights the safety and efficacy of compound **1** *in vivo*, it also sheds light on the limitations of testing this drug in mouse models of neurodegenerative disease. One of the major drawbacks of compound **1** is the fact that it must be delivered twice daily to achieve sustained therapeutic levels in the CNS, both because of its low metabolic stability and of its relatively limited brain exposure (Goodfellow et al., 2013). Dosing strategies involving multiple daily injections increase the risk of handling stress in treated animals (Ryabinin et al., 1999), which can, in turn, lead to the induction of MAPK pathways in the CNS (Liu et al., 2004) and may confound the effects of kinase inhibitors in the context of neurodegeneration. We therefore set out to enhance the metabolic stability of the potent and neuroprotective compound **1** analogs described above.

To evaluate the metabolic stability of compound **1** derivatives, we incubated them with mouse liver microsomes and analyzed samples collected over 2 h by LC-MS/MS. Under these conditions, compounds with a half-life of less than 30 min were considered to have a high clearance rate and were not suitable therapeutic candidates. In accordance with previous findings (Goodfellow et al., 2013), we found that compound **1** had a half-life of 15 min (Table S7). Initially, we selected 11 analogs for further analysis based on their structural variety and their activity profiles in the motor neuron survival assay. Only two of these analogs (**7y** and **7ad**) exhibited a half-life $\geq$30 min (Table S7).

Next, we set out to improve the half-life of the analogs through further structural modification. Computational docking experiments indicated that the N-methylpiperazine moiety is solvent-exposed, suggesting that its modifications might alter pharmacokinetic properties of compounds, while maintaining their potency in the ER stress assay (Schemes 2A and 2B, **12a**-**12l**).

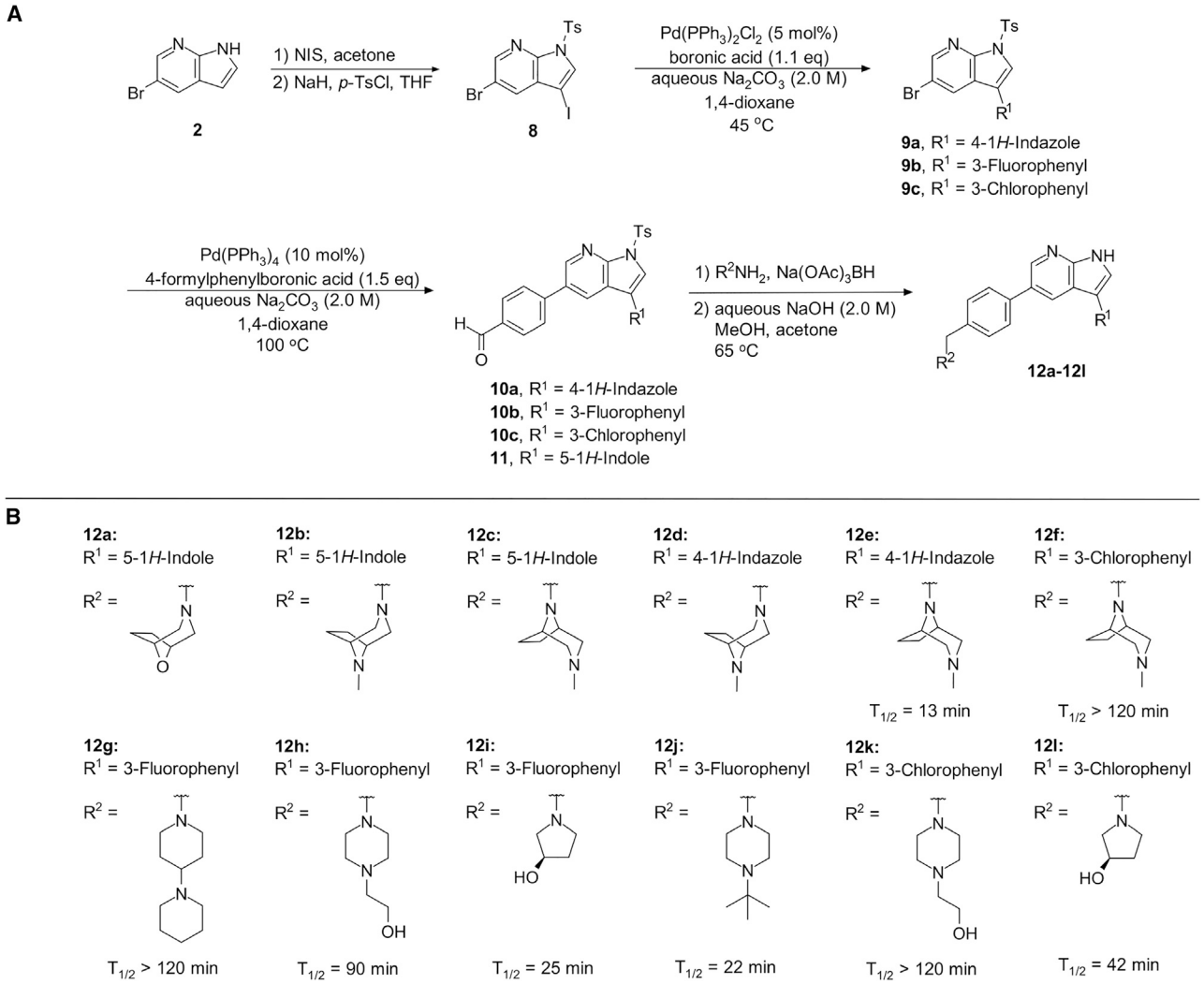

Scheme 2. Synthesis and metabolic stability of compounds 12a–12l

(A and B) (A) Synthesis of compounds **12a–12l**; (B) structures of analogs **12a–12l** and half-life in mouse liver microsomes (CD-1) of analogs **12e–12l**.

Introduction of a bicyclic N-methylpiperazine to one of the most potent analogs (Scheme 2) only slightly increased the half-life from 9 to 13 min (compound **12e**; Table S7). To further enhance the microsomal stability of these analogs, we introduced the same bicyclic piperazine to one of the analogs from the initial series that had a half-life of $\geq$30 min (compound **7ad**; Table S7). In this case, we were able to considerably increase the half-life from 38 to >120 min (compound **12f**; Table S7).

Compound **12f** was more potent than compound **1** in the motor neuron survival assay, with an EC_{50} of 0.11 μM (Table S1) but was toxic at concentrations above 0.3 μM. To mitigate this increase in toxicity, while maintaining potency and microsomal stability, we synthesized a new series of analogs (Scheme 2; **12g–12l**) containing the *m*-chlorophenyl or *m*-fluorophenyl substituent on the 3-position of the 7-azaindole scaffold. We evaluated the potency of these compounds in the ER stress assay, and their stability in the microsomal stability assay. Two of these compounds, **12g** and **12j**, either had a shorter half-life than desired or showed a decrease in potency in the ER stress assay (Tables S1 and S7). The remaining four compounds (**12h**, **12i**, **12k**, and **12l**) completely blocked the effects of CPA treatment at concentrations <0.3 μM (Table S1). We also confirmed by western blot that they effectively inhibit the same JNK pathway components as compound **1** (Figure S2). One of the resulting compounds, **12k** (Figure 4B), had a half-life of >120 min in the microsome assay (Figure 4C) and rescued CPA-induced neurodegeneration with an improved EC_{50} of 0.10 μM (Table S1; Figures 4D–4H). We termed this compound **Prostetin/12k** (Figure 4B).

To determine whether the computationally and functionally guided structural modifications made to **Prostetin/12k** corresponded to a decrease in the half maximal inhibitory concentration (IC_{50}) of HGK, we measured HGK activity in cell-free radiolabeled ATP assays for each compound. The IC_{50} of HGK was 5.93 nM for compound **1** and 0.30 nM for **Prostetin/12k**

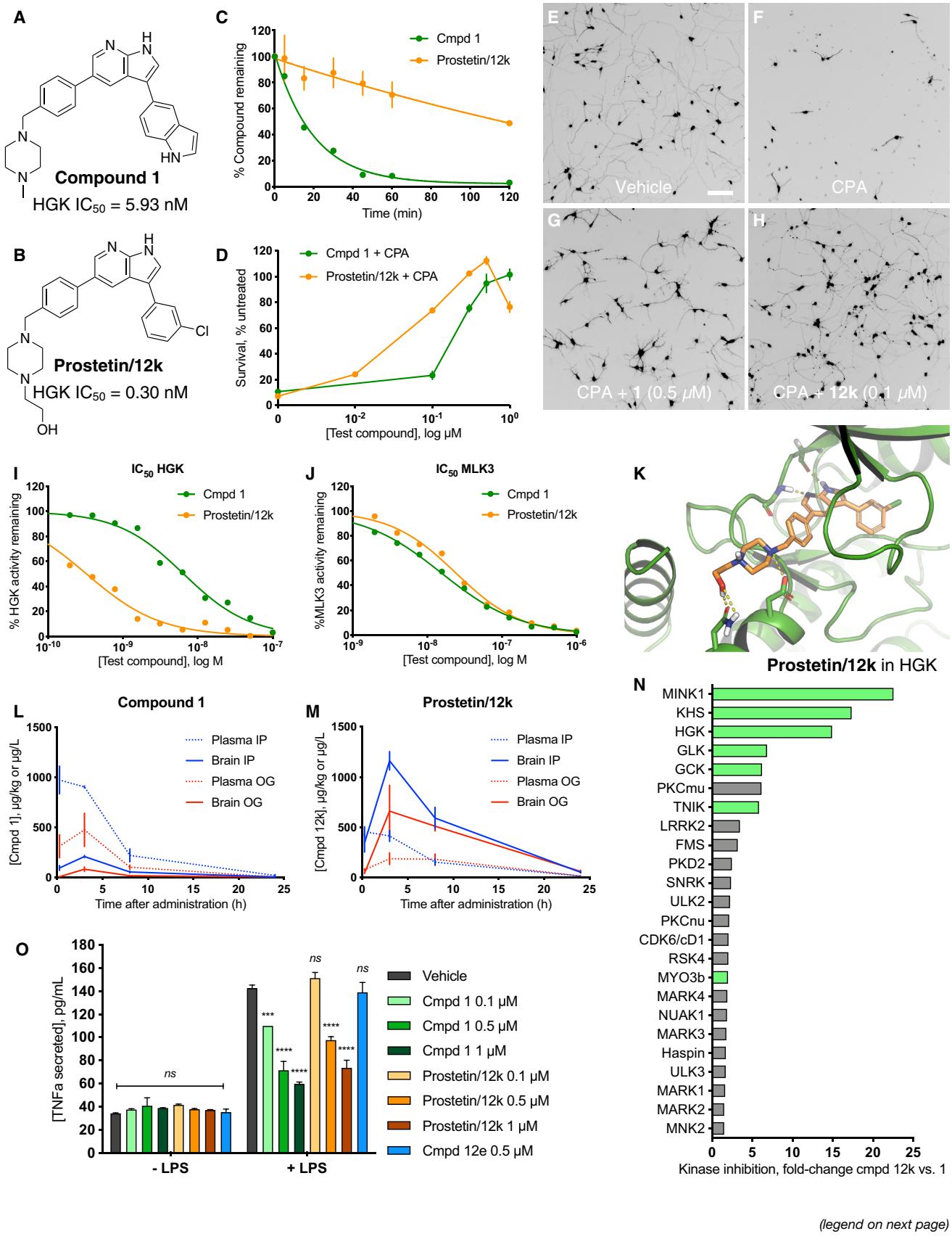

(legend on next page)

Table 1. Pharmacokinetic Parameters for Compound 1 versus Prostetin/12k Administered by i.p. Injection or by o.g.

Parameter	Compound **1**, i.p.	Compound **1**, o.g.	**Prostetin/12k**, i.p.	**Prostetin/12k**, o.g.
Plasma AUC (μg/L·h)	7,328 (±1,000)	3,401 (±908.8)	3,899 (±539.3)	2,785 (±797.0)
Brain AUC (μg/L· h)	1,568 (±147.1)	567.2 (±110.5)	11,570 (±1,655)	8,429 (±1,458)
Plasma mean C_{max} (μg/L)	971.7 (±138.2)	476.2 (±165.3)	454.0 (±48.62)	184.1 (±57.26)
Brain mean C_{max} (μg/kg)	208.8 (±10.21)	83.35 (±21.40)	1,162 (±91.99)	658.9 (±257.7)
Mean brain/plasma ratio at 3 h	0.23 (±0.014)	0.19 (±0.019)	3.0 (±0.59)	3.3 (±0.53)

Error is ± SEM. AUC, area under the curve.

(Figures 4A, 4B, and 4I). Meanwhile, the IC_{50} of MLK3 was 18.60 nM for compound **1** and 23.70 for **Prostetin/12k** (Figure 4J), indicating that the improvement in EC_{50} observed for **Prostetin/12k** in CPA-treated motor neurons was independent of MLK3. Similar trends were observed for MLK1, a homolog of MLK3, and MINK1, a homolog of HGK (Figure S3). Together, these findings provided further support for the idea that MAP4K inhibition drives neuroprotection. The docking pose of **Prostetin/12k** in HGK (PDB: 5DI1; Figure 4K) revealed that it had a similar binding mode to compound **1** (Figure 2A), but formed an additional hydrogen bond through the hydroxyl group that may underlie its reduced IC_{50}.

Prostetin/12k Is Stable, Orally Bioavailable, and Brain Penetrant *In Vivo*

In additional to its low metabolic stability, another critical hurdle in the administration of compound **1** in translational models of neurodegeneration is its low oral bioavailability, which is compounded by its low brain-to-plasma ratio. Goodfellow et al. (2013) reported that the bioavailability (%F) of compound **1** as measured in the plasma was 41. The %F of compound **1** in the brain was not evaluated in that study, but given that the brain-to-plasma ratios that were observed for intravenous administration (<1 at all time points measured [Goodfellow et al., 2013]), the %F in the brain would be expected to be even lower than that observed in the plasma. The limited oral bioavailability of compound **1** in the CNS precludes the possibility of implementing more translational routes of administration, such as oral gavage, in preclinical assessments of the drug.

To evaluate the brain exposure and oral bioavailability of **Prostetin/12k** versus compound **1**, each drug was administered to mice at 10 mg/kg through i.p. injection or oral gavage (o.g.). The pharmacokinetic properties of **Prostetin/12k** were improved relative to **1** across several measures. The area under the curve was greatly increased for **Prostetin/12k** in the brain after both i.p. and o.g. administration, consistent with the decreased rate of clearance predicted by the *in vitro* microsomal stability assay (Table 1). The concentration of **Prostetin/12k** in the brain was increased across all time points and routes of administration assessed, as were brain-to-plasma ratios (Figures 4L and 4M; Table 1), indicating improved brain penetrance. The brain C_{max} of **Prostetin/12k** in i.p.-injected animals was 1,162 ng/g (2.60 μM; Figures 4L and 4M; Table 1), which exceeds the concentration at which E_{max} was observed in CPA-treated motor neurons (0.5 μM; Figure 4D). Oral bioavailability (%F) based on plasma measurements in i.p. versus o.g.-treated animals was 46 for compound **1**, which is in line with the %F of 41 reported by Goodfellow et al. (2013). Meanwhile, the %F for **Prostetin/12k** was 73, a marked increase compared with **1**. Similar results were obtained for **Prostetin/12k** by comparing brain measurements (%F = 73). Taken together, these results indicate that **Prostetin/12k** is well suited to future use *in vivo*, particularly in the study of CNS disorders.

Figure 4. *In Vitro* and *In Vivo* Characterization of Prostetin/12k

(A and B) Structures of compound **1** and **Prostetin/12k**.

(C) *In vitro* microsomal stability curves for compound **1** and **Prostetin/12k**. **Prostetin/12k** has a markedly longer half-life in this assay than compound **1**. Data are means ± SEM; n = 3 replicates per compound per time point.

(D) Survival curves for $SOD1^{A4V}$ mutant ALS motor neurons treated with CPA and compound **1** or **Prostetin/12k**. **Prostetin/12k** shows improved potency and efficacy. Data are means ± SEM of motor neurons treated with CPA + test compounds normalized to vehicle controls. n = 3 replicate wells from a 96-well plate for each test compound dose.

(E–H) Representative fields from whole-well images of $SOD1^{A4V}$ motor neurons treated with vehicle (DMSO) alone (E); CPA alone (F); CPA + compound **1** (G); or CPA + compound **12k** (H).

(I and J) IC_{50} determination for HGK (I) and MLK3 (J) in cell-free assays. Compared with compound **1**, **Prostetin/12k** shows a reduced IC_{50} for HGK but little change in IC_{50} for MLK3. See also Figure S3.

(K) Docking pose of **Prostetin/12k** in HGK. **Prostetin/12k** has a similar binding mode as compound **1**, but forms an additional hydrogen bond through the hydroxyl group with Asn119.

(L and M) Concentration of compounds **1** (L) versus **Prostetin/12k** (M) in brain and plasma samples over 24 h following i.p. or o.g. administration. **Prostetin/12k** is more effective than **1** at reaching the CNS. Pharmacokinetic parameters are further described in Table 1. Data are means ± SEM of plasma (μg/L) or brain (μg/kg) concentrations. n = 3 mice per treatment per time point.

(N) Ranked fold-changes in kinase inhibition for **Prostetin 12k** versus compound **1** for all kinases assayed in Table S6, where fold-change >1.5. MAP4Ks (green) are among the most enhanced targets of **Prostetin/12k**.

(O) Suppression of cytokine release in LPS-stimulated microglia. Microglial N9 cells were treated with compound **1**, **Prostetin/12k**, or **12e** ± LPS. TNF-α release was measured by ELISA. **Prostetin/12k** was ~5× less potent than compound **1**, but significantly attenuated TNF-α release at concentrations of 0.5 μM and above. Compound **12e**, which strongly inhibits HGK but has little activity at MLK3, did not inhibit TNF-α release at 0.5 μM. Data are mean ± SEM. n = 2 replicate wells of a 96-well plate. ***p < 0.001, ****p < 0.0001.

Identification of Additional Kinase Targets of Prostetin/12k

The increased potency and favorable pharmacokinetic profile of **Prostetin/12k** make it a strong candidate for future studies *in vivo*, where off-target effects will be a concern. To obtain global kinase inhibition profiles, compound **1** and **Prostetin/12k** were tested in cell-free radiolabeled ATP assays across a panel of 371 human kinases (Table S6). We found that the MAP4Ks MINK1, KHS, HGK, GLK, and GCK exhibited the greatest degree of change in activity following **Prostetin/12k** exposure compared with **1** (Figure 4N). However, several unrelated kinases were inhibited more effectively (>1.5-fold) by **Prostetin/12k** than by compound **1**, including kinases that have previously been implicated in neurodegeneration, such as NUAK1 (Lasagna-Reeves et al., 2016) and LRRK2 (Islam and Moore, 2017). These observations raised the possibility that additional kinase targets beyond the MAP4Ks might contribute to the enhanced potency of **Prostetin/12k** in ER stress-mediated neurodegeneration.

Prostetin/12k Maintains the Anti-inflammatory Properties of Compound 1

Compound **1** was originally validated in *in vitro* and *in vivo* models of HIV-associated neuroinflammation, where it was shown to attenuate inflammatory cytokine production by microglia (Marker et al., 2013). Our aim in developing the compound **1** analogs described herein was primarily to generate potent, metabolically stable drugs that could prevent neuronal death; but, given the fact that neurodegenerative disorders such as ALS are also accompanied by aggressive microgliosis (Hall et al., 1998), and that drug-mediated inhibition of microgliosis is protective in a rodent model of ALS (Trias et al., 2016), we asked whether the optimized compound could also modulate microglial cytokine release. This question was also prompted by the fact that, according to Marker et al. (2013), the anti-inflammatory effects of compound **1** are orchestrated by MLK3 in microglia; meanwhile, all of the analogs tested here showed diminished activity at MLK3 compared with **1** (Table S3).

To model microglial activation *in vitro*, we stimulated mouse N9 microglial cells with *E.-coli*-derived lipopolysaccharides (LPS) and measured the release of the pro-inflammatory cytokine tumor necrosis factor alpha (TNF-α) into cell culture media. The LPS concentration selected here strongly induced TNF-α secretion (Figure 4O), but did not induce N9 cell death (data not shown). We then compared TNF-α secretion in cultures co-treated with LPS and compound **1** or the optimized analog **Prostetin/12k**, which showed increased inhibition of MAP4Ks (Figure 4N), but slightly decreased inhibition of MLK3 (Table S6). We also tested compound **12e**, which strongly inhibited HGK activity (Table S4) and was highly neuroprotective (Table S1) but had little activity at MLK3 (Table S3).

We found that compound **1** significantly and dose-dependently decreased TNF-α secretion in LPS-stimulated microglia, consistent with its previously reported anti-inflammatory effects (EC_{50} = 0.20 μM; Figure 4O). **Prostetin/12k** also significantly decreased TNF-α secretion, although it was less potent in this assay than compound **1** (EC_{50} = 0.47 μM; Figure 4O). Meanwhile, compound **12e** did not significantly decrease TNF-α levels (Figure 4O). Taken together, these findings suggest that MAP4K inhibition does not mitigate TNF-α release in this context, and that the retention of non-MAP4K targets, such as MLK3 may confer anti-inflammatory activity to compound **1** analogs.

DISCUSSION

Our previous work in human motor neurons subjected to ER stress pointed to broad-spectrum kinase inhibitors as potent neuroprotective agents. Here we determined that one of the shared targets of these protective compounds was HGK, a MAP4K. Using compound **1** as a scaffold, we developed an array of neuroprotective, pharmacologically stable compounds that potently inhibit HGK, culminating in **Prostetin/12k**.

Although our initial focus was on HGK, a kinase previously implicated in motor neuron degeneration (Wu et al., 2019; Yang et al., 2013), we found that the efficacy of compound **1** derivatives also correlated with other closely related MAP4Ks, including MINK1, GCK, KHS, and TNIK, raising the possibility that multiple MAP4Ks may be involved in ER-stress-mediated neurodegeneration. In support of this idea, Larhammar et al. (2017) showed that siRNA-mediated knockdown of HGK, MINK1, and TNIK simultaneously—but not individually—was neuroprotective in dorsal root ganglia neurons subjected to neurotrophic factor withdrawal. They argue that the roles of related MAP4Ks in their neurodegeneration assay are redundant, and that the effects of inhibiting a single kinase can be overcome by the activity of the remaining kinases. Therefore, it is possible that the combined inhibition of multiple MAP4Ks underlies the robust neuroprotective effects of compound **1** and its analogs in CPA-treated motor neurons.

At the same time, kinome-wide profiles of **1** and **Prostetin/12k** (Figure 4N; Table S6) make it clear that neither compound is perfectly selective for MAP4Ks. It is possible that some of the additional targets of compound **1** and its analogs may enhance their neuroprotective effects. Other kinases whose inhibition correlated strongly with neuroprotection included PRKD3, ABL1, and ABL2 (Figure 3D). Accordingly, we have observed that kinase inhibitors targeting PKC or ABL kinases in a non-subtype-specific manner (e.g., Ro-318220 mesylate and bosutinib, respectively) are mildly protective in CPA-treated motor neurons (data not shown). Furthermore, both the addition of bosutinib and the genetic ablation of ABL1 have been shown to be neuroprotective in a human stem cell-derived motor neuron model of ALS (Imamura et al., 2017). Although it is unclear how these might be activated in the context of CPA, the combined inhibition of multiple kinase subtypes by compound **1** and its analogs may be critical to their success in the *in vitro* motor neuron survival assay.

Furthermore, the anti-inflammatory properties of compound **1** analogs, which may be linked to MLK3 inhibition (Marker et al., 2013), could prove to be an additional benefit. Microgliosis is a hallmark of many neurodegenerative disorders and is readily observed in murine models of ALS (Hall et al., 1998). There is an ongoing debate as to whether microglia are helpful or harmful in the context of ALS (Chiu et al., 2013; Gowing et al., 2008; Spiller et al., 2018), but treatment with the kinase inhibitor masitinib has been shown to attenuate microgliosis and slow disease progression in late-stage $SOD1^{G93A}$ mutant rats (Trias et al., 2016). Thus, **Prostetin/12k** and the other compound **1** analogs

generated here that target both neuroinflammatory and neurodegenerative pathways may be particularly strong therapeutic candidates for ALS.

Finally, MAP4Ks have been directly implicated in multiple, diverse disorders outside of the CNS, including obesity (Danai et al., 2015), insulin resistance (Ammirati et al., 2015; Bouzakri and Zierath, 2007; Chuang et al., 2014; Flach et al., 2016; Tang et al., 2006; Tesz et al., 2007), atherosclerosis (Aouadi et al., 2009; Virbasius and Czech, 2016), hepatocellular carcinoma (Han et al., 2010), lung adenocarcinoma (Qiu et al., 2012), colorectal cancer (Lin et al., 2018; Salem et al., 2018), and general transformation and metastatic processes in many types of human tumors (Wright et al., 2003). The compounds generated here may therefore have broad therapeutic potential across a wide range of human diseases.

SIGNIFICANCE

ALS and other neurodegenerative diseases are characterized by the accumulation of misfolded proteins, which trigger ER stress and, if left unchecked, ultimately lead to neuronal death (Yoshida, 2007). Because the therapeutic options for these diseases are currently limited, we used a human motor neuron-based screening platform to identify compounds that could reverse the neurotoxic effects of ER stress. We found that the hits resulting from this screen shared the MAP4 kinase HGK as their target. We selected an orally bioavailable HGK inhibitor with a strong safety profile for further optimization, and developed analogs with enhanced efficacy, potency, metabolic stability, and blood-brain barrier penetration. These compounds, including Prostetin/12k, are now primed for further investigation into their therapeutic potential in animal models of neurodegeneration.

STAR★METHODS

Detailed methods are provided in the online version of this paper and include the following:

- KEY RESOURCES TABLE
- LEAD CONTACT AND MATERIALS AVAILABILITY
- EXPERIMENTAL MODEL AND SUBJECT DETAILS
  - Generation of Human and Mouse Stem Cell Lines
  - Human Motor Neuron Differentiation
  - Mouse Motor Neuron Differentiation
  - N9 Microglia Culture Details
  - Mouse Maintenance
- METHOD DETAILS
  - Human Motor Neuron Survival Assays
  - Biochemical Analysis of JNK Pathway Regulation
  - General Experimental Details for the Synthesis of Compound 1 Analogs and Intermediates
  - *In Vitro* Microsomal Stability
  - *In Vivo* Pharmacokinetics
  - Commercial In Vitro Kinase Inhibition Assays
  - Microglia LPS Treatment and TNFα ELISAs
- QUANTIFICATION AND STATISTICAL ANALYSIS
- DATA AND CODE AVAILABILITY

SUPPLEMENTAL INFORMATION

Supplemental Information can be found online at https://doi.org/10.1016/j.chembiol.2019.10.005.

ACKNOWLEDGMENTS

We thank V. Jackson-Lewis and H. Melikyan for their assistance in animal tissue collection. This research was funded by a grant from the United States Department of Defense to B.R.S. and H.W. (CDMRP/USAMRAA GG012467), by a grant from the NIH to H.W. (R21NS109661), and by Project ALS. E.R.L. is a Project ALS Women and the Brain fellow. H.W. holds an endowed chair from Jerry and Emily Spiegel. Work performed in the Columbia Chemistry Department NMR facility was supported by a 500 Ascend grant (S10RR025431). The graphical abstract was created with BioRender.com.

AUTHOR CONTRIBUTIONS

P.H.B., A.Z., and B.R.S. designed compound **1** analogs. E.R.L., S.T., and H.W. designed *in vitro* motor neuron survival and western blotting experiments. E.R.L. and H.W. designed *in vitro* microglial cytokine release experiments. E.R.L., P.H.B., and H.W. designed *in vivo* pharmacokinetic experiments. B.R.S., P.H.B. and A.Z. performed computational modeling and ligand design of compound **1** analogs and designed synthetic routes. P.H.B. performed compound synthesis and analysis under supervision of A.Z. and B.R.S. P.H.B. performed *in vitro* microsomal stability studies under the supervision of B.R.S. E.R.L. and J.C. performed and analyzed *in vitro* motor neuron survival, *in vitro* cytokine release, and western blotting experiments. A.G.-D. differentiated and characterized the wild-type human motor neuron iPS line. E.R.L. collected blood and brain samples for pharmacokinetic experiments. E.R.L. analyzed correlations between motor neuron survival and kinase activity. E.R.L., P.H.B., A.Z., H.W., and B.R.S. wrote the manuscript.

DECLARATION OF INTERESTS

B.R.S., H.W., A.Z., P.H.B., E.R.L., and S.T. have filed an application for a patent for the use of compound **1** analogs to suppress ER stress-related toxicity and inflammation. B.R.S. holds equity in and serves as a consultant to Inzen Therapeutics.

Received: March 31, 2019
Revised: September 14, 2019
Accepted: October 10, 2019
Published: October 29, 2019

REFERENCES

Ammirati, M., Bagley, S.W., Bhattacharya, S.K., Buckbinder, L., Carlo, A.A., Conrad, R., Cortes, C., Dow, R.L., Dowling, M.S., El-Kattan, A., et al. (2015). Discovery of an in vivo tool to establish proof-of-concept for MAP4K4-based antidiabetic treatment. ACS Med. Chem. Lett. *6*, 1128–1133.

Anastassiadis, T., Deacon, S.W., Devarajan, K., Ma, H., and Peterson, J.R. (2011). Comprehensive assay of kinase catalytic activity reveals features of kinase inhibitor selectivity. Nat. Biotechnol. *29*, 1039.

Aouadi, M., Tesz, G.J., Nicoloro, S.M., Wang, M., Chouinard, M., Soto, E., Ostroff, G.R., and Czech, M.P. (2009). Orally delivered siRNA targeting macrophage Map4k4 suppresses systemic inflammation. Nature *458*, 1180–1184.

Banerjee, S., Buhrlage, S.J., Huang, H.-T., Deng, X., Zhou, W., Wang, J., Traynor, R., Prescott, A.R., Alessi, D.R., and Gray, N.S. (2014). Characterization of WZ4003 and HTH-01-015 as selective inhibitors of the LKB1-tumour-suppressor-activated NUAK kinases. Biochem. J. *457*, 215–225.

Boillée, S., Yamanaka, K., Lobsiger, C.S., Copeland, N.G., Jenkins, N.A., Kassiotis, G., Kollias, G., and Cleveland, D.W. (2006). Onset and progression in inherited ALS determined by motor neurons and microglia. Science *312*, 1389–1392.

Bouzakri, K., and Zierath, J.R. (2007). MAP4K4 gene silencing in human skeletal muscle prevents tumor necrosis factor-α-induced insulin resistance. J. Biol. Chem. *282*, 7783–7789.

Chiu, I.M., Morimoto, E., Goodarzi, H., Liao, J.T., O'Keeffe, S., Phatnani, H.P., Muratet, M., Carroll, M.C., Levy, S., Tavazoie, S., et al. (2013). A neurodegeneration-specific gene-expression signature of acutely isolated microglia from an amyotrophic lateral sclerosis mouse model. Cell Rep. *4*, 385–401.

Chuang, H.-C., Sheu, W.H., Lin, Y.-T., Tsai, C.-Y., Yang, C.-Y., Cheng, Y.-J., Huang, P.-Y., Li, J.-P., Chiu, L.-L., Wang, X., et al. (2014). HGK/MAP4K4 deficiency induces TRAF2 stabilization and Th17 differentiation leading to insulin resistance. Nat. Commun. *5*, 4602–4615.

Corradin, S., Mauël, J., Donini, S., Quattrocchi, E., and Ricciardi-Castagnoli, P. (1993). Inducible nitric oxide synthase activity of cloned murine microglial cells. Glia *7*, 255–262.

Danai, L.V., Flach, R.J., Virbasius, J.V., Menendez, L., Jung, D., Kim, J., Kim, J.K., and Czech, M.P. (2015). Inducible deletion of protein kinase Map4k4 in obese mice improves insulin sensitivity in liver and adipose tissues. Mol. Cell. Biol. *35*, 2356–2365.

Deacon, K., and Blank, J.L. (1997). Characterization of the mitogen-activated protein kinase kinase 4 (MKK4)/c-Jun NH2-terminal kinase 1 and MKK3/p38 pathways regulated by MEK kinases 2 and 3 MEK kinase 3 activates MKK3 but does not cause activation of p38 kinase in vivo. J. Biol. Chem. *272*, 14489–14496.

Dow, R.L., Ammirati, M., Bagley, S.W., Bhattacharya, S.K., Buckbinder, L., Cortes, C., El-Kattan, A.F., Ford, K., Freeman, G.B., Guimaraes, C.R., et al. (2018). 2-Aminopyridine-based mitogen-activated protein kinase kinase kinase kinase 4 (MAP4K4) inhibitors: assessment of mechanism-based safety. J. Med. Chem. *7*, 3114–3125.

Flach, R.J., Danai, L.V., DiStefano, M.T., Kelly, M., Menendez, L., Jurczyk, A., Sharma, R.B., Jung, D., Kim, J., Kim, J.K., et al. (2016). Protein kinase mitogen-activated protein kinase kinase kinase kinase 4 (MAP4K4) promotes obesity-induced hyperinsulinemia. J. Biol. Chem. *291*, 16221–16230.

Gallo, K.A., and Johnson, G.L. (2002). Mixed-lineage kinase control of JNK and p38 MAPK pathways. Nat. Rev. Mol. Cell Biol. *3*, 663–672.

Goodfellow, V.S., Loweth, C.J., Ravula, S.B., Wiemann, T., Nguyen, T., Xu, Y., Todd, D.E., Sheppard, D., Pollack, S., Polesskaya, O., et al. (2013). Discovery, synthesis, and characterization of an orally bioavailable, brain penetrant inhibitor of mixed lineage kinase 3. J. Med. Chem. *56*, 8032–8048.

Gowing, G., Philips, T., Wijmeersch, B., Audet, J.-N., Dewil, M., Bosch, L., Billiau, A.D., Robberecht, W., and Julien, J.-P. (2008). Ablation of proliferating microglia does not affect motor neuron degeneration in amyotrophic lateral sclerosis caused by mutant superoxide dismutase. J. Neurosci. *28*, 10234–10244.

Greenwald, R.B., Zhao, H., Xia, J., Wu, D., Nervi, S., Stinson, S.F., Majerova, E., Bramhall, C., and Zaharevitz, D.W. (2004). Poly(ethylene glycol) prodrugs of the CDK inhibitor, alsterpaullone (NSC 705701): synthesis and pharmacokinetic studies. Bioconjug. Chem. *15*, 1076–1083.

Hall, E.D., Oostveen, J.A., and Gurney, M.E. (1998). Relationship of microglial and astrocytic activation to disease onset and progression in a transgenic model of familial ALS. Glia *23*, 249–256.

Han, S.-X., Zhu, Q., Ma, J.-L., Zhao, J., Huang, C., Jia, X., and Zhang, D. (2010). Lowered HGK expression inhibits cell invasion and adhesion in hepatocellular carcinoma cell line HepG2. World J. Gastroenterol. *16*, 4541–4548.

Hayakawa, J., Mittal, S., Wang, Y., Korkmaz, K.S., Adamson, E., English, C., Ohmichi, M., McClelland, M., and Mercola, D. (2005). Identification of promoters bound by c-jun/ATF2 during rapid large-scale gene activation following genotoxic stress. Mol. Cell *16*, 521–535.

Imamura, K., Izumi, Y., Watanabe, A., Tsukita, K., Woltjen, K., Yamamoto, T., Hotta, A., Kondo, T., Kitaoka, S., Ohta, A., et al. (2017). The Src/c-Abl pathway is a potential therapeutic target in amyotrophic lateral sclerosis. Sci. Transl. Med. *9*, eaaf3962.

Islam, M., and Moore, D.J. (2017). Mechanisms of LRRK2-dependent neurodegeneration: role of enzymatic activity and protein aggregation. Biochem. Soc. Trans. *45*, 163–172.

Kiskinis, E., Sandoe, J., Williams, L.A., Boulting, G.L., Moccia, R., Wainger, B.J., Han, S., Peng, T., Thams, S., Mikkilineni, S., et al. (2014). Pathways disrupted in human ALS motor neurons identified through genetic correction of mutant SOD1. Cell Stem Cell *14*, 781–795.

Larhammar, M., Huntwork-Rodriguez, S., Rudhard, Y., Sengupta-Ghosh, A., and Lewcock, J.W. (2017). The Ste20 family kinases MAP4K4, MINK1, and TNIK converge to regulate stress-induced JNK signaling in neurons. J. Neurosci. *37*, 11074–11084.

Lasagna-Reeves, C.A., de Haro, M., Hao, S., Park, J., Rousseaux, M., Al-Ramahi, I., Jafar-Nejad, P., Vilanova-Velez, L., See, L., De Maio, A., et al. (2016). Reduction of Nuak1 decreases Tau and reverses phenotypes in a tauopathy mouse model. Neuron *92*, 407–418.

Lin, J.-C., Lee, Y.-C., Tan, T.-H., Liang, Y.-C., Chuang, H.-C., Fann, Y.C., Johnson, K.R., and Lin, Y.-J. (2018). RBM4-SRSF3-MAP4K4 splicing cascade modulates the metastatic signature of colorectal cancer cell. Biochim. Biophys. Acta Mol. Cell Res. *1865*, 259–272.

Liu, Y., Bertram, K., Perides, G., McEwen, B.S., and Wang, D. (2004). Stress induces activation of stress-activated kinases in the mouse brain. J. Neurochem. *89*, 1034–1043.

Marker, D.F., Tremblay, M.-È., Puccini, J.M., Barbieri, J., Marker, M.A., Loweth, C.J., Muly, C.E., Lu, S.-M., Goodfellow, V.S., Dewhurst, S., et al. (2013). The new small-molecule mixed-lineage kinase 3 inhibitor URMC-099 is neuroprotective and anti-inflammatory in models of human immunodeficiency virus-associated neurocognitive disorders. J. Neurosci. *33*, 9998–10010.

Maury, Y., Côme, J., Piskorowski, R.A., Salah-Mohellibi, N., Chevaleyre, V., Peschanski, M., Martinat, C., and Nedelec, S. (2014). Combinatorial analysis of developmental cues efficiently converts human pluripotent stem cells into multiple neuronal subtypes. Nat. Biotechnol. *33*, 89–96.

Medinas, D.B., Cabral-Miranda, F., and Hetz, C. (2019). ER stress links aging to sporadic ALS. Aging *11*, 5–6.

Ndubaku, C.O., Crawford, T.D., Chen, H., Boggs, J.W., Drobnick, J., Harris, S.F., Jesudason, R., McNamara, E., Nonomiya, J., Sambrone, A., et al. (2015). Structure-based design of GNE-495, a potent and selective MAP4K4 inhibitor with efficacy in retinal angiogenesis. ACS Med. Chem. Lett. *6*, 913–918.

Paliulis, O., Peters, D., Holzer, W., and Sackus, A. (2013). Synthesis of 10-methyl-8,10-diazabicyclo[4.3.1]decane as a new building block for nicotinic modulators. Arkivoc, 240–250.

Pulverer, B.J., Kyriakis, J.M., Avruch, J., Nikolakaki, E., and Woodgett, J.R. (1991). Phosphorylation of c-jun mediated by MAP kinases. Nature *353*, 670–674.

Qiu, M.-H., Qian, Y.-M., Zhao, X.-L., Wang, S.-M., Feng, X.-J., Chen, X.-F., and Zhang, S.-H. (2012). Expression and prognostic significance of MAP4K4 in lung adenocarcinoma. Pathol. Res. Pract. *208*, 541–548.

Read, J., Collie, I.T., Nguyen-McCarty, M., Lucaj, C., Robinson, J., Conway, L., Mukherjee, J., McCall, E., Donohoe, G., Flavell, E., et al. (2019). Tool inhibitors and assays to interrogate the biology of the TRAF2 and NCK interacting kinase. Bioorg. Med. Chem. Lett. *29*, 1962–1967.

Robertson, G.S., Crocker, S.J., Nicholson, D.W., and Schulz, J.B. (2000). Neuroprotection by the inhibition of apoptosis. Brain Pathol. *10*, 283–292.

Roussel, B.D., Kruppa, A.J., Miranda, E., Crowther, D.C., Lomas, D.A., and Marciniak, S.J. (2013). Endoplasmic reticulum dysfunction in neurological disease. Lancet Neurol. *12*, 105–118.

Ryabinin, A.E., Wang, Y.-M., and Finn, D.A. (1999). Different levels of Fos immunoreactivity after repeated handling and injection stress in two inbred strains of mice. Pharmacol. Biochem. Behav. *63*, 143–151.

Salem, S.M., Hamed, A.R., Fayez, A.G., and Eldeen, G. (2018). Non-target genes regulate miRNAs-mediated migration steering of colorectal carcinoma. Pathol. Oncol. Res. *25*, 559–566.

Saxena, S., Cabuy, E., and Caroni, P. (2009). A role for motoneuron subtype-selective ER stress in disease manifestations of FALS mice. Nat. Neurosci. *12*, 627–636.

Scott, S., Kranz, J.E., Cole, J., Lincecum, J.M., Thompson, K., Kelly, N., Bostrom, A., Theodoss, J., Al-Nakhala, B.M., Vieira, F.G., et al. (2009). Design, power, and interpretation of studies in the standard murine model of ALS. Amyotroph. Lateral Scler. *9*, 4–15.

Spiller, K.J., Restrepo, C.R., Khan, T., Dominique, M.A., Fang, T.C., Canter, R.G., Roberts, C.J., Miller, K.R., Ransohoff, R.M., Trojanowski, J.Q., et al. (2018). Microglia-mediated recovery from ALS-relevant motor neuron degeneration in a mouse model of TDP-43 proteinopathy. Nat. Neurosci. *21*, 329–340.

Tang, X., Guilherme, A., Chakladar, A., Powelka, A.M., Konda, S., Virbasius, J.V., Nicoloro, S.M., Straubhaar, J., and Czech, M.P. (2006). An RNA interference-based screen identifies MAP4K4/NIK as a negative regulator of PPARγ, adipogenesis, and insulin-responsive hexose transport. Proc. Natl. Acad. Sci. U S A *103*, 2087–2092.

Tang, S., Lagas, J.S., Lankheet, N., Poller, B., Hillebrand, M.J., Rosing, H., Beijnen, J.H., and Schinkel, A.H. (2012). Brain accumulation of sunitinib is restricted by P-glycoprotein (ABCB1) and breast cancer resistance protein (ABCG2) and can be enhanced by oral elacridar and sunitinib coadministration. Int. J. Cancer *130*, 223–233.

Tesz, G.J., Guilherme, A., Guntur, K.V., Hubbard, A.C., Tang, X., Chawla, A., and Czech, M.P. (2007). Tumor necrosis factor α (TNFα) stimulates Map4k4 expression through TNFα receptor 1 signaling to c-jun and activating transcription factor 2. J. Biol. Chem. *282*, 19302–19312.

Thams, S., Lowry, E.R., Larraufie, M.-H., Spiller, K.J., Li, H., Williams, D.J., Hoang, P., Jiang, E., Williams, L.A., Sandoe, J., et al. (2019). A stem cell-based screening platform identifies compounds that desensitize motor neurons to endoplasmic reticulum stress. Mol. Ther. *27*, 87–101.

Trias, E., Ibarburu, S., Barreto-Núñez, R., Babdor, J., Maciel, T.T., Guillo, M., Gros, L., Dubreuil, P., Díaz-Amarilla, P., Cassina, P., et al. (2016). Post-paralysis tyrosine kinase inhibition with masitinib abrogates neuroinflammation and slows disease progression in inherited amyotrophic lateral sclerosis. J. Neuroinflamm. *13*, 177–188.

Virbasius, J.V., and Czech, M.P. (2016). Map4k4 signaling nodes in metabolic and cardiovascular diseases. Trends Endocrinol. Metab. *27*, 484–492.

Wichterle, H., Lieberam, I., Porter, J.A., and Jessell, T.M. (2002). Directed differentiation of embryonic stem cells into motor neurons. Cell *110*, 385–397.

Wright, J.H., Wang, X., Manning, G., LaMere, B.J., Le, P., Zhu, S., Khatry, D., Flanagan, P.M., Buckley, S.D., Whyte, D.B., et al. (2003). The STE20 kinase HGK is broadly expressed in human tumor cells and can modulate cellular transformation, invasion, and adhesion. Mol. Cell. Biol. *23*, 2068–2082.

Wu, C., Watts, M.E., and Rubin, L.L. (2019). MAP4K4 activation mediates motor neuron degeneration in amyotrophic lateral sclerosis. Cell Rep. *26*, 1143–1156.

Yang, Y.M., Gupta, S.K., Kim, K.J., Powers, B.E., Cerqueira, A., Wainger, B.J., Ngo, H.D., Rosowski, K.A., Schein, P.A., Ackeifi, C.A., et al. (2013). A small molecule screen in stem-cell-derived motor neurons identifies a kinase inhibitor as a candidate therapeutic for ALS. Cell Stem Cell *12*, 713–726.

Yao, Z., Zhou, G., Wang, X., Brown, A., Diener, K., Gan, H., and Tan, T.-H. (1999). A novel human STE20-related protein kinase, HGK, that specifically activates the c-jun N-terminal kinase signaling pathway. J. Biol. Chem. *274*, 2118–2125.

Yoshida, H. (2007). ER stress and diseases. FEBS J. *274*, 630–658.

STAR★METHODS

KEY RESOURCES TABLE

REAGENT or RESOURCE	SOURCE	IDENTIFIER
Antibodies		
Rabbit polyclonal anti-Cleaved caspase 3 (Asp175)	Cell Signaling Technology	Cat # 9661; RRID: AB_2341188
Rabbit monoclonal anti-c-Jun	Cell Signaling Technology	Cat # 9165; RRID: AB_213065
Rabbit polyclonal anti-Phospho-c-Jun (Ser63)	Cell Signaling Technology	Cat # 9261; RRID: AB_2130162
Rabbit polyclonal anti-JNK	Cell Signaling Technology	Cat # 9252; RRID: AB_2250373
Rabbit monoclonal anti-Phospho-JNK (Thr183/Tyr185)	Cell Signaling Technology	Cat # 4668; RRID: AB_823588
Rabbit polyclonal anti-MKK4	Cell Signaling Technology	Cat# 9152; RRID: AB_330905
Rabbit monoclonal anti-Phospho-MKK4 (Ser257)	Cell Signaling Technology	Cat # 4514; RRID: AB_2140946
Rabbit polyclonal GAPDH (FL-335)	Santa Cruz Biotechnologies	Cat # sc-25778; RRID: AB_10167688
Goat anti-rabbit HRP-linked	Cell Signaling Technology	Cat # 7074; RRID: AB_2099233
Biological Samples		
Mouse CD-1 microsomes	Thermo Fisher	Cat # MSMCPL
Chemicals, Peptides, and Recombinant Proteins		
Knockout serum replacement	Life Technologies	Cat # 10828-028
Human recombinant fibroblast growth factor 2	Peprotech	Cat # PHG0263
N-2 supplement	Thermo Fisher	Cat # 17502048
B-27 supplement	Thermo Fisher	Cat # 17504044
Ascorbic acid	Sigma-Aldrich	Cat # A4403
Y-27632 dihydrochloride	Abcam	Cat # ab120129
SB 431542 hydrate	Sigma-Aldrich	Cat # S4317
LDN193189	Stemgent	Cat # 04-0074
CHIR 99021	Tocris	Cat # 4423
Retinoic acid (all trans)	Sigma-Aldrich	Cat # R2625
Sonic Hedgehog agonist	Millipore	Cat # 566660
Human recombinant brain-derived neurotrophic factor	Peprotech	Cat # 450-02
DAPT	Tocris	Cat # 2643
Human recombinant glial-derived neurotrophic factor	R&D Systems	Cat # 212-GD-050
Poly-Ornithine	Sigma-Aldrich	Cat # 3655
Mouse laminin	Thermo Fisher	Cat # 23017-015
Uridine	Sigma-Aldrich	Cat # U3750
Fluorodeoxyuridine	Sigma-Aldrich	Cat # F0503
Human recombinant ciliary neurotrophic factor	Peprotech	Cat # 257-NT-050
Human recombinant insulin-like growth factor 1	Peprotech	Cat # 291-G1
Cyclopiazonic acid	Tocris	Cat # 1235
WZ4003	Tocris	Cat # 5177
HTH 01-015	Selleckchem	Cat # S7318
PF-6260933	Tocris	Cat # 5752
GNE-495	Cayman Chemical	Cat # 21808
URMC-099	Selleckchem	Cat # S7343
Brilliant Black	Sigma	Cat # 211842
Fetal Bovine Serum, embryonic stem cell grade	Fisher Scientific	Cat # SH3007003E
Forskolin	Sigma-Aldrich	Cat # F6886

(*Continued on next page*)

Continued

REAGENT or RESOURCE	SOURCE	IDENTIFIER
IBMX	Tocris	Cat # 2845
Lipopolysaccharides from E. coli O111:B4	Sigma-Aldrich	Cat # L2640
PhosSTOP phosphatase inhibitor tablets	Sigma-Aldrich	Cat # 4906845001
Complete protease inhibitor cocktail	Sigma-Aldrich	Cat # 1183617001
7-Ethoxycoumarin	Sigma-Aldrich	Cat # 1379
PEG-400	Sigma-Aldrich	Cat # 202398
(2-hydroxypropyl)-beta-cyclodextrins	Sigma-Aldrich	Cat # 332607
5-Bromo-1H-pyrrolo[2,3-b]pyridine	AK Scientific	183208-35-7
4-formylphenylboronic acid	Sigma-Aldrich	87199-17-5
trans-Dichlorobis(triphenylphosphine)palladium(II), 99%	Strem	13965-03-2
1-methylpiperazine	Sigma-Aldrich	109-01-3
N-iodosuccinimide	Sigma-Aldrich	516-12-1
Di-tert-butyl dicarbonate 99% (GC)	AK Scientific	24424-99-5
4-(Dimethylamino)pyridine	Sigma-Aldrich	1122-58-3
Tetrakis(triphenylphosphine)palladium(0)	Strem	14221-01-3
5-indolylboronic acid	Sigma-Aldrich	144104-59-6
indole-2-boronic acid pinacol ester	Sigma-Aldrich	476004-81-6
6-ethoxy-3-pyridinylboronic acid	Sigma-Aldrich	612845-44-0
4-(dibenzofuranyl)boronic acid	Sigma-Aldrich	100124-06-9
1,4-benzodioxane-6-boronic acid	Sigma-Aldrich	164014-95-3
4-aminophenylboronic acid pinacol ester	Sigma-Aldrich	214360-73-3
benzo[b]thien-3-ylboronic acid	Sigma-Aldrich	113893-08-6
benzo[b]thien-2-ylboronic acid	Sigma-Aldrich	98437-23-1
3-Aminophenylboronic acid hydrochloride	Sigma-Aldrich	85006-23-1
3-carboxy-4-fluorophenylboronic acid	AK Scientific	872460-12-3
3-carboxyphenylboronic acid	Sigma-Aldrich	25487-66-5
2-aminopyrimidine-5-boronic acid	Sigma-Aldrich	936250-22-5
2-amino-3-methylpyridine-5-boronic acid pinacol ester	AK Scientific	1111637-91-2
2-aminopyridine-5-boronic acid pinacol ester	Sigma-Aldrich	827614-64-2
4-pyridinylboronic acid	Sigma-Aldrich	1692-15-5
4-cyanophenylboronic acid	Sigma-Aldrich	126747-14-6
3-nitrophenylboronic acid	Sigma-Aldrich	13331-27-6
4-isopropoxyphenylboronic acid	Sigma-Aldrich	153624-46-5
3-hydroxyphenylboronic acid	Sigma-Aldrich	87199-18-6
1-methylpyrazole-4-boronic acid pinacol ester	Sigma-Aldrich	761446-44-0
5-(morpholinomethyl)-2-thiopheneboronic acid pinacol ester	Sigma-Aldrich	950603-39-1
6-(methylsulfonyl)pyridine-3-boronic acid	Sigma-Aldrich	1088496-41-6
1*H*-indazole-5-boronic acid	Sigma-Aldrich	338454-14-1
3-furanylboronic acid	Sigma-Aldrich	55552-70-0
4-acetylphenylboronic acid	Sigma-Aldrich	149104-90-5
3-fluorophenylboronic acid	Sigma-Aldrich	768-35-4
4-(trifluoromethoxy)phenylboronic acid	Sigma-Aldrich	139301-27-2
1H-Indazole-5-boronic acid	Sigma-Aldrich	338454-14-1
3-(trifluoromethyl)phenylboronic acid	Sigma-Aldrich	1423-26-3
phenylboronic acid	Sigma-Aldrich	98-80-6
3-chlorophenylboronic acid	AK Scientific	63503-60-6
2,4-dichlorophenylboronic acid	Sigma-Aldrich	68716-47-2
2,5-dimethylphenylboronic acid	Sigma-Aldrich	85199-06-0

(*Continued on next page*)

Continued

REAGENT or RESOURCE	SOURCE	IDENTIFIER
1-methyl-1*H*-indazole-6-boronic acid	Sigma-Aldrich	1150114-80-9
1-benzyl-1H-pyrazole-4-boronic acid	Sigma-Aldrich	852362-22-2
1,3,5-trimethyl-1H-pyrazole-4-boronic acid pinacol ester	Sigma-Aldrich	844891-04-9
3,5-bis(trifluoromethyl)phenylboronic acid	Sigma-Aldrich	73852-19-4
4-(4-methoxybenzyloxy)phenylboronic acid	Sigma-Aldrich	156635-90-4
3,4,5-trimethoxyphenylboronic acid	Sigma-Aldrich	182163-96-8
4-methoxy-3-methylphenylboronic acid	Sigma-Aldrich	175883-62-2
3-(benzyloxy)phenylboronic acid	Sigma-Aldrich	156682-54-1
2-chlorophenylboronic acid	Sigma-Aldrich	3900-89-8
2-methoxyphenylboronic acid	Sigma-Aldrich	5720-06-9
N-(3-Dimethylaminopropyl)-N′-ethylcarbodiimide hydrochloride (EDC.HCl)	Sigma-Aldrich	25952-53-8
1-Hydroxybenzotriazole hydrate (HOBT)	Sigma-Aldrich	123333-53-9
Furfurylamine	Sigma-Aldrich	617-89-0
Triphosgene	Sigma-Aldrich	32315-10-9
cyclohexylamine	Sigma-Aldrich	108-91-8
(R)-(+)-α-methylbenzylamine	Sigma-Aldrich	3886-69-9
2-methoxyethan-1-amine	Sigma-Aldrich	109-85-3
8-oxa-3-azabicyclo[3.2.1]octane	Sigma-Aldrich	280-13-7
4-piperidinopiperidine	Sigma-Aldrich	4897-50-1
1-(2-hydroxyethyl)piperazine	Sigma-Aldrich	103-76-4
(*R*)-3-pyrrolidinol	Sigma-Aldrich	2799-21-5
1-tert-butylpiperazine	Ark Pharm	38216-72-7
t-Butyl-3,8-diazabicyclo[3.2.1]octane-3-carboxylate	Ark Pharm	201162-53-0
t-Butyl-3,8-diazabicyclo[3.2.1]octane-8-carboxylate	Ark Pharm	149771-44-8
Formaldehyde (37% in H_2O)	Sigma-Aldrich	50-00-0
Sodium triacetoxyborohydride	Sigma-Aldrich	56553-60-7
Critical Commercial Assays		
CellTrace Calcein AM	Life Technologies	Cat # C3100MP
SuperSignal West Femto	Thermo Fisher	Cat # 34096
BCA Protein Assay	Pierce	Cat # PI23227
Mouse TNF-alpha DuoSet ELISA	R&D Systems	Cat # DY410-05
AlamarBlue Cell Viability Reagent	Thermo Fisher	Cat # DAL1025
Gentest 3P NADPH Regenerating System	Corning	Cat # 451220
Experimental Models: Cell Lines		
Human: NCRM-1 (male)	NIH Center for Regenerative Medicine (CRM); Bethesda; USA.	RRID: CVCL_1E71
Human: HUES3 Hb9::GFP-hSOD1^{A4V} (male)	Thams et al., 2019	N/a
Mouse: HB9::GFP-hSOD^{G93A} (male)	Thams et al., 2019	N/a
Mouse: Immortalized N9 Microglia (male)	Corradin et al., 1993	RRID: CVCL_0452
Experimental Models: Organisms/Strains		
Mouse: B6SJLF1/J	The Jackson Laboratory	Cat #100012; RRID: IMSR_JAX:100012
Software and Algorithms		
Prism 8	GraphPad	https://www.graphpad.com/scientific-software/prism/
Metamorph (version 2010)	Molecular Devices	https://www.moleculardevices.com/products/cellular-imaging/acquisition-and-analysis-software/metamorph-microscopy#gref

(*Continued on next page*)

Continued

REAGENT or RESOURCE	SOURCE	IDENTIFIER
Spotfire (version 2017)	TIBCO	https://www.tibco.com/spotfire-trial?lp=y&utm_medium=3Q_cpc&utm_source=3Q_google&utm_content=s&utm_campaign=ggl_s_us_en_spt_brand_alpha&utm_term=spotfire%20software&_bt=309951201993&_bm=e&_bn=g&gclid=CjwKCAjwxrzoBRBBEiwAbtX1n_tLuGHFVl9ABZePIWVSY7zp8ytQw9wyxyYC68KCS8wwawwTl2MoChoCDv8QAvD_BwE
Glide (versions 2012-2016)	Schrödinger	https://www.schrodinger.com/glide
Schrödinger Maestro (version 2017)	Schrödinger	https://www.schrodinger.com/maestro
ChemDraw Professional (version 16.0)	Perkin Elmer	https://www.perkinelmer.com/category/chemdraw
ImageStudio Lite (version 2018)	LiCor	https://www.licor.com/bio/image-studio-lite/

LEAD CONTACT AND MATERIALS AVAILABILITY

Requests for resources, reagents, and further information should be directed to Brent Stockwell (bstockwell@columbia.edu).

EXPERIMENTAL MODEL AND SUBJECT DETAILS

Generation of Human and Mouse Stem Cell Lines

Preliminary survival assays to identify lead compounds were performed in human motor neurons derived from a wild-type male iPS cell line, NCRM-1 (RRID:CVCL_1E71).

Survival assays to characterized compound **1** analogs were performed in human motor neurons derived from an HB9:GFP motor neuron reporter embryonic stem cell line carrying a heterozygous SOD1A4V point mutation (HUES3 Hb9::GFP-hSOD1A4V) that was generated as described previously (Thams et al., 2019).

Western blot experiments were carried out in ES-derived mouse motor neurons (HB9::GFP-hSOD1G93A) generated by Thams et al. (2019) from crosses of heterozygous Tg(Hlxb9-GFP)1Tmj motor neuron reporter mice (RRID:IMSR_JAX:005029) and mice expressing wild-type human SOD1 (B6SJL-Tg(SOD1)2Gur/J, RRID:IMSR_JAX:002726).

All stem cell lines were routinely tested for mycoplasma.

Human Motor Neuron Differentiation

Human motor neurons were differentiated from the above human ES or iPS cells as previously described (Maury et al., 2014; Thams et al., 2019). Stem cells were maintained in humidified incubators at 37°C on irradiated CF-1 mouse embryonic fibroblast (MEF) feeder layers (Thermo Fisher) in serum-free media (DMEM/F12, Life Technologies) supplemented with knockout serum replacement (20%, Life Technologies), Glutamax (1%, Life Technologies), non-essential amino acids (1%, Millipore), beta-mercaptoethanol (0.1%, Sigma), and human recombinant fibroblast growth factor 2 (FGF2, 20 ng/mL, Life Technologies).

On day 0, stem cells were dissociated into single cells using Accutase (Thermo Fisher) and differentiated into motor neurons over the course of 16 days as embryoid bodies cultured in suspension at 37°C. Differentiations were carried out in N2B27 media, which was comprised of a 1:1 mixture of Advanced DMEM/F12 and Neurobasal media (Life Technologies), Glutamax (1%), beta-mercaptoethanol (0.1%), N-2 (1%, Thermo Fisher), B-27 (2%, Thermo Fisher), and ascorbic acid (10 μM, Sigma). From day 0-1, differentiation medium was supplemented with FGF2 (10 ng/mL), Y-27632 dihydrochloride (10 μM, Abcam), SB 431542 hydrate (SB, 20 μM, Sigma), LDN193189 (LDN, 0.1 μM, Stemgent) and CHIR 99021 (CHIR, 3 μM, Tocris). From days 2-7, differentiation medium was supplemented with SB (20 μM), LDN (0.1 μM), CHIR (3 μM), retinoic acid (100 nM, Sigma), and sonic hedgehog agonist (SAG, 500 nM; Millipore). From days 7-9, differentiation medium was supplemented with retinoic acid (100 nM), and SAG (500 nM), and brain-derived neurotrophic factor (BDNF, 10 ng/mL, Peprotech). From days 9-14, differentiation medium was supplemented with retinoic acid (100 nM), SAG (500 nM), BDNF (10 ng/mL, Peprotech), and DAPT (10 μM, Tocris). From days 14-6, differentiation medium was supplemented with retinoic acid (100 nM), SAG (500 nM), BDNF (10 ng/mL), DAPT (10 μM), and glial-derived neurotrophic factor (GDNF, 10 ng/mL; R&D Systems).

On day 16 of differentiation, embryoid bodies were dissociated using 0.05% trypsin (Life Technologies) and mechanical trituration, and motor neurons were plated at 2000 cells / well in 96-well plates (Greiner) coated with poly-ornithine (100 μg/mL, Sigma) and mouse laminin (3 μg/mL, Thermo Fisher). Cultures were maintained at 37°C in serum-free neurobasal media (Life Technologies) supplemented with N-2 (1%), B-27 (2%), a 1:1 cocktail of uridine and fluorodeoxyuridine as anti-mitotics (1 μM, Sigma), and the following recombinant human neurotrophic factors: GDNF, BDNF, ciliary neurotrophic factor (CNTF; R&D Systems), and insulin-like growth factor 1 (IGF-1; R&D systems), all at 10 ng/mL.

Mouse Motor Neuron Differentiation

We used mouse rather than human motor neurons for biochemistry assays because mouse motor neurons can be rapidly generated in the quantities required for protein extraction. Differentiations were carried out as described (Thams et al., 2019; Wichterle et al., 2002). In brief, ES cells were maintained at 37°C on CF-1 MEF feeder layers, then dissociated and differentiated for 6 days using retinoic acid (1 μM) and SAG (0.5 μM). Motor neurons were maintained at 37°C in media containing 2% fetal bovine serum (FBS, Fisher Scientific), GDNF (400 pg/mL), Forskolin (10 μM, Sigma-Aldrich), and IBMX (100 μM, Tocris).

N9 Microglia Culture Details

Immortalized N9 mouse microglia cells (Corradin et al., 1993) were kindly provided by Serge Przedborski, Columbia University. Cultures were maintained at 37°C in DMEM (Life Technologies) containing FBS (10%, Fisher Scientific) and Glutamax (1%, Life Technologies) on gelatinized plates. This cell line was not authenticated upon receipt, but appeared and behaved as expected.

Mouse Maintenance

All animal procedures were approved by the Columbia University Institutional Animal Care and Use committee under protocol number AC-AAAU6461, and were performed in accordance with all relevant regulatory standards. Mice were housed 4 per cage under 12h light/dark cycle conditions. Food and water were provided ad libitum. All experiments described here involved 8-week-old male wild-type B6SJLF1/J mice (The Jackson Laboratory; RRID_IMSR_JAX:100012). This strain was chosen because it shares the same background as the most commonly used ALS mouse model (B6SJL-Tg(SOD1*G93A)1Gur/J; RRID:IMSR_JAX:002726). The preliminary pharmacokinetic studies described here only involved male mice in anticipation of future studies in ALS mice where male and female phenotypes diverge (Scott et al., 2009), and where single-sex studies in males are common. All mice were drug-naïve prior to the initiation of the pharmacokinetic studies. Mice used in this study were bred by Jackson laboratories, and all were born within ± 3 days of each other. Experimental groups (n = 3 mice per treatment per time point) were balanced by average mouse weight on the day before treatment.

METHOD DETAILS

Human Motor Neuron Survival Assays

48 h after dissociation and plating (DIV2), motor neurons were treated simultaneously with CPA (33 μM, Tocris) and test compounds. DMSO (Sigma) was used as a vehicle control. For all test compounds, stock solutions were prepared in DMSO, and working solutions were prepared in motor neuron media. WZ4003 (Tocris) and HTH 01-015 (Selleckchem) were tested in 8-point, 2-fold dilution series from 0.25-32 μM in 3 replicate wells. PF-6260933 (Tocris), GNE-495 (Cayman Chemical), and URMC-099 (Selleckchem) were tested in 8-point, 2-fold dilution series from 0.075-9.6 μM in 3 replicate wells. Compound **1** analogs were evaluated at 0.1, 0.3, 0.5, 1, and 3 μM in 3 replicate wells. The EC50 of compound **1** analogs were determined using Prism 8 software (GraphPad) from experiments where compound **1** and 53 analogs were assayed simultaneously.

Motor neurons were incubated with CPA and test compounds for 72 h. Live cells were visualized using CellTrace Calcein AM (1.3 μM, Life Technologies) and background fluorescence was quenched with a solution of 10% brilliant black (Sigma) in PBS. Whole-well images were acquired using a Plate RunnerHD system (Trophos). Cells were counted using Metamorph software (Molecular Devices). All cell counts are expressed as a percentage of surviving vehicle (DMSO)-treated cells.

Biochemical Analysis of JNK Pathway Regulation

Whole mouse embryoid bodies at day 6 of differentiation were treated with CPA (10 μM) and test compounds (0.5 μM) for 4 h, then lysed and sonicated in ice-cold buffer containing HEPES (50 mM), NaCl (100 mM), Triton-X (1%), SDS (0.1%), DTT (1 mM), EDTA (1 mM), plus protease and phosphatase inhibitor cocktails (Sigma-Aldrich). Total protein content was analyzed using a BCA kit according to the manufacturer's instructions (Pierce). For each sample, 30 μg total protein was reduced with dithiothreitol (DTT, 100 mM) for 10 mins at 70°C and loaded into a NuPAGE Novex 4-12% bis-tris gel (Thermo Fisher) with LDS loading buffer (Thermo Fisher). Samples were run for 4h at 100V at 4°C, then transferred to 0.2 μ nitrocellulose membranes overnight at 15V at 4°C. Membranes were blocked with tris-buffered saline (TBS) containing 5% bovine serum albumen (BSA, Cell Signaling Technologies), then incubated with primary antibodies in a buffer containing 5% BSA and 0.1% Tween-20 (Sigma) in TBS overnight at 4°C. Primary antibodies against cleaved caspase 3 (Asp175, Cell Signaling Technology) were added at 1:1000; primary antibodies against c-Jun (Cell Signaling Technology) were added at 1:1000; primary antibodies against phospho-c-Jun (Ser63, Cell Signaling Technology) were added at 1:1000; primary antibodies against JNK (Cell Signaling Technology) were added at 1:1000; primary antibodies against phospho-JNK (Thr183/Tyr185, Cell Signaling Technology) were added at 1:1000; primary antibodies against MKK4 (Cell Signaling Technology) were added at 1:1000; primary antibodies against phospho-MKK4 (Ser257, Cell Signaling Technology) were added at 1:1000; primary antibodies against GAPDH (Santa Cruz Biotechnologies) were added at 1:3000 as a loading control. Following washes in TBS containing 0.1% Tween, membranes were incubated in goat anti-rabbit HRP-conjugated secondary antibody solutions (1:5000; Cell Signaling Technology) for 1h. Membranes were washed again in TBS containing 0.1% Tween, then incubated in

SuperSignal West Femto reagent (Thermo Fisher) for 5 min. Chemiluminescence was visualized using a LiCor Odyssey. Band intensities were quantified using ImageStudio Lite (LiCor). Cleaved caspase 3, c-Jun, phospho-c-Jun, JNK, phospho-JNK, MKK4, and phospho-MKK4 intensities were normalized to GAPDH. Intensities for phospho-c-Jun, phospho-JNK, and phospho-MKK4 were then normalized to c-Jun, JNK, and MKK4. Treatment-mediated changes in normalized intensities were expressed as a percentage of CPA-treated samples.

General Experimental Details for the Synthesis of Compound 1 Analogs and Intermediates

Starting materials were purchased form Sigma-Aldrich, Fisher Scientific, Ark Pharm, Oakwood Chemical, Cambridge Isotope Laboratory, or AK Scientific and were used as received unless stated otherwise. All solvents were reagent grade. Column chromatography was performed on a Teledyne ISCO CombiFlash® Rf+ using RediSep® Normal-phase silica flash columns. Thin layer chromatography (TLC) was performed on Silicycle SiliaPlate™ Glass TLC Plates (250 μm, 20 x 20 cm). Where indicated, compounds were purified by preparatory HPLC on a Phenomenex Gemini NX-C18 column (250 x 21.2 mm, particle size: 5 μm, pore size: 110 Å) using a Gilson HPLC with GX-271 liquid handler. 1H NMR spectra were recorded at ambient temperature using 400 MHz, or 500 MHz spectrometers as indicated. Chemical shifts are reported in ppm relative to the residual solvent peaks (1H NMR: DMSO-*d6*, δ 2.50; chloroform-*d*, δ 7.26; methanol-*d4*, δ 3.31). The following abbreviations are used to indicate multiplicity: s (singlet), d (doublet), t (triplet), q (quartet), hept (heptuplet), m (multiplet), br (broad). High resolution mass spectra (HRMS) were acquired on a time-of-flight spectrometer with atmospheric pressure chemical ionization (APCI) or electrospray ionization (ESI), as indicated, and were obtained by peak matching. All reactions were run under an atmosphere of nitrogen or argon in glassware that was flame-dried under argon unless otherwise stated. Aqueous solutions were prepared from nanopure water with a resistivity over 18 MΩ·cm. Unless otherwise noted, all reagents were commercially available.

Synthesis Route for the Synthesis of Piperazine Analogs

Routes for the synthesis of piperazine analogs are shown in Scheme 1.

4-(1H-Pyrrolo[2,3-*b*]pyridin-5-yl)benzaldehyde (3).

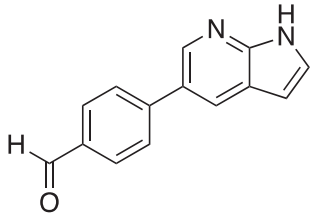

5-Bromo-1*H*-pyrrolo[2,3-*b*]pyridine (**2**, 3.94 g, 20 mmol, 1.0 eq) and 4-formylphenylboronic acid (3.30 g, 22 mmol, 1.1 eq) were added to a pressure tube and acetonitrile (80 mL) and 1,4-dioxane (20 mL) were added. The reaction mixture was degassed and kept under argon. $Pd(PPh_3)_2Cl_2$ (0.70 g, 1.0 mmol, 5 mol%) was added followed by addition of aqueous Na_2CO_3 (2.0 M, 50 mL). The reaction mixture was stirred for 5 min, transferred to an oil bath and stirred at 130°C overnight. After cooling to room temperature, the reaction mixture was partitioned between ethyl acetate and brine, separated and the aqueous layer extracted with ethyl acetate (3x). The combined organic layers were dried with anhydrous sodium sulfate and filtered over Celite. The solvent was evaporated, and the crude product purified by column chromatography (0–100% EtOAc in hexanes) to give 4-(1*H*-pyrrolo[2,3-*b*]pyridin-5-yl)benzaldehyde (**3**, 2.15 g, 48% yield) as a colorless solid. ^{1}H NMR (400 MHz, DMSO-d_6) δ 11.80 (s, 1H), 10.06 (s, 1H), 8.63 (d, J = 2.2 Hz, 1H), 8.35 (d, J = 2.2 Hz, 1H), 8.05 – 7.94 (m, 4H), 7.55 (d, J = 3.5 Hz, 1H), 6.54 (d, J = 3.4 Hz, 1H) ppm. HRMS (APCI$^+$, m/z): calcd. for $C_{14}H_{11}N_2O$ [M+H$^+$]: 223.0872, found: 223.0872.

5-(4-((4-Methylpiperazin-1-yl)methyl)phenyl)-1H-pyrrolo[2,3-*b*]pyridine (4).

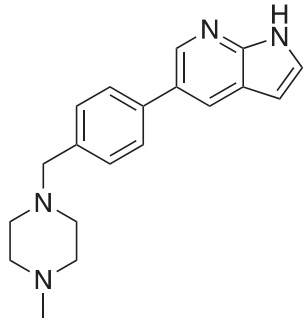

4-(1*H*-Pyrrolo[2,3-*b*]pyridin-5-yl)benzaldehyde (**3**, 2.15 g, 9.66 mmol, 1.0 eq) was suspended in dichloromethane (~0.1 M), and 1-methylpiperazine (1.93 g, 2.14 mL, 19.3 mmol, 2.0 eq), and $Na(OAc)_3BH$ (3.07 g, 14.5 mmol, 1.5 eq) were added and the reaction mixture was stirred overnight at room temperature. The reaction mixture was partitioned between dichloromethane and brine, the

layers separated, and the aqueous layer was extracted with dichloromethane. The combined organic layer was washed with brine, dried with sodium sulfate, filtered over Celite, and the solvent evaporated to give 5-(4-((4-methylpiperazin-1-yl)methyl)phenyl)-1*H*-pyrrolo[2,3-*b*]pyridine (**4**, 2.2 gram, 74% yield) as a colorless solid. The product was used in the next step without further purification. ^{1}H NMR (400 MHz, Methanol-d_4) δ 8.43 (d, J = 2.1 Hz, 1H), 8.21 (d, J = 2.1 Hz, 1H), 7.64 (d, J = 8.2 Hz, 2H), 7.45 (d, J = 8.2 Hz, 2H), 7.42 (d, J = 3.5 Hz, 1H), 6.55 (d, J = 3.5 Hz, 1H), 3.64 (s, 2H), 2.71 (bs, 4H), 2.63 (bs, 4H), 2.44 (s, 3H) ppm. HRMS (APCI$^+$, m/z): calcd. for $C_{19}H_{23}N_4$ [M+H$^+$]: 307.1923, found: 307.1918.

3-Iodo-5-(4-((4-methylpiperazin-1-yl)methyl)phenyl)-1H-pyrrolo[2,3-*b*]pyridine (5).

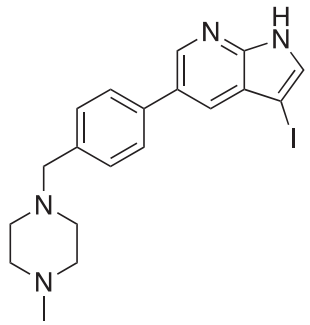

5-(4-((4-Methylpiperazin-1-yl)methyl)phenyl)-1*H*-pyrrolo[2,3-*b*]pyridine (**4**, 2.2 g, 7.18 mmol, 1.0 eq) was suspended in acetone (0.015 M, 480 mL) and *N*-iodosuccinimide (1.78 g, 7.9 mmol, 1.1 eq) was added and the reaction mixture was stirred at room temperature overnight. The solvent was evaporated and the crude product was purified by column chromatography (0–10% MeOH in DCM containing 1% Et_3N) to give 3-iodo-5-(4-((4-methylpiperazin-1-yl)methyl)phenyl)-1*H*-pyrrolo[2,3-*b*]pyridine (**5**, 2.3 g, 74% yield) as a tan-colored solid. ^{1}H NMR (400 MHz, Methanol-d_4) δ 8.46 (d, J = 2.1 Hz, 1H), 7.88 (d, J = 2.1 Hz, 1H), 7.64 (d, J = 8.2 Hz, 2H), 7.57 (s, 1H), 7.47 (d, J = 8.2 Hz, 2H), 3.71 (s, 2H), 3.35 (s, 1H), 3.21 (bs, 8H), 2.80 (s, 3H) ppm. HRMS (APCI$^+$, m/z): calcd. for $C_{19}H_{22}N_4I$ [M+H$^+$]: 433.0889, found: 433.0883.

tert-Butyl 3-iodo-5-(4-((4-methylpiperazin-1-yl)methyl)phenyl)-1*H*-pyrrolo[2,3-*b*]pyridine-1-carboxylate (6).

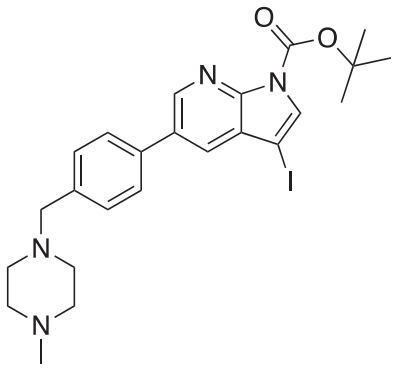

3-Iodo-5-(4-((4-methylpiperazin-1-yl)methyl)phenyl)-1*H*-pyrrolo[2,3-*b*]pyridine (**5**, 2.3 g, 5.32 mmol, 1.0 eq) was dissolved in a mixture of THF (250 mL) and DMF (20 mL). Boc_2O (3.48 g, 15.96 mmol, 3.0 eq) and DMAP (0.97 g, 7.98 mmol, 1.5 eq) were added and the mixture was stirred at room temperature overnight. Water was added and the reaction mixture was extracted with ethyl acetate (3x). The combined organic layers were washed with brine, dried with sodium sulfate, filtered and the solvent evaporated. The crude material was purified by column chromatography on silica (0–10% MeOH in DCM containing 1% Et_3N) to give *tert*-butyl 3-iodo-5-(4-((4-methylpiperazin-1-yl)methyl)phenyl)-1*H*-pyrrolo[2,3-*b*]pyridine-1-carboxylate as a tan-colored solid (**6**, 2.0 g, 71% yield). ^{1}H NMR (400 MHz, Chloroform-*d*) δ 8.73 (d, J = 2.1 Hz, 1H), 7.84 (d, J = 2.1 Hz, 1H), 7.82 (s, 1H), 7.59 (d, J = 8.2 Hz, 2H), 7.45 (d, J = 8.2 Hz, 2H), 3.58 (s, 2H), 2.53 (bs, 4H), 2.47 (bs, 4H), 2.30 (s, 3H), 1.69 (s, 9H) ppm. HRMS (APCI$^+$, m/z): calcd. for $C_{24}H_{30}N_4O_2I$ [M+H$^+$]: 533.1413, found: 533.1423.

General Procedure for the Suzuki Coupling and In Situ *Deprotection*

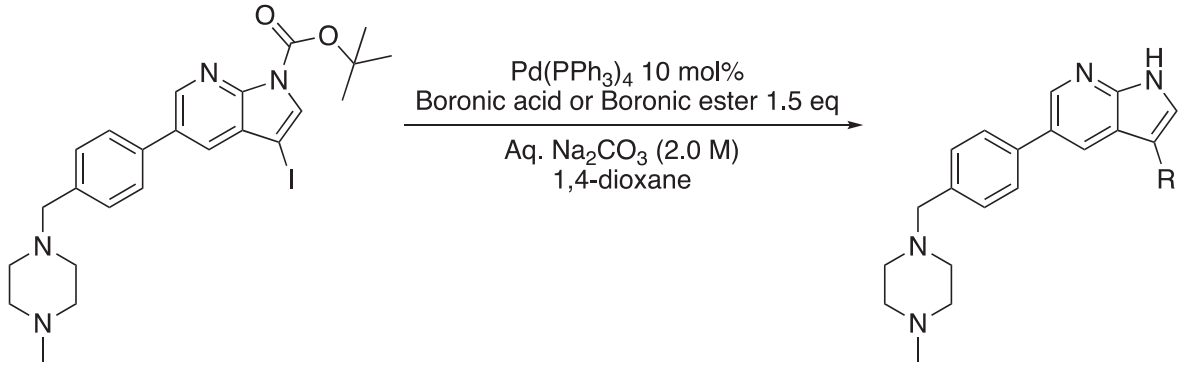

tert-butyl 3-iodo-5-(4-((4-methylpiperazin-1-yl)methyl)phenyl)-1*H*-pyrrolo[2,3-*b*]pyridine-1-carboxylate (**6**, 26.2 mg, 0.05 mmol, 1.0 eq) was dissolved in 1,4-dioxane (2.0 mL) in a 1 dram glass vial with Teflon lined cap. The boronic acid or boronic ester (0.075 mmol, 1.5 eq) was added, followed by addition of Tetrakis(triphenylphosphine)palladium(0) ($Pd(PPh_3)_4$, 5.8 mg, 5 mol%). The reaction mixture was degassed, aqueous Na_2CO_3 (2.0 M, 0.5 mL) was added, and was stirred overnight at 100°C. The reaction mixture was filtered over Celite and the Celite was washed with ethyl acetate. The solvent was evaporated and the crude product was purified by preparatory HPLC purification to give the pure material.

3-(1H-Indol-5-yl)-5-(4-((4-methylpiperazin-1-yl)methyl)phenyl)-1*H*-pyrrolo[2,3-*b*]pyridine (1).

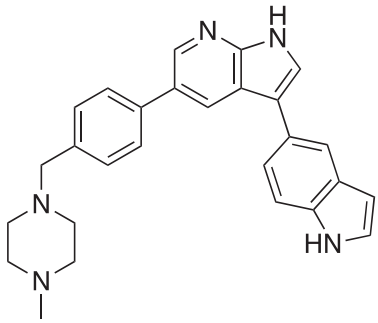

Compound **1** was prepared according to the general procedure for the Suzuki coupling and *in situ* deprotection as described above using 5-indolylboronic acid (12.1 mg, 0.075 mmol, 1.5 eq). The crude product was purified by preparatory HPLC purification to afford 3-(1*H*-indol-5-yl)-5-(4-((4-methylpiperazin-1-yl)methyl)phenyl)-1*H*-pyrrolo[2,3-*b*]pyridine (**1**, 14.8 mg, 70% yield). ^{1}H NMR (400 MHz, Methanol-d_4) δ 8.61 (d, *J* = 2.0 Hz, 1H), 8.52 (d, *J* = 2.0 Hz, 1H), 7.86 (dd, *J* = 1.7, 0.7 Hz, 1H), 7.70 (d, *J* = 8.2 Hz, 2H), 7.67 (s, 1H), 7.50 (m, 3H), 7.44 (dd, *J* = 8.4, 1.7 Hz, 1H), 7.28 (d, *J* = 3.2 Hz, 1H), 6.51 (dd, *J* = 3.2, 0.9 Hz, 1H), 3.84 (s, 2H), 3.00 – 2.80 (bs, 8H), 2.87 (s, 3H) ppm. The spectroscopic data matched those reported in literature (Goodfellow et al., 2013).

3-(1H-Indol-2-yl)-5-(4-((4-methylpiperazin-1-yl)methyl)phenyl)-1*H*-pyrrolo[2,3-*b*]pyridine (7*a*).

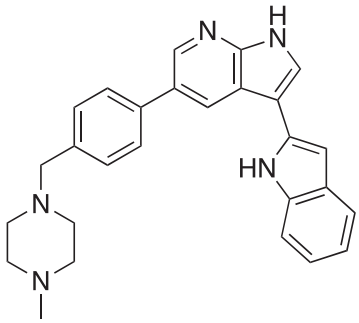

Compound **7a** was prepared according to the general procedure for the Suzuki coupling and *in situ* deprotection as described above using indole-2-boronic acid pinacol ester (18.2 mg, 0.075 mmol, 1.5 eq). The crude product was purified by preparatory HPLC purification to afford 3-(1*H*-Indol-2-yl)-5-(4-((4-methylpiperazin-1-yl)methyl)phenyl)-1*H*-pyrrolo[2,3-*b*]pyridine

(**7a**, 14.1 mg, 67% yield). ^{1}H NMR (400 MHz, Methanol-d_4) δ 8.54 (d, J = 2.1 Hz, 1H), 8.49 (d, J = 2.1 Hz, 1H), 7.82 (s, 1H), 7.65 (d, J = 8.2 Hz, 2H), 7.54 (dt, J = 7.8, 1.0 Hz, 1H), 7.41 (d, J = 8.1 Hz, 2H), 7.42 – 7.35 (m, 1H), 7.07 (ddd, J = 8.0, 7.2, 1.1 Hz, 1H), 7.00 (ddd, J = 8.0, 7.1, 1.1 Hz, 1H), 6.78 (d, J = 1.0 Hz, 1H), 3.56 (s, 2H), 2.75 – 2.40 (bs, 8H), 2.34 (s, 3H) ppm. HRMS (APCI$^+$, m/z): calcd. for $C_{27}H_{28}N_5$ [M+H$^+$]: 422.2339, found: 422.2336.

3-(6-Ethoxypyridin-3-yl)-5-(4-((4-methylpiperazin-1-yl)methyl)phenyl)-1H-pyrrolo[2,3-*b*]pyridine (7b).

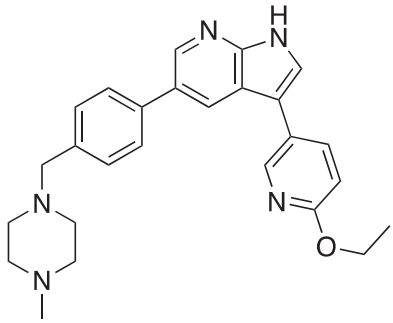

Compound **7b** was prepared according to the general procedure for the Suzuki coupling and *in situ* deprotection as described above using 6-ethoxy-3-pyridinylboronic acid (12.5 mg, 0.075 mmol, 1.5 eq). The crude product was purified by preparatory HPLC purification to afford 3-(6-ethoxypyridin-3-yl)-5-(4-((4-methylpiperazin-1-yl)methyl)phenyl)-1*H*-pyrrolo[2,3-*b*]pyridine (**7b**, 16.2 mg, 76% yield). ^{1}H NMR (400 MHz, Methanol-d_4) δ 8.48 (d, J = 2.1 Hz, 1H), 8.42 (dd, J = 2.6, 0.8 Hz, 1H), 8.33 (d, J = 2.1 Hz, 1H), 7.99 (dd, J = 8.6, 2.5 Hz, 1H), 7.66 (s, 1H), 7.63 (d, J = 8.0 Hz, 2H), 7.43 (d, J = 8.0 Hz, 2H), 6.88 (dd, J = 8.6, 0.8 Hz, 1H), 4.34 (q, J = 7.0 Hz, 2H), 2.80 – 2.45 (bs, 8H), 2.40 (s, 3H), 1.40 (t, J = 7.1 Hz, 3H) ppm. HRMS (APCI$^+$, m/z): calcd. for $C_{26}H_{30}N_5O$ [M+H$^+$]: 428.2450, found: 428.2449.

*3-(Dibenzo[b,d]*furan-4-yl)-5-(4-((4-methylpiperazin-1-yl)methyl)phenyl)-1*H*-pyrrolo[2,3-*b*]pyridine (7c).

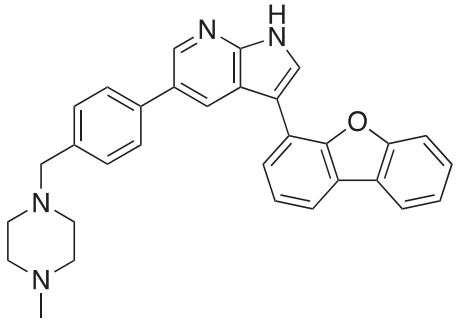

Compound **7c** was prepared according to the general procedure for the Suzuki coupling and *in situ* deprotection as described above using 4-(dibenzofuranyl)boronic acid (15.9 mg, 0.075 mmol, 1.5 eq). The crude product was purified by preparatory HPLC purification to afford 3-(dibenzo[*b*,*d*]furan-4-yl)-5-(4-((4-methylpiperazin-1-yl)methyl)phenyl)-1*H*-pyrrolo[2,3-*b*]pyridine (**7c**, 12.6 mg, 58% yield). ^{1}H NMR (400 MHz, Methanol-d_4) δ 8.57 (s, 2H), 8.18 (s, 1H), 8.12 (dt, J = 7.7, 1.2 Hz, 1H), 8.00 (dd, J = 7.7, 1.2 Hz, 1H), 7.94 (dd, J = 7.6, 1.2 Hz, 1H), 7.72 (d, J = 8.2 Hz, 2H), 7.70 – 7.65 (m, 2H), 7.57 – 7.48 (m, 4H), 3.69 (s, 2H), 3.05 – 2.75 (bs, 4H), 2.85 – 2.55 (bs, 4H), 2.59 (s, 3H) ppm. HRMS (APCI$^+$, m/z): calcd. for $C_{31}H_{29}N_4O$ [M+H$^+$]: 473.2341, found: 473.2345.

3-(2,3-Dihydrobenzo[b][1,4]dioxin-6-yl)-5-(4-((4-methylpiperazin-1-yl)methyl)phenyl)-1*H*-pyrrolo[2,3-*b*]pyridine (7d).

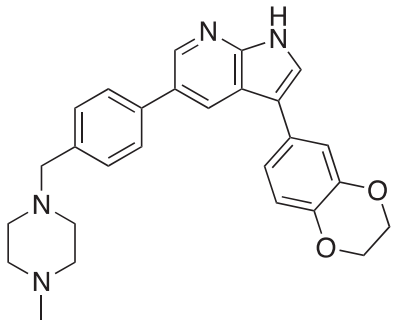

Compound **7d** was prepared according to the general procedure for the Suzuki coupling and *in situ* deprotection as described above using 1,4-benzodioxane-6-boronic acid (13.5 mg, 0.075 mmol, 1.5 eq). The crude product was purified by preparatory HPLC purification to afford 3-(2,3-dihydrobenzo[*b*][1,4]dioxin-6-yl)-5-(4-((4-methylpiperazin-1-yl)methyl)phenyl)-1*H*-pyrrolo[2,3-*b*]pyridine (**7d**, 10.2 mg, 46% yield). ^{1}H NMR (400 MHz, Methanol-d_4) δ 8.45 (d, *J* = 2.1 Hz, 1H), 8.34 (d, *J* = 2.1 Hz, 1H), 7.61 (d, *J* = 8.2 Hz, 2H), 7.55 (s, 1H), 7.43 (d, *J* = 8.2 Hz, 2H), 7.17 – 7.10 (m, 2H), 6.91 (d, *J* = 8.8 Hz, 1H), 4.27 (s, 4H), 3.60 (s, 2H), 2.77 – 2.46 (bs, 8H), 2.39 (s, 3H) ppm. HRMS (APCI$^+$, m/z): calcd. for $C_{27}H_{29}N_4O_2$ [M+H$^+$]: 441.2291, found: 441.2287.

4-(5-(4-((4-Methylpiperazin-1-yl)methyl)phenyl)-1H-pyrrolo[2,3-*b*]pyridin-3-yl)aniline (7e).

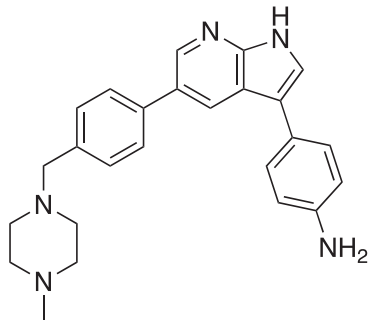

Compound **7e** was prepared according to the general procedure for the Suzuki coupling and *in situ* deprotection as described above using 4-aminophenylboronic acid pinacol ester (17.0 mg, 0.075 mmol, 1.5 eq). The crude product was purified by preparatory HPLC purification to afford 4-(5-(4-((4-methylpiperazin-1-yl)methyl)phenyl)-1*H*-pyrrolo[2,3-*b*]pyridin-3-yl)aniline (**7e**, 14.4 mg, 73% yield). ^{1}H NMR (400 MHz, Methanol-d_4) δ 8.43 (d, *J* = 2.1 Hz, 1H), 8.34 (d, *J* = 2.1 Hz, 1H), 7.61 (d, *J* = 8.2 Hz, 2H), 7.50 (s, 1H), 7.46 –7.39 (m, 4H), 6.84 (d, *J* = 8.5 Hz, 2H), 3.62 (s, 2H), 2.79 (bs, 4H), 2.63 (bs, 4H), 2.49 (s, 3H) ppm. HRMS (APCI$^+$, m/z): calcd. for $C_{25}H_{28}N_5$ [M+H$^+$]: 398.2345, found: 398.2344.

*3-(Benzo[b]*thiophen-3-yl)-5-(4-((4-methylpiperazin-1-yl)methyl)phenyl)-1*H*-pyrrolo[2,3-*b*]pyridine (7f).

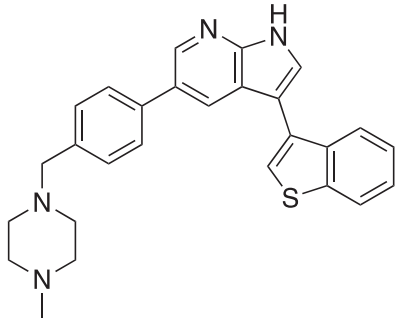

Compound **7f** was prepared according to the general procedure for the Suzuki coupling and *in situ* deprotection as described above using benzo[b]thien-3-ylboronic acid (14.0 mg, 0.075 mmol, 1.5 eq). The crude product was purified by preparatory HPLC purification to afford 3-(benzo[*b*]thiophen-3-yl)-5-(4-((4-methylpiperazin-1-yl)methyl)phenyl)-1*H*-pyrrolo[2,3-*b*]pyridine (**7f**, 16.0 mg, 73% yield). ^{1}H NMR (400 MHz, Methanol-d_4) δ 8.50 (d, *J* = 2.1 Hz, 1H), 8.17 (d, *J* = 2.1 Hz, 1H), 7.97 – 7.87 (m, 2H), 7.71 (s, 1H), 7.63 (s, 1H), 7.55 (d, *J* = 8.2 Hz, 2H), 7.44 – 7.33 (m, 4H), 3.55 (s, 2H), 2.71 – 2.45 (bs, 8H), 2.37 (s, 3H) ppm. HRMS (APCI$^+$, m/z): calcd. for $C_{27}H_{27}N_4S$ [M+H$^+$]: 439.1956, found: 439.1955.

3-(Benzo[b]thiophen-2-yl)-5-(4-((4-methylpiperazin-1-yl)methyl)phenyl)-1H-pyrrolo[2,3-b]pyridine (7g).

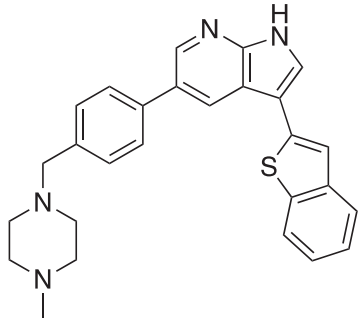

Compound **7g** was prepared according to the general procedure for the Suzuki coupling and *in situ* deprotection as described above using benzo[b]thien-2-ylboronic acid (14.0 mg, 0.075 mmol, 1.5 eq). The crude product was purified by preparatory HPLC purification to afford 3-(benzo[b]thiophen-2-yl)-5-(4-((4-methylpiperazin-1-yl)methyl)phenyl)-1H-pyrrolo[2,3-b]pyridine (**7g**, 15.9 mg, 73% yield). ^{1}H NMR (400 MHz, Methanol-d_4) δ 8.52 (d, J = 2.1 Hz, 1H), 8.50 (d, J = 2.1 Hz, 1H), 7.83 – 7.74 (m, 3H), 7.64 (d, J = 8.2 Hz, 2H), 7.57 (d, J = 0.7 Hz, 1H), 7.43 (d, J = 8.2 Hz, 2H), 7.32 (ddd, J = 7.9, 7.2, 1.2 Hz, 1H), 7.26 (ddd, J = 8.4, 7.2, 1.2 Hz, 1H), 3.59 (s, 2H), 2.72 – 2.48 (bs, 8H), 2.38 (s, 3H) ppm. HRMS (APCI$^+$, m/z): calcd. for $C_{27}H_{27}N_4S$ [M+H$^+$]: 439.1956, found: 439.1959.

3-(5-(4-((4-Methylpiperazin-1-yl)methyl)phenyl)-1H-pyrrolo[2,3-*b*]pyridin-3-yl)aniline (7h).

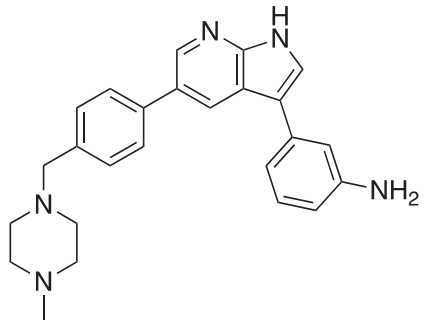

Compound **7h** was prepared according to the general procedure for the Suzuki coupling and *in situ* deprotection as described above using 3-aminophenylboronic acid hydrochloride (13.3 mg, 0.075 mmol, 1.5 eq). The crude product was purified by preparatory HPLC purification to afford 3-(5-(4-((4-methylpiperazin-1-yl)methyl)phenyl)-1*H*-pyrrolo[2,3-*b*]pyridin-3-yl)aniline (**7h**, 14.9 mg, 75% yield). ^{1}H NMR (400 MHz, Methanol-d_4) δ 8.47 (d, J = 2.1 Hz, 1H), 8.45 (d, J = 2.1 Hz, 1H), 7.64 (d, J = 8.2 Hz, 2H), 7.61 (s, 1H), 7.44 (d, J = 8.2 Hz, 2H), 7.19 (t, J = 7.8 Hz, 1H), 7.11 (t, J = 2.0 Hz, 1H), 7.03 (ddd, J = 7.6, 1.7, 1.0 Hz, 1H), 6.68 (ddd, J = 7.8, 2.3, 1.0 Hz, 1H), 3.60 (s, 2H), 2.58 (bs, 8H), 2.34 (s, 3H) ppm. HRMS (APCI$^+$, m/z): calcd. for $C_{25}H_{28}N_5$ [M+H$^+$]: 398.2345, found: 398.2337.

2-Fluoro-5-(5-(4-((4-methylpiperazin-1-yl)methyl)phenyl)-1H-pyrrolo[2,3-*b*]pyridin-3-yl)benzoic acid (7i).

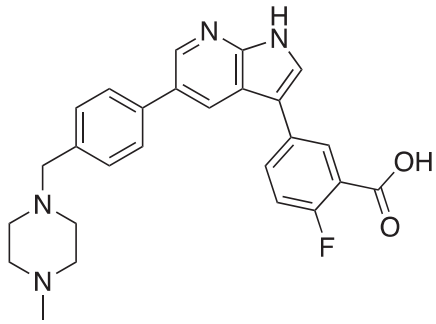

Compound **7i** was prepared according to the general procedure for the Suzuki coupling and *in situ* deprotection as described above using 3-carboxy-4-fluorophenylboronic acid (13.8 mg, 0.075 mmol, 1.5 eq). The crude product was purified by preparatory HPLC purification to afford 2-fluoro-5-(5-(4-((4-methylpiperazin-1-yl)methyl)phenyl)-1*H*-pyrrolo[2,3-*b*]pyridin-3-yl)benzoic acid (**7i**, 8.9 mg, 40% yield). ^{1}H NMR (500 MHz, Methanol-d_4) δ 8.56 (d, J = 2.0 Hz, 1H), 8.53 (d, J = 2.0 Hz, 1H), 8.24 (dd, J = 6.8, 2.5 Hz, 1H), 7.95 (ddd, J = 8.6, 4.5, 2.5 Hz, 1H), 7.81 (s, 1H), 7.75 (d, J = 8.2 Hz, 2H), 7.55 (d, J = 8.2 Hz, 2H), 7.32 (dd, J = 10.6, 8.6 Hz, 1H), 3.96 (s, 2H), 3.38 (bs, 4H), 3.05 (bs, 4H), 2.91 (s, 3H) ppm. HRMS (APCI$^+$, m/z): calcd. for $C_{26}H_{26}FN_4O_2$ [M+H$^+$]: 445.2040, found: 445.2035.

3-(5-(4-((4-Methylpiperazin-1-yl)methyl)phenyl)-1H-pyrrolo[2,3-*b*]pyridin-3-yl)benzoic acid (7j).

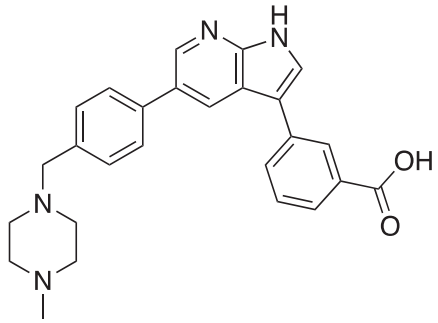

Compound **7j** was prepared according to the general procedure for the Suzuki coupling and *in situ* deprotection as described above using 3-carboxyphenylboronic acid (12.5 mg, 0.075 mmol, 1.5 eq). The crude product was purified by preparatory HPLC purification to afford 3-(5-(4-((4-methylpiperazin-1-yl)methyl)phenyl)-1*H*-pyrrolo[2,3-*b*]pyridin-3-yl)benzoic acid (**7j**, 12.0 mg, 56% yield). ^{1}H NMR (400 MHz, Methanol-d_4) δ 8.62 – 8.56 (m, 2H), 8.36 (s, 1H), 8.02 – 7.94 (m, 2H), 7.85 (s, 1H), 7.76 (d, *J* = 8.0 Hz, 2H), 7.60 (d, *J* = 7.8 Hz, 1H), 7.56 (d, *J* = 8.0 Hz, 2H), 3.97 (s, 2H), 3.39 (bs, 4H), 3.05 (bs, 4H), 2.91 (s, 3H) ppm. HRMS (APCI$^+$, m/z): calcd. for $C_{26}H_{27}N_4O_2$ [M+H$^+$]: 427.2134, found: 427.2137.

5-(5-(4-((4-Methylpiperazin-1-yl)methyl)phenyl)-1H-pyrrolo[2,3-*b*]pyridin-3-yl)pyrimidin-2-amine (7k).

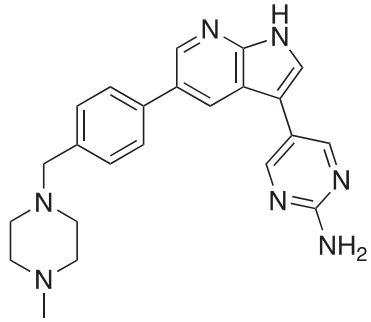

Compound **7k** was prepared according to the general procedure for the Suzuki coupling and *in situ* deprotection as described above using 2-aminopyrimidine-5-boronic acid (11.0 mg, 0.075 mmol, 1.5 eq). The crude product was purified by preparatory HPLC purification to afford 5-(5-(4-((4-methylpiperazin-1-yl)methyl)phenyl)-1*H*-pyrrolo[2,3-*b*]pyridin-3-yl)pyrimidin-2-amine (**7k**, 16.4 mg, 82%). ^{1}H NMR (400 MHz, Methanol-d_4) δ 8.87 (s, 2H), 8.58 (d, *J* = 2.1 Hz, 1H), 8.46 (d, *J* = 2.1 Hz, 1H), 7.87 (s, 1H), 7.76 (d, *J* = 8.2 Hz, 2H), 7.54 (d, *J* = 8.2 Hz, 2H), 3.93 (s, 2H), 3.37 (bs, 4H), 3.01 (bs, 4H), 2.90 (s, 3H) ppm. HRMS (APCI$^+$, m/z): calcd. for $C_{23}H_{26}N_7$ [M+H$^+$]: 400.2250, found: 400.2250.

3-Methyl-5-(5-(4-((4-methylpiperazin-1-yl)methyl)phenyl)-1H-pyrrolo[2,3-*b*]pyridin-3-yl)pyridin-2-amine (7l).

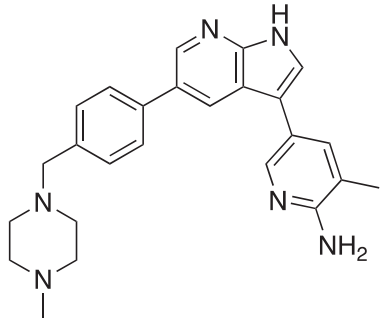

Compound **7l** was prepared according to the general procedure for the Suzuki coupling and *in situ* deprotection as described above using 2-amino-3-methylpyridine-5-boronic acid pinacol ester (18.3 mg, 0.075 mmol, 1.5 eq). The crude product was purified by preparatory HPLC purification to afford 3-methyl-5-(5-(4-((4-methylpiperazin-1-yl)methyl)phenyl)-1*H*-pyrrolo[2,3-*b*]pyridin-3-yl) pyridin-2-amine (**7l**, 8.2 mg, 40% yield). ^{1}H NMR (400 MHz, Methanol-d_4) δ 8.55 (s, 1H), 8.42 (d, *J* = 2.0 Hz, 1H), 8.24 (dd, *J* = 2.2, 1.1 Hz, 1H), 8.14 – 8.08 (m, 1H), 7.83 (s, 1H), 7.73 (d, *J* = 8.2 Hz, 2H), 7.51 (d, *J* = 8.1 Hz, 2H), 3.79 (s, 2H), 3.04 – 2.68 (bs, 8H), 2.87 (s, 3H), 2.37 (s, 3H) ppm. HRMS (APCI$^+$, m/z): calcd. for $C_{25}H_{29}N_6$ [M+H$^+$]: 413.2454, found: 413.2457.

5-(5-(4-((4-Methylpiperazin-1-yl)methyl)phenyl)-1H-pyrrolo[2,3-*b*]pyridin-3-yl)pyridin-2-amine (7m).

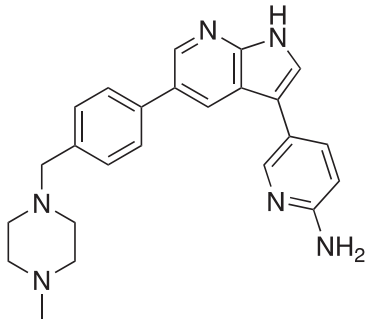

Compound **7m** was prepared according to the general procedure for the Suzuki coupling and *in situ* deprotection as described above using 2-aminopyridine-5-boronic acid pinacol ester (16.5 mg, 0.075 mmol, 1.5 eq). The crude product was purified by preparatory HPLC purification to afford 5-(5-(4-((4-methylpiperazin-1-yl)methyl)phenyl)-1*H*-pyrrolo[2,3-*b*]pyridin-3-yl)pyridin-2-amine (**7m**, 15.2 mg, 76% yield). ^{1}H NMR (400 MHz, Methanol-d_4) δ 8.60 (d, *J* = 2.0 Hz, 1H), 8.52 (d, *J* = 2.0 Hz, 1H), 8.35 (dd, *J* = 9.3, 2.2 Hz, 1H), 8.22 (dd, *J* = 2.2, 0.7 Hz, 1H), 7.87 (s, 1H), 7.80 (d, *J* = 8.2 Hz, 2H), 7.59 (d, *J* = 8.2 Hz, 2H), 7.16 (dd, *J* = 9.2, 0.7 Hz, 1H), 4.10 (s, 2H), 3.46 (bs, 4H), 3.20 (s, 4H), 2.93 (s, 3H) ppm. HRMS (APCI$^+$, m/z): calcd. for $C_{24}H_{27}N_6$ [M+H$^+$]: 399.2297, found: 399.2307.

5-(4-((4-Methylpiperazin-1-yl)methyl)phenyl)-3-(pyridin-4-yl)-1H-pyrrolo[2,3-*b*]pyridine (7n).

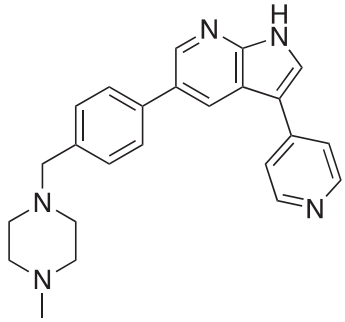

Compound **7n** was prepared according to the general procedure for the Suzuki coupling and *in situ* deprotection as described above using 4-pyridinylboronic acid (10.3 mg, 0.075 mmol, 1.5 eq). The crude product was purified by preparatory HPLC purification to afford 5-(4-((4-methylpiperazin-1-yl)methyl)phenyl)-3-(pyridin-4-yl)-1*H*-pyrrolo[2,3-*b*]pyridine (**7n**, 8.7 mg, 45% yield). ^{1}H NMR (400 MHz, Methanol-d_4) δ 8.74 (d, *J* = 2.0 Hz, 1H), 8.68 – 8.64 (m, 3H), 8.57 (s, 1H), 8.43 (d, *J* = 7.1 Hz, 2H), 7.83 (d, *J* = 8.2 Hz, 2H), 7.60 (d, *J* = 8.2 Hz, 2H), 4.04 (s, 2H), 3.43 (bs, 4H), 3.13 (bs, 4H), 2.92 (s, 3H) ppm. HRMS (APCI$^+$, m/z): calcd. for $C_{24}H_{26}N_5$ [M+H$^+$]: 384.2188, found: 384.2194.

4-(5-(4-((4-Methylpiperazin-1-yl)methyl)phenyl)-1H-pyrrolo[2,3-*b*]pyridin-3-yl)benzonitrile (7o).

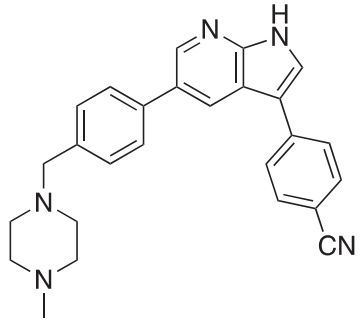

Compound **7o** was prepared according to the general procedure for the Suzuki coupling and *in situ* deprotection as described above using 4-cyanophenylboronic acid (11.0 mg, 0.075 mmol, 1.5 eq). The crude product was purified by preparatory HPLC purification to afford 4-(5-(4-((4-methylpiperazin-1-yl)methyl)phenyl)-1*H*-pyrrolo[2,3-*b*]pyridin-3-yl)benzonitrile (**7o**, 14.4 mg, 71% yield). ^{1}H NMR (400 MHz, Methanol-d_4) δ 8.56 (d, *J* = 2.1 Hz, 1H), 8.54 (d, *J* = 2.1 Hz, 1H), 7.97 – 7.91 (m, 3H), 7.83 – 7.77 (m, 2H), 7.75 (d, *J* = 8.2 Hz, 2H), 7.54 (d, *J* = 8.2 Hz, 2H), 3.89 (s, 2H), 3.35 (bs, 4H), 2.96 (bs, 4H), 2.89 (s, 3H) ppm. HRMS (APCI$^+$, m/z): calcd. for $C_{26}H_{26}N_5$ [M+H$^+$]: 408.2188, found: 408.2198.

5-(4-((4-Methylpiperazin-1-yl)methyl)phenyl)-3-(3-nitrophenyl)-1H-pyrrolo[2,3-*b*]pyridine (7p).

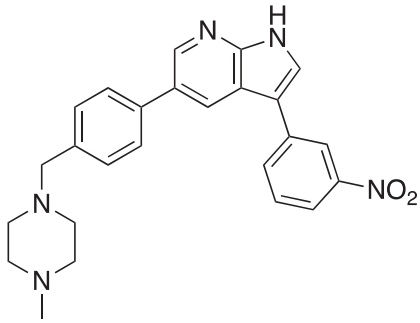

Compound **7p** was prepared according to the general procedure for the Suzuki coupling and *in situ* deprotection as described above using 3-nitrophenylboronic acid (12.5 mg, 0.075 mmol, 1.5 eq). The crude product was purified by preparatory HPLC purification to afford 5-(4-((4-methylpiperazin-1-yl)methyl)phenyl)-3-(3-nitrophenyl)-1*H*-pyrrolo[2,3-*b*]pyridine (**7p**, 15.4 mg, 72% yield). ^{1}H NMR (400 MHz, Methanol-d_4) δ 8.59 (d, *J* = 2.0 Hz, 1H), 8.58 (d, *J* = 2.0 Hz, 1H), 8.54 (t, *J* = 2.0 Hz, 1H), 8.15 (dddd, *J* = 7.7, 4.3, 2.1, 1.0 Hz, 2H), 7.96 (s, 1H), 7.77 (d, *J* = 8.2 Hz, 2H), 7.71 (t, *J* = 8.0 Hz, 1H), 7.58 (d, *J* = 8.2 Hz, 2H), 4.08 (s, 2H), 3.44 (bs, 4H), 3.17 (bs, 4H), 2.93 (s, 3H) ppm. HRMS (APCI$^+$, m/z): calcd. for $C_{25}H_{26}N_5O_2$ [M+H$^+$]: 428.2087, found: 428.2081.

3-(4-Isopropoxyphenyl)-5-(4-((4-methylpiperazin-1-yl)methyl)phenyl)-1H-pyrrolo[2,3-*b*]pyridine (7q).

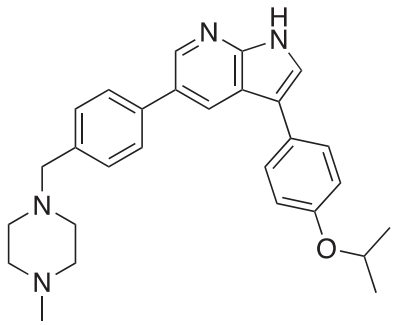

Compound **7q** was prepared according to the general procedure for the Suzuki coupling and *in situ* deprotection as described above using 4-isopropoxyphenylboronic acid (13.5 mg, 0.075 mmol, 1.5 eq). The crude product was purified by preparatory HPLC purification to afford 3-(4-isopropoxyphenyl)-5-(4-((4-methylpiperazin-1-yl)methyl)phenyl)-1*H*-pyrrolo[2,3-*b*]pyridine (**7q**, 18.2 mg, 83% yield). ^{1}H NMR (400 MHz, Methanol-d_4) δ 8.61 (d, *J* = 2.0 Hz, 1H), 8.56 (d, *J* = 2.0 Hz, 1H), 7.75 (d, *J* = 8.2 Hz, 2H), 7.69 (s, 1H), 7.64 – 7.58 (m, 2H), 7.55 (d, *J* = 8.2 Hz, 2H), 7.08 – 6.98 (m, 2H), 4.65 (hept, *J* = 6.0 Hz, 1H), 3.94 (s, 2H), 3.37 (bs, 4H), 3.02 (bs, 4H), 2.90 (s, 3H), 1.35 (d, *J* = 6.0 Hz, 6H) ppm. HRMS (APCI$^+$, m/z): calcd. for $C_{28}H_{33}N_4O$ [M+H$^+$]: 441.2654, found: 441.2646.

3-(5-(4-((4-Methylpiperazin-1-yl)methyl)phenyl)-1H-pyrrolo[2,3-*b*]pyridin-3-yl)phenol (7r).

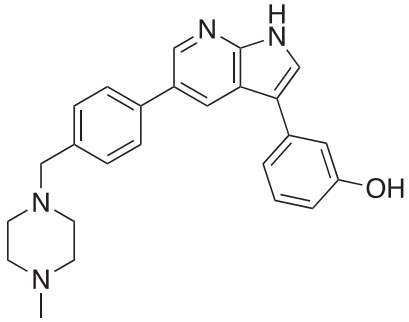

Compound **7r** was prepared according to the general procedure for the Suzuki coupling and *in situ* deprotection as described above using 3-hydroxyphenylboronic acid (10.3 mg, 0.075 mmol, 1.5 eq). The crude product was purified by preparatory HPLC purification to afford 3-(5-(4-((4-methylpiperazin-1-yl)methyl)phenyl)-1*H*-pyrrolo[2,3-*b*]pyridin-3-yl)phenol (**7r**, 9.8 mg, 49% yield). ^{1}H NMR (400 MHz, Methanol-d_4) δ 8.68 (d, *J* = 1.9 Hz, 1H), 8.60 (s, 1H), 7.80 – 7.73 (m, 3H), 7.58 (d, *J* = 8.2 Hz, 2H), 7.30

(t, *J* = 7.8 Hz, 1H), 7.24 – 7.17 (m, 1H), 7.16 (t, *J* = 2.0 Hz, 1H), 6.78 (ddd, *J* = 8.1, 2.5, 1.0 Hz, 1H), 4.04 (s, 2H), 3.42 (bs, 4H), 3.13 (bs, 4H), 2.92 (s, 3H) ppm. HRMS (APCI$^+$, m/z): calcd. for $C_{25}H_{27}N_4O$ [M+H$^+$]: 399.2185, found: 399.2180.

3-(1-Methyl-1H-pyrazol-4-yl)-5-(4-((4-methylpiperazin-1-yl)methyl)phenyl)-1*H*-pyrrolo[2,3-*b*]pyridine (7s).

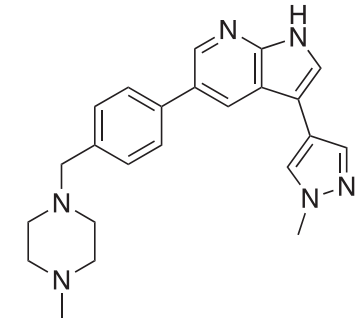

Compound **7s** was prepared according to the general procedure for the Suzuki coupling and *in situ* deprotection as described above using 1-methylpyrazole-4-boronic acid pinacol ester (16.1 mg, 0.075 mmol, 1.5 eq). The crude product was purified by preparatory HPLC purification to afford 3-(1-methyl-1*H*-pyrazol-4-yl)-5-(4-((4-methylpiperazin-1-yl)methyl)phenyl)-1*H*-pyrrolo[2,3-*b*]pyridine (**7s**, 14.8 mg, 77% yield). ^{1}H NMR (400 MHz, Methanol-d_4) δ 8.62 (d, *J* = 2.0 Hz, 1H), 8.31 (d, *J* = 2.0 Hz, 1H), 7.80 (s, 1H), 7.76 (d, *J* = 8.2 Hz, 2H), 7.64 (d, *J* = 2.0 Hz, 1H), 7.58 (d, *J* = 8.2 Hz, 2H), 6.60 (d, *J* = 2.1 Hz, 1H), 4.14 (s, 2H), 3.95 (s, 3H), 3.48 (bs, 4H), 3.25 (bs, 4H), 2.94 (s, 3H) ppm. HRMS (APCI$^+$, m/z): calcd. for $C_{23}H_{27}N_6$ [M+H$^+$]: 387.2297, found: 387.2303.

4-((5-(5-(4-((4-Methylpiperazin-1-yl)methyl)phenyl)-1H-pyrrolo[2,3-*b*]pyridin-3-yl)thiophen-2-yl)methyl)morpholine (7t).

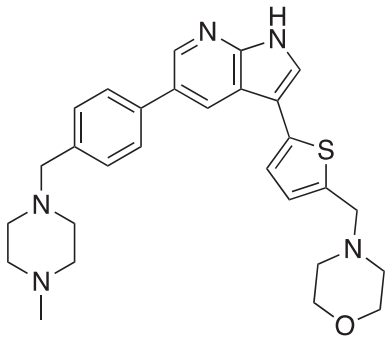

Compound **7t** was prepared according to the general procedure for the Suzuki coupling and *in situ* deprotection as described above using 5-(morpholinomethyl)-2-thiopheneboronic acid pinacol ester (24.4 mg, 0.075 mmol, 1.5 eq). The crude product was purified by preparatory HPLC purification to afford 4-((5-(5-(4-((4-methylpiperazin-1-yl)methyl)phenyl)-1*H*-pyrrolo[2,3-*b*]pyridin-3-yl)thiophen-2-yl)methyl)morpholine (**7t**, 10.0 mg, 41% yield). ^{1}H NMR (400 MHz, Methanol-d_4) δ 8.57 (d, *J* = 2.1 Hz, 1H), 8.52 (d, *J* = 2.1 Hz, 1H), 7.84 (s, 1H), 7.75 (d, *J* = 8.2 Hz, 2H), 7.57 (d, *J* = 8.2 Hz, 2H), 7.42 (d, *J* = 3.7 Hz, 1H), 7.37 (d, *J* = 3.7 Hz, 1H), 4.64 (s, 2H), 4.06 (bs, 4H), 4.01 (s, 2H), 3.80 (bs, 4H), 3.41 (bs, 4H), 3.09 (bs, 4H), 2.92 (s, 3H) ppm. HRMS (APCI$^+$, m/z): calcd. for $C_{28}H_{34}N_5OS$ [M+H$^+$]: 488.2484, found: 488.2475.

5-(4-((4-Methylpiperazin-1-yl)methyl)phenyl)-3-(6-(methylsulfonyl)pyridin-3-yl)-1H-pyrrolo[2,3-*b*]pyridine (7u).

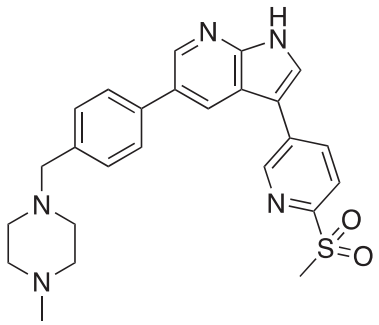

Compound **7u** was prepared according to the general procedure for the Suzuki coupling and *in situ* deprotection as described above using 6-(methylsulfonyl)pyridine-3-boronic acid (15.0 mg, 0.075 mmol, 1.5 eq). The crude product was purified by preparatory

HPLC purification to afford 5-(4-((4-methylpiperazin-1-yl)methyl)phenyl)-3-(6-(methylsulfonyl)pyridin-3-yl)-1*H*-pyrrolo[2,3-*b*]pyridine (**7u**, 11.0 mg, 48% yield). ^{1}H NMR (400 MHz, Methanol-d_4) δ 9.14 (dd, *J* = 2.2, 0.8 Hz, 1H), 8.59 (q, *J* = 2.1 Hz, 2H), 8.46 (dd, *J* = 8.2, 2.2 Hz, 1H), 8.15 (dd, *J* = 8.2, 0.8 Hz, 1H), 8.08 (s, 1H), 7.78 (d, *J* = 8.2 Hz, 2H), 7.57 (d, *J* = 8.2 Hz, 2H), 4.02 (s, 2H), 3.41 (bs, 4H), 3.27 (s, 3H), 3.11 (bs, 4H), 2.92 (s, 3H) ppm. HRMS (APCI$^+$, m/z): calcd. for $C_{25}H_{28}N_5O_2S$ [M+H$^+$]: 462.1964, found: 462.1968.

5-(5-(4-((4-Methylpiperazin-1-yl)methyl)phenyl)-1H-pyrrolo[2,3-*b*]pyridin-3-yl)-1*H*-indazole (7v).

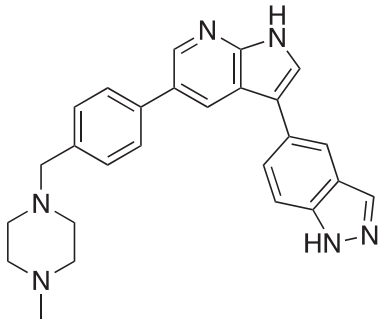

Compound **7v** was prepared according to the general procedure for the Suzuki coupling and *in situ* deprotection as described above using 1*H*-indazole-5-boronic acid (12.1 mg, 0.075 mmol, 1.5 eq). The crude product was purified by preparatory HPLC purification to afford 5-(5-(4-((4-methylpiperazin-1-yl)methyl)phenyl)-1*H*-pyrrolo[2,3-*b*]pyridin-3-yl)-1*H*-indazole (**7v**, 8.4 mg, 40% yield). ^{1}H NMR (400 MHz, Methanol-d_4) δ 8.67 (d, *J* = 1.9 Hz, 1H), 8.58 (d, *J* = 1.9 Hz, 1H), 8.13 – 8.09 (m, 2H), 7.79 (s, 1H), 7.80 – 7.73 (m, 3H), 7.67 (dt, *J* = 8.7, 0.9 Hz, 1H), 7.55 (d, *J* = 8.3 Hz, 2H), 3.95 (s, 2H), 3.38 (bs, 4H), 3.03 (bs, 4H), 2.90 (s, 3H) ppm. HRMS (APCI$^+$, m/z): calcd. for $C_{26}H_{27}N_6$ [M+H$^+$]: 423.2297, found: 423.2298.

3-(Furan-3-yl)-5-(4-((4-methylpiperazin-1-yl)methyl)phenyl)-1H-pyrrolo[2,3-*b*]pyridine (7w).

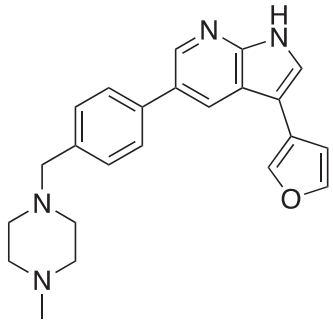

Compound **7w** was prepared according to the general procedure for the Suzuki coupling and *in situ* deprotection as described above using 3-furanylboronic acid (**7w**, 8.4 mg, 0.075 mmol, 1.5 eq). The crude product was purified by preparatory HPLC purification to afford 3-(furan-3-yl)-5-(4-((4-methylpiperazin-1-yl)methyl)phenyl)-1*H*-pyrrolo[2,3-*b*]pyridine (12.9 mg, 69% yield). ^{1}H NMR (500 MHz, Methanol-d_4) δ 8.58 (s, 2H), 8.08 (t, *J* = 1.1 Hz, 1H), 7.80 (d, *J* = 8.2 Hz, 2H), 7.76 (s, 1H), 7.62 (t, *J* = 1.7 Hz, 1H), 7.58 (d, *J* = 8.2 Hz, 2H), 6.87 (dd, *J* = 1.8, 1.1 Hz, 1H), 4.00 (s, 2H), 3.41 (bs, 4H), 3.07 (bs, 4H), 2.92 (s, 3H) ppm. HRMS (APCI$^+$, m/z): calcd. for $C_{23}H_{25}N_4O$ [M+H$^+$]: 373.2028, found: 373.2036.

1-(4-(5-(4-((4-Methylpiperazin-1-yl)methyl)phenyl)-1H-pyrrolo[2,3-*b*]pyridin-3-yl)phenyl)ethan-1-one (7x).

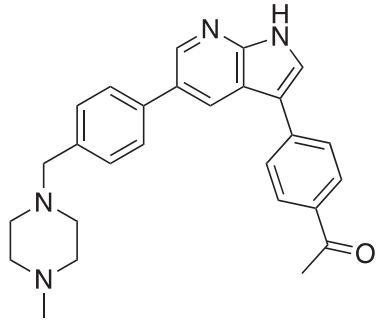

Compound **7x** was prepared according to the general procedure for the Suzuki coupling and *in situ* deprotection as described above using 4-acetylphenylboronic acid (12.3 mg, 0.075 mmol, 1.5 eq). The crude product was purified by preparatory HPLC

purification to afford 1-(4-(5-(4-((4-methylpiperazin-1-yl)methyl)phenyl)-1*H*-pyrrolo[2,3-*b*]pyridin-3-yl)phenyl)ethan-1-one(**7x**, 15.1 mg, 71% yield). ^{1}H NMR (500 MHz, Methanol-d_4) δ 8.63 (d, *J* = 2.0 Hz, 1H), 8.58 (d, *J* = 2.0 Hz, 1H), 8.11 (d, *J* = 8.4 Hz, 2H), 7.95 (s, 1H), 7.90 (d, *J* = 8.4 Hz, 2H), 7.78 (d, *J* = 8.2 Hz, 2H), 7.57 (d, *J* = 8.2 Hz, 2H), 4.01 (s, 2H), 3.41 (bs, 4H), 3.09 (bs, 4H), 2.92 (s, 3H), 2.65 (s, 3H) ppm. HRMS (APCI$^+$, m/z): calcd. for $C_{27}H_{29}N_4O$ [M+H$^+$]: 425.2341, found: 425.2347.

3-(3-Fluorophenyl)-5-(4-((4-methylpiperazin-1-yl)methyl)phenyl)-1H-pyrrolo[2,3-*b*]pyridine (7y).

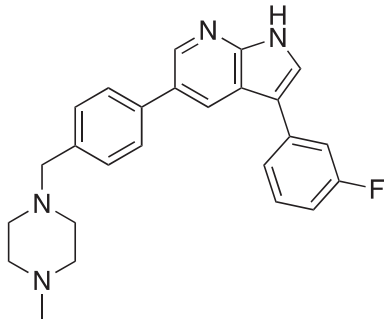

Compound **7y** was prepared according to the general procedure for the Suzuki coupling and *in situ* deprotection as described above using 3-fluorophenylboronic acid (10.5 mg, 0.075 mmol, 1.5 eq). The crude product was purified by preparatory HPLC purification to afford 3-(3-fluorophenyl)-5-(4-((4-methylpiperazin-1-yl)methyl)phenyl)-1*H*-pyrrolo[2,3-*b*]pyridine (**7y**, 12.8 mg, 64% yield). ^{1}H NMR (500 MHz, Methanol-d_4) δ 8.59 (d, *J* = 2.0 Hz, 1H), 8.58 (d, *J* = 2.2 Hz, 1H), 7.85 (s, 1H), 7.78 (d, *J* = 8.2 Hz, 2H), 7.61 – 7.55 (m, 3H), 7.52 – 7.44 (m, 2H), 7.11 – 7.02 (m, 1H), 4.02 (s, 2H), 3.41 (bs, 4H), 3.09 (bs, 4H), 2.92 (s, 3H) ppm. HRMS (APCI$^+$, m/z): calcd. for $C_{25}H_{26}N_4F$ [M+H$^+$]: 401.2142, found: 401.2146.

5-(4-((4-Methylpiperazin-1-yl)methyl)phenyl)-3-(4-(trifluoromethoxy)phenyl)-1H-pyrrolo[2,3-*b*]pyridine (7z).

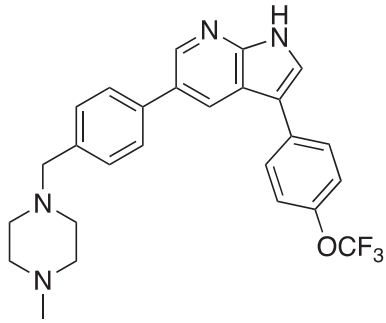

Compound **7z** was prepared according to the general procedure for the Suzuki coupling and *in situ* deprotection as described above using 4-(trifluormethoxy)phenylboronic acid (15.4 mg, 0.075 mmol, 1.5 eq). The crude product was purified by preparatory HPLC purification to afford 5-(4-((4-methylpiperazin-1-yl)methyl)phenyl)-3-(4-(trifluoromethoxy)phenyl)-1*H*-pyrrolo[2,3-*b*]pyridine (**7z**, 17.4 mg, 75% yield). ^{1}H NMR (500 MHz, Methanol-d_4) δ 8.62 (d, *J* = 2.0 Hz, 1H), 8.59 (d, *J* = 2.0 Hz, 1H), 7.85 (s, 1H), 7.86 – 7.80 (m, 2H), 7.79 (d, *J* = 8.2 Hz, 2H), 7.58 (d, *J* = 8.2 Hz, 2H), 7.40 (d, *J* = 8.0 Hz, 2H), 4.05 (s, 2H), 3.43 (bs, 4H), 3.13 (bs, 4H), 2.92 (s, 3H) ppm. HRMS (APCI$^+$, m/z): calcd. for $C_{26}H_{26}F_3N_4O$ [M+H$^+$]: 467.2059, found: 467.2062.

4-(5-(4-((4-Methylpiperazin-1-yl)methyl)phenyl)-1H-pyrrolo[2,3-*b*]pyridin-3-yl)-1*H*-indazole (7aa).

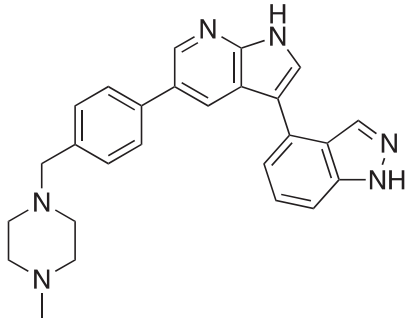

Compound **7aa** was prepared according to the general procedure for the Suzuki coupling and *in situ* deprotection as described above using 1*H*-Indazole-5-boronic acid (12.5 mg, 0.075 mmol, 1.5 eq). The crude product was purified by preparatory HPLC

purification to afford 4-(5-(4-((4-methylpiperazin-1-yl)methyl)phenyl)-1*H*-pyrrolo[2,3-*b*]pyridin-3-yl)-1*H*-indazole (**7aa**, 15.6 mg, 74% yield). ^{1}H NMR (400 MHz, Methanol-d_4) δ 8.62 (d, *J* = 2.0 Hz, 1H), 8.52 (d, *J* = 2.0 Hz, 1H), 8.18 (s, 1H), 7.94 (s, 1H), 7.73 (d, *J* = 8.2 Hz, 2H), 7.58 – 7.51 (m, 4H), 7.44 (dd, *J* = 6.2, 1.7 Hz, 1H), 3.97 (s, 2H), 3.38 (bs, 4H), 3.05 (bs, 4H), 2.90 (s, 3H) ppm. HRMS (APCI$^+$, m/z): calcd. for $C_{26}H_{27}N_6$ [M+H$^+$]: 423.2297, found: 423.2303.

5-(4-((4-Methylpiperazin-1-yl)methyl)phenyl)-3-(3-(trifluoromethyl)phenyl)-1H-pyrrolo[2,3-*b*]pyridine (7ab).

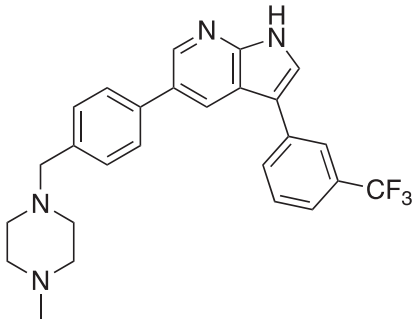

Compound **7ab** was prepared according to the general procedure for the Suzuki coupling and *in situ* deprotection as described above using 3-(trifluoromethyl)phenylboronic acid (14.2 mg, 0.075 mmol, 1.5 eq). The crude product was purified by preparatory HPLC purification to afford 5-(4-((4-methylpiperazin-1-yl)methyl)phenyl)-3-(3-(trifluoromethyl)phenyl)-1*H*-pyrrolo[2,3-*b*]pyridine (**7ab**, 17.0 mg, 75% yield). ^{1}H NMR (400 MHz, Methanol-d_4) δ 8.59 (d, *J* = 2.0 Hz, 1H), 8.54 (d, *J* = 2.0 Hz, 1H), 8.00 (d, *J* = 7.8 Hz, 1H), 7.97 (s, 1H), 7.89 (s, 1H), 7.76 (d, *J* = 8.2 Hz, 2H), 7.68 (t, *J* = 7.7 Hz, 1H), 7.61 (d, *J* = 8.4 Hz, 1H), 7.57 (d, *J* = 8.2 Hz, 2H), 4.03 (s, 2H), 3.42 (bs, 4H), 3.12 (bs, 4H), 2.92 (s, 3H) ppm. HRMS (APCI$^+$, m/z): calcd. for $C_{26}H_{26}F_3N_4$ [M+H$^+$]: 451.2110, found: 451.2115.

5-(4-((4-Methylpiperazin-1-yl)methyl)phenyl)-3-phenyl-1H-pyrrolo[2,3-*b*]pyridine (7ac).

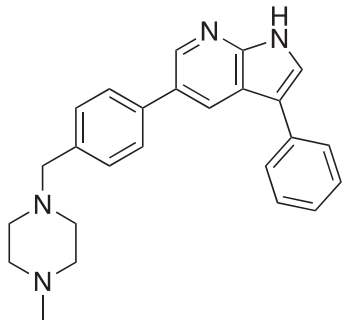

Compound **7ac** was prepared according to the general procedure for the Suzuki coupling and *in situ* deprotection as described above using phenylboronic acid (9.6 mg, 0.075 mmol, 1.5 eq). The crude product was purified by preparatory HPLC purification to afford 5-(4-((4-methylpiperazin-1-yl)methyl)phenyl)-3-phenyl-1*H*-pyrrolo[2,3-*b*]pyridine (**7ac**, 16.2 mg, 85% yield). ^{1}H NMR (400 MHz, Methanol-d_4) δ 8.69 (d, *J* = 1.9 Hz, 1H), 8.61 (d, *J* = 1.9 Hz, 1H), 7.82 (s, 1H), 7.78 (d, *J* = 8.2 Hz, 2H), 7.76 – 7.69 (m, 2H), 7.59 (d, *J* = 8.3 Hz, 2H), 7.53 – 7.44 (m, 2H), 7.39 – 7.29 (m, 1H), 4.08 (s, 2H), 3.45 (bs, 4H), 3.17 (bs, 4H), 2.93 (s, 3H) ppm. HRMS (APCI$^+$, m/z): calcd. for $C_{25}H_{27}N_4$ [M+H$^+$]: 383.2236, found: 383.2236.

3-(3-Chlorophenyl)-5-(4-((4-methylpiperazin-1-yl)methyl)phenyl)-1H-pyrrolo[2,3-*b*]pyridine (7ad).

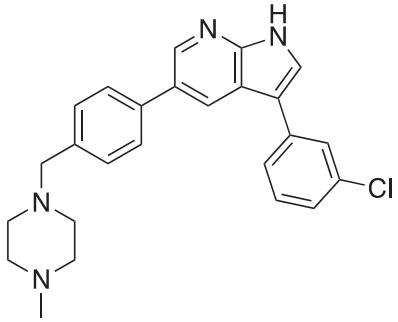

Compound **7ad** was prepared according to the general procedure for the Suzuki coupling and *in situ* deprotection as described above using 3-chlorophenylboronic acid (11.7 mg, 0.075 mmol, 1.5 eq). The crude product was purified by preparatory HPLC purification to afford 3-(3-chlorophenyl)-5-(4-((4-methylpiperazin-1-yl)methyl)phenyl)-1*H*-pyrrolo[2,3-*b*]pyridine (**7ad**, 18.4 mg, 88% yield). ^{1}H NMR (400 MHz, Methanol-d_4) δ 8.60 (d, *J* = 1.3 Hz, 2H), 7.85 (s, 1H), 7.79 (d, *J* = 8.2 Hz, 2H), 7.71 (t, *J* = 1.9 Hz, 1H), 7.66 (dt, *J* = 7.8, 1.3 Hz, 1H), 7.61 (d, *J* = 8.2 Hz, 2H), 7.46 (t, *J* = 7.9 Hz, 1H), 7.32 (ddd, *J* = 8.1, 2.1, 1.0 Hz, 1H), 4.17 (s, 2H), 3.49 (bs, 4H), 3.29 (bs, 4H), 2.94 (s, 3H) ppm. HRMS (APCI$^+$, m/z): calcd. for $C_{25}H_{26}ClN_4$ [M+H$^+$]: 417.1846, found: 417.1843.
3-(2,4-Dichlorophenyl)-5-(4-((4-methylpiperazin-1-yl)methyl)phenyl)-1H-pyrrolo[2,3-*b*]pyridine (7ae).

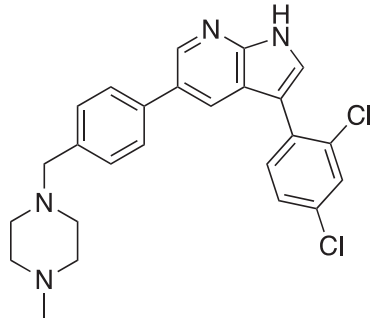

Compound **7ae** was prepared according to the general procedure for the Suzuki coupling and *in situ* deprotection as described above using 2,4-dichlorophenylboronic acid (14.3 mg, 0.075 mmol, 1.5 eq). The crude product was purified by preparatory HPLC purification to afford 3-(2,4-dichlorophenyl)-5-(4-((4-methylpiperazin-1-yl)methyl)phenyl)-1*H*-pyrrolo[2,3-*b*]pyridine (**7ae**, 14.9 mg, 66% yield). ^{1}H NMR (400 MHz, Methanol-d_4) δ 8.61 (d, *J* = 2.0 Hz, 1H), 8.32 (d, *J* = 2.0 Hz, 1H), 7.77 (s, 1H), 7.75 (d, *J* = 8.3 Hz, 2H), 7.64 (d, *J* = 2.2 Hz, 1H), 7.58 (dd, *J* = 8.3, 1.4 Hz, 3H), 7.44 (dd, *J* = 8.3, 2.2 Hz, 1H), 4.16 (s, 2H), 3.49 (bs, 4H), 3.27 (bs, 4H), 2.94 (s, 3H) ppm. HRMS (APCI$^+$, m/z): calcd. for $C_{25}H_{25}Cl_2N_4$ [M+H$^+$]: 451.1456, found: 451.1447.
3-(2,5-Dimethylphenyl)-5-(4-((4-methylpiperazin-1-yl)methyl)phenyl)-1H-pyrrolo[2,3-*b*]pyridine (7af).

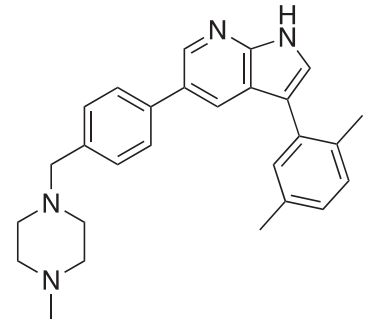

Compound **7af** was prepared according to the general procedure for the Suzuki coupling and *in situ* deprotection as described above using 2,5-dimethylphenylboronic acid (11.2 mg, 0.075 mmol, 1.5 eq). The crude product was purified by preparatory HPLC purification to afford 3-(2,5-dimethylphenyl)-5-(4-((4-methylpiperazin-1-yl)methyl)phenyl)-1*H*-pyrrolo[2,3-*b*]pyridine (**7af**, 14.0 mg, 68% yield). ^{1}H NMR (400 MHz, Methanol-d_4) δ 8.65 (d, *J* = 1.9 Hz, 1H), 8.36 (d, *J* = 1.9 Hz, 1H), 7.75 (d, *J* = 8.2 Hz, 2H), 7.63 (s, 1H), 7.60 (d, *J* = 8.2 Hz, 2H), 7.25 (d, *J* = 7.8 Hz, 1H), 7.21 (s, 1H), 7.13 (dd, *J* = 7.4, 1.7 Hz, 1H), 4.18 (s, 2H), 3.50 (bs, 4H), 3.30 (bs, 4H), 2.94 (s, 3H), 2.35 (s, 3H), 2.26 (s, 3H) ppm. HRMS (APCI$^+$, m/z): calcd. for $C_{27}H_{31}N_4$ [M+H$^+$]: 411.2549, found: 411.2556.
1-Methyl-6-(5-(4-((4-methylpiperazin-1-yl)methyl)phenyl)-1H-pyrrolo[2,3-*b*]pyridin-3-yl)-1*H*-indazole (7ag).

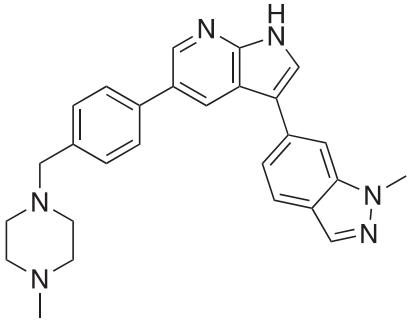

Compound **7ag** was prepared according to the general procedure for the Suzuki coupling and *in situ* deprotection as described above using 1-methyl-1*H*-indazole-6-boronic acid (13.2 mg, 0.075 mmol, 1.5 eq). The crude product was purified by preparatory HPLC purification to afford 1-methyl-6-(5-(4-((4-methylpiperazin-1-yl)methyl)phenyl)-1*H*-pyrrolo[2,3-*b*]pyridin-3-yl)-1*H*-indazole (**7ag**, 13.2 mg, 60% yield). ^{1}H NMR (400 MHz, Methanol-d_4) δ 8.67 (d, *J* = 2.0 Hz, 1H), 8.58 (d, *J* = 2.0 Hz, 1H), 8.01 (d, *J* = 0.9 Hz, 1H), 7.88 (s, 1H), 7.84 (dd, *J* = 8.4, 0.9 Hz, 1H), 7.81 (d, *J* = 1.2 Hz, 1H), 7.76 (d, *J* = 8.2 Hz, 2H), 7.60 – 7.52 (m, 3H), 4.11 (s, 3H), 3.99 (s, 2H), 3.40 (bs, 4H), 3.09 (bs, 4H), 2.91 (s, 3H) ppm. HRMS (APCI$^+$, m/z): calcd. for $C_{27}H_{29}N_6$ [M+H$^+$]: 437.2454, found: 437.2449.

3-(1-Benzyl-1H-pyrazol-4-yl)-5-(4-((4-methylpiperazin-1-yl)methyl)phenyl)-1*H*-pyrrolo[2,3-*b*]pyridine (7ah).

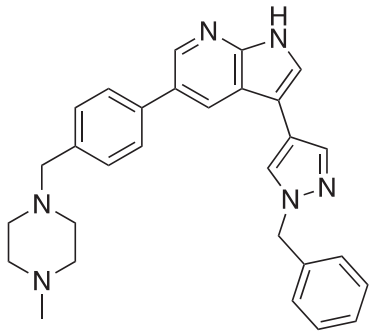

Compound **7ah** was prepared according to the general procedure for the Suzuki coupling and *in situ* deprotection as described above using 1-benzyl-1*H*-pyrazole-4-boronic acid (15.2 mg, 0.075 mmol, 1.5 eq). The crude product was purified by preparatory HPLC purification to afford 3-(1-benzyl-1*H*-pyrazol-4-yl)-5-(4-((4-methylpiperazin-1-yl)methyl)phenyl)-1*H*-pyrrolo[2,3-*b*]pyridine (**7ah**, 14.3 mg, 62% yield). ^{1}H NMR (400 MHz, Methanol-d_4) δ 8.61 (d, *J* = 2.0 Hz, 1H), 8.57 (d, *J* = 2.0 Hz, 1H), 8.19 (d, *J* = 0.8 Hz, 1H), 7.94 (d, *J* = 0.8 Hz, 1H), 7.79 (d, *J* = 8.2 Hz, 2H), 7.75 (s, 1H), 7.57 (d, *J* = 8.2 Hz, 2H), 7.39 – 7.26 (m, 5H), 5.42 (s, 2H), 4.01 (s, 2H), 3.41 (bs, 4H), 3.09 (bs, 4H), 2.92 (s, 3H) ppm. HRMS (APCI$^+$, m/z): calcd. for $C_{29}H_{31}N_6$ [M+H$^+$]: 463.2610, found: 463.2612.

5-(4-((4-Methylpiperazin-1-yl)methyl)phenyl)-3-(1,3,5-trimethyl-1H-pyrazol-4-yl)-1*H*-pyrrolo[2,3-*b*]pyridine (7ai).

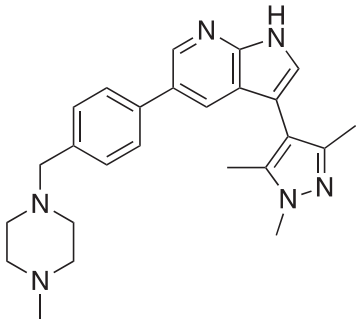

Compound **7ai** was prepared according to the general procedure for the Suzuki coupling and *in situ* deprotection as described above using 1,3,5-trimethyl-1*H*-pyrazole-4-boronic acid pinacol ester (17.7 mg, 0.075 mmol, 1.5 eq). The crude product was purified by preparatory HPLC purification to afford 5-(4-((4-methylpiperazin-1-yl)methyl)phenyl)-3-(1,3,5-trimethyl-1*H*-pyrazol-4-yl)-1*H*-pyrrolo[2,3-*b*]pyridine (**7ai**, 7.6 mg, 37% yield). ^{1}H NMR (400 MHz, Methanol-d_4) δ 8.59 (d, *J* = 2.0 Hz, 1H), 8.16 (d, *J* = 2.0 Hz, 1H), 7.70 (d, *J* = 8.2 Hz, 2H), 7.56 – 7.50 (m, 3H), 3.93 (s, 2H), 3.88 (s, 3H), 3.37 (bs, 4H), 3.01 (bs, 4H), 2.90 (s, 3H), 2.28 (s, 3H), 2.22 (s, 3H) ppm. HRMS (APCI$^+$, m/z): calcd. for $C_{25}H_{31}N_6$ [M+H$^+$]: 415.2610, found: 415.2604.

3-(3,5-Bis(trifluoromethyl)phenyl)-5-(4-((4-methylpiperazin-1-yl)methyl)phenyl)-1H-pyrrolo[2,3-*b*]pyridine (7aj).

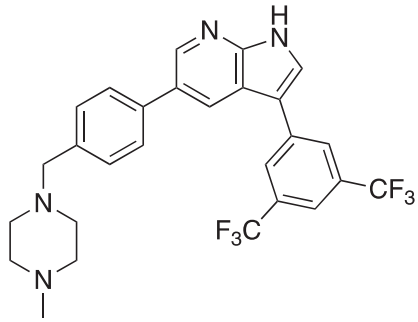

Compound **7aj** was prepared according to the general procedure for the Suzuki coupling and *in situ* deprotection as described above using 3,5-bis(trifluoromethyl)phenylboronic acid (19.3 mg, 0.075 mmol, 1.5 eq). The crude product was purified by preparatory HPLC purification to afford 3-(3,5-bis(trifluoromethyl)phenyl)-5-(4-((4-methylpiperazin-1-yl)methyl)phenyl)-1*H*-pyrrolo[2,3-*b*]pyridine (**7aj**, 11.2 mg, 43% yield). ^{1}H NMR (400 MHz, Methanol-d_4) δ 8.58 (d, J = 2.0 Hz, 1H), 8.44 (d, J = 2.0 Hz, 1H), 8.29 – 8.23 (m, 2H), 8.02 (s, 1H), 7.86 (s, 1H), 7.74 (d, J = 8.2 Hz, 2H), 7.56 (d, J = 8.2 Hz, 2H), 3.96 (s, 2H), 3.38 (bs, 4H), 3.04 (bs, 4H), 2.90 (s, 3H) ppm. HRMS (APCI$^+$, m/z): calcd. for $C_{27}H_{25}F_6N_4$ [M+H$^+$]: 519.1983, found: 519.1983.

1-Methyl-3-(3-(5-(4-((4-methylpiperazin-1-yl)methyl)phenyl)-1H-pyrrolo[2,3-*b*]pyridin-3-yl)phenyl)urea (7ak).

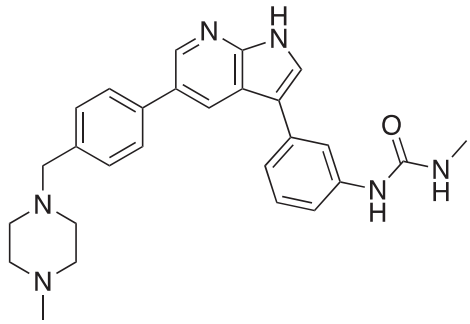

Compound **7ak** was prepared according to the general procedure for the Suzuki coupling and *in situ* deprotection as described above using (3-(3-methylureido)phenyl)boronic acid (**13a**, 14.6 mg, 0.075 mmol, 1.5 eq). The crude product was purified by preparatory HPLC purification to afford 1-methyl-3-(3-(5-(4-((4-methylpiperazin-1-yl)methyl)phenyl)-1*H*-pyrrolo[2,3-*b*]pyridin-3-yl)phenyl) urea (**7ak**, 6.4 mg, 14% yield). ^{1}H NMR (400 MHz, Methanol-d_4) δ 8.70 (d, J = 2.0 Hz, 1H), 8.57 (d, J = 2.0 Hz, 1H), 7.96 (t, J = 1.8 Hz, 1H), 7.81 – 7.75 (m, 3H), 7.54 (d, J = 8.2 Hz, 2H), 7.39 – 7.31 (m, 2H), 7.18 (dt, J = 7.3, 2.0 Hz, 1H), 3.91 (s, 2H), 3.35 (bs, 4H), 2.98 (bs, 4H), 2.89 (s, 3H), 2.80 (s, 3H) ppm. HRMS (APCI$^+$, m/z): calcd. for $C_{27}H_{31}N_6O$ [M+H$^+$]: 455.2559, found: 455.2559.

Methyl (3-(5-(4-((4-methylpiperazin-1-yl)methyl)phenyl)-1H-pyrrolo[2,3-*b*]pyridin-3-yl)phenyl)carbamate (7al).

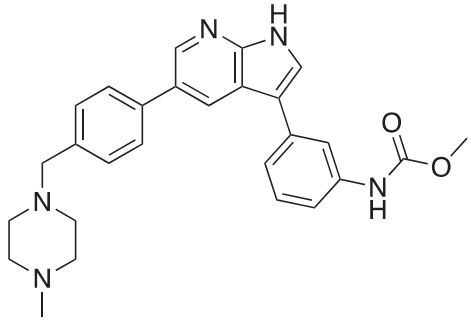

Compound **7al** was prepared according to the general procedure for the Suzuki coupling and *in situ* deprotection as described above using (3-((methoxycarbonyl)amino)phenyl)boronic acid (**13b**, 14.6 mg, 0.075 mmol, 1.5 eq). The crude product was purified by preparatory HPLC purification to afford methyl (3-(5-(4-((4-methylpiperazin-1-yl)methyl)phenyl)-1*H*-pyrrolo[2,3-*b*]pyridin-3-yl) phenyl)carbamate (**7al**, 8.5 mg, 19% yield). ^{1}H NMR (400 MHz, Methanol-d_4) δ 8.74 (d, J = 2.0 Hz, 1H), 8.59 (d, J = 2.0 Hz, 1H), 7.98 (s, 1H), 7.83 – 7.78 (m, 3H), 7.56 (d, J = 8.2 Hz, 2H), 7.41 – 7.37 (m, 2H), 7.36 – 7.27 (m, 1H), 3.97 (s, 2H), 3.77 (s, 3H), 3.38 (bs, 4H), 3.04 (bs, 4H), 2.91 (s, 3H) ppm. HRMS (APCI$^+$, m/z): calcd. for $C_{27}H_{30}N_5O_2$ [M+H$^+$]: 456.2400, found: 456.2400.

1-Methyl-3-(4-(5-(4-((4-methylpiperazin-1-yl)methyl)phenyl)-1H-pyrrolo[2,3-*b*]pyridin-3-yl)phenyl)urea (7am).

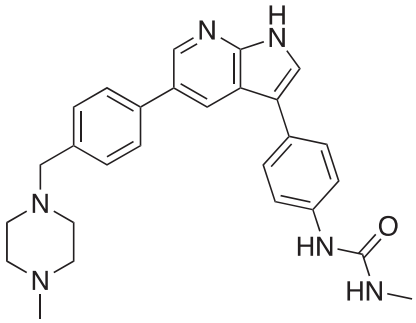

Compound **7am** was prepared according to the general procedure for the Suzuki coupling and *in situ* deprotection as described above using (4-(3-methylureido)phenyl)boronic acid (**13c**, 14.6 mg, 0.075 mmol, 1.5 eq). The crude product was purified by preparatory HPLC purification to afford 1-methyl-3-(4-(5-(4-((4-methylpiperazin-1-yl)methyl)phenyl)-1*H*-pyrrolo[2,3-*b*]pyridin-3-yl)phenyl) urea (**7am**, 5.1 mg, 22% yield). ^{1}H NMR (400 MHz, Methanol-d_4) δ 8.63 (d, J = 2.0 Hz, 1H), 8.56 (d, J = 2.0 Hz, 1H), 7.76 (s, 1H), 7.74 (d, J = 4.6 Hz, 2H), 7.65 – 7.60 (m, 2H), 7.55 (d, J = 8.1 Hz, 2H), 7.52 – 7.45 (m, 2H), 3.92 (s, 2H), 3.36 (bs, 4H), 2.99 (bs, 4H), 2.90 (s, 3H), 2.80 (s, 3H) ppm. HRMS (APCI$^+$, m/z): calcd. for $C_{27}H_{31}N_6O$ [M+H$^+$]: 455.2559, found: 455.2566.

Methyl (4-(5-(4-((4-methylpiperazin-1-yl)methyl)phenyl)-1H-pyrrolo[2,3-*b*]pyridin-3-yl)phenyl)carbamate (7an).

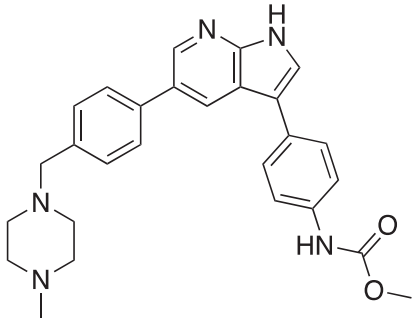

Compound **7an** was prepared according to the general procedure for the Suzuki coupling and *in situ* deprotection as described above using (4-((methoxycarbonyl)amino)phenyl)boronic acid (**13d**, 14.6 mg, 0.075 mmol, 1.5 eq). The crude product was purified by preparatory HPLC purification to afford methyl (4-(5-(4-((4-methylpiperazin-1-yl)methyl)phenyl)-1*H*-pyrrolo[2,3-*b*]pyridin-3-yl)phenyl) carbamate (**7an**, 7.6 mg, 33% yield). ^{1}H NMR (400 MHz, Methanol-d_4) δ 8.68 (d, J = 1.9 Hz, 1H), 8.59 (d, J = 2.0 Hz, 1H), 7.82 – 7.72 (m, 3H), 7.65 (d, J = 8.7 Hz, 2H), 7.61 – 7.51 (m, 4H), 4.04 (s, 3H), 3.76 (s, 2H), 3.43 (bs, 4H), 3.13 (bs, 4H), 2.92 (s, 3H) ppm. HRMS (APCI$^+$, m/z): calcd. for $C_{27}H_{30}N_5O_2$ [M+H$^+$]: 456.2400, found: 456.2397.

3-(4-((4-Methoxybenzyl)oxy)phenyl)-5-(4-((4-methylpiperazin-1-yl)methyl)phenyl)-1H-pyrrolo[2,3-*b*]pyridine (7ao).

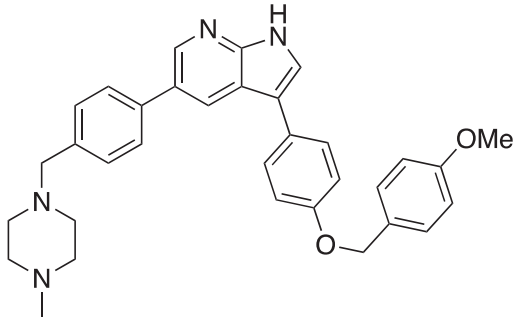

Compound **7ao** was prepared according to the general procedure for the Suzuki coupling and *in situ* deprotection as described above using 4-(4-methoxybenzyloxy)phenylboronic acid (19.4 mg, 0.075 mmol, 1.5 eq). The crude product was purified by

preparatory HPLC purification to afford 3-(4-((4-methoxybenzyl)oxy)phenyl)-5-(4-((4-methylpiperazin-1-yl)methyl)phenyl)-1*H*-pyrrolo[2,3-*b*]pyridine (**7ao**, 20.4 mg, 79% yield). ^{1}H NMR (400 MHz, Methanol-d_4) δ 8.69 (dd, *J* = 7.3, 1.9 Hz, 2H), 8.59 (d, *J* = 1.8 Hz, 1H), 7.77 (dd, *J* = 8.3, 1.6 Hz, 2H), 7.72 (d, *J* = 8.2 Hz, 1H), 7.66 – 7.51 (m, 3H), 7.37 (dd, *J* = 8.7, 6.9 Hz, 2H), 7.28 – 7.03 (m, 1H), 6.98 – 6.77 (m, 3H), 5.05 (s, 2H), 4.06 (s, 2H), 3.80 (s, 3H), 3.44 (bs, 4H), 3.16 (bs, 4H), 2.92 (s, 3H) ppm. HRMS (APCI$^+$, m/z): calcd. for $C_{33}H_{35}N_4O_2$ [M+H$^+$]: 519.2760, found: 519.2755.

5-(4-((4-Methylpiperazin-1-yl)methyl)phenyl)-3-(3,4,5-trimethoxyphenyl)-1H-pyrrolo[2,3-*b*]pyridine (7ap).

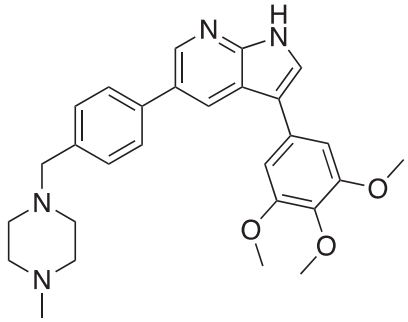

Compound **7ap** was prepared according to the general procedure for the Suzuki coupling and *in situ* deprotection as described above using 3,4,5-trimethoxyphenylboronic acid (15.9 mg, 0.075 mmol, 1.5 eq). The crude product was purified by preparatory HPLC purification to afford 5-(4-((4-methylpiperazin-1-yl)methyl)phenyl)-3-(3,4,5-trimethoxyphenyl)-1*H*-pyrrolo[2,3-*b*]pyridine (**7ap**, 19.2 mg, 81% yield). ^{1}H NMR (400 MHz, Methanol-d_4) δ 8.67 (d, *J* = 1.9 Hz, 1H), 8.60 (d, *J* = 1.9 Hz, 1H), 7.81 (s, 1H), 7.78 (d, *J* = 8.2 Hz, 2H), 7.59 (d, *J* = 8.2 Hz, 2H), 6.96 (s, 2H), 4.10 (s, 2H), 3.92 (s, 6H), 3.82 (s, 3H), 3.46 (bs, 4H), 3.20 (bs, 4H), 2.93 (s, 3H) ppm. HRMS (APCI$^+$, m/z): calcd. for $C_{28}H_{33}N_4O_3$ [M+H$^+$]: 473.2553, found: 473.2554.

3-(4-Methoxy-3-methylphenyl)-5-(4-((4-methylpiperazin-1-yl)methyl)phenyl)-1H-pyrrolo[2,3-*b*]pyridine (7aq).

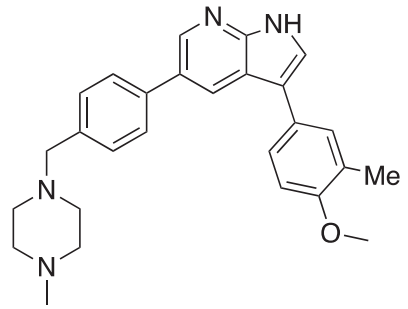

Compound **7aq** was prepared according to the general procedure for the Suzuki coupling and *in situ* deprotection as described above using 4-methoxy-3-methylphenylboronic acid (12.4 mg, 0.075 mmol, 1.5 eq). The crude product was purified by preparatory HPLC purification to afford 3-(4-methoxy-3-methylphenyl)-5-(4-((4-methylpiperazin-1-yl)methyl)phenyl)-1*H*-pyrrolo[2,3-*b*]pyridine (**7aq**, 17.2 mg, 81% yield). ^{1}H NMR (400 MHz, Methanol-d_4) δ 8.69 (d, *J* = 1.9 Hz, 1H), 8.59 (d, *J* = 1.9 Hz, 1H), 7.77 (d, *J* = 8.2 Hz, 2H), 7.72 (s, 1H), 7.59 (d, *J* = 8.2 Hz, 2H), 7.51 (dd, *J* = 8.4, 2.3 Hz, 1H), 7.48 – 7.44 (m, 1H), 7.03 (d, *J* = 8.4 Hz, 1H), 4.03 (s, 2H), 3.88 (s, 3H), 3.43 (bs, 4H), 3.12 (bs, 4H), 2.92 (s, 3H), 2.28 (s, 3H) ppm. HRMS (APCI$^+$, m/z): calcd. for $C_{27}H_{31}N_4O$ [M+H$^+$]: 427.2498, found: 427.2501.

3-(3-(Benzyloxy)phenyl)-5-(4-((4-methylpiperazin-1-yl)methyl)phenyl)-1H-pyrrolo[2,3-*b*]pyridine (7ar).

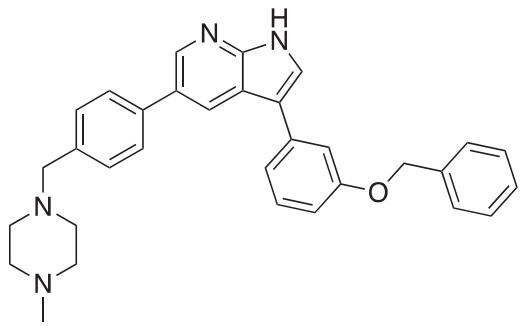

Compound **7ar** was prepared according to the general procedure for the Suzuki coupling and *in situ* deprotection as described above using 3-(benzyloxy)phenylboronic acid (17.1 mg, 0.075 mmol, 1.5 eq). The crude product was purified by preparatory HPLC purification to afford 3-(3-(benzyloxy)phenyl)-5-(4-((4-methylpiperazin-1-yl)methyl)phenyl)-1*H*-pyrrolo[2,3-*b*]pyridine (**7ar**, 15.4 mg, 63% yield). ^{1}H NMR (400 MHz, Methanol-d_4) δ 8.58 (s, 2H), 7.79 (s, 1H), 7.74 (d, *J* = 8.2 Hz, 2H), 7.58 (d, *J* = 8.2 Hz, 2H), 7.49 – 7.43 (m, 2H), 7.43 – 7.22 (m, 6H), 7.06 – 6.96 (m, 1H), 5.17 (s, 2H), 4.06 (s, 2H), 3.43 (bs, 4H), 3.15 (bs, 4H), 2.92 (s, 3H) ppm. HRMS (APCI$^+$, m/z): calcd. for $C_{32}H_{33}N_4O$ [M+H$^+$]: 489.2654, found: 489.2657.

3-(2-Chlorophenyl)-5-(4-((4-methylpiperazin-1-yl)methyl)phenyl)-1H-pyrrolo[2,3-*b*]pyridine (7as).

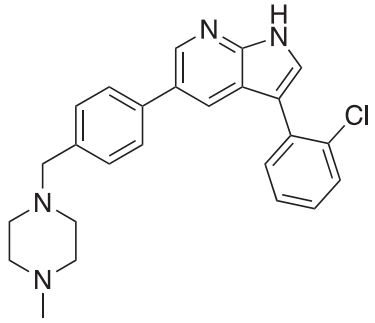

Compound **7as** was prepared according to the general procedure for the Suzuki coupling and *in situ* deprotection as described above using 2-chlorophenylboronic acid (17.1 mg, 0.075 mmol, 1.5 eq). The crude product was purified by preparatory HPLC purification to afford 3-(2-chlorophenyl)-5-(4-((4-methylpiperazin-1-yl)methyl)phenyl)-1*H*-pyrrolo[2,3-*b*]pyridine (**7as**, 16.6 mg, 80% yield). ^{1}H NMR (400 MHz, Methanol-d_4) δ 8.60 (d, *J* = 2.0 Hz, 1H), 8.32 (d, *J* = 2.0 Hz, 1H), 7.74 (s, 1H), 7.72 (d, *J* = 8.2 Hz, 2H), 7.59 (ddd, *J* = 7.7, 4.0, 1.7 Hz, 2H), 7.55 (d, *J* = 8.2 Hz, 2H), 7.43 (td, *J* = 7.5, 1.7 Hz, 1H), 7.38 (td, *J* = 7.5, 2.0 Hz, 1H), 4.01 (s, 2H), 3.41 (bs, 4H), 3.10 (bs, 4H), 2.91 (s, 3H) ppm. HRMS (APCI$^+$, m/z): calcd. for $C_{25}H_{26}N_4Cl$ [M+H$^+$]: 417.1846, found: 417.1849.

3-(2-Methoxyphenyl)-5-(4-((4-methylpiperazin-1-yl)methyl)phenyl)-1H-pyrrolo[2,3-*b*]pyridine (7at).

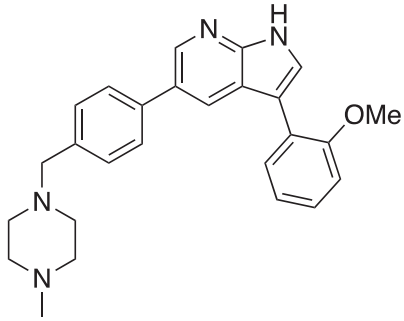

Compound **7at** was prepared according to the general procedure for the Suzuki coupling and *in situ* deprotection as described above using 2-methoxyphenylboronic acid (11.4 mg, 0.075 mmol, 1.5 eq). The crude product was purified by preparatory HPLC purification to afford 3-(2-methoxyphenyl)-5-(4-((4-methylpiperazin-1-yl)methyl)phenyl)-1*H*-pyrrolo[2,3-*b*]pyridine (**7at**, 17.1 mg, 83% yield). ^{1}H NMR (400 MHz, Methanol-d_4) δ 8.61 (d, *J* = 1.9 Hz, 1H), 8.58 (d, *J* = 1.9 Hz, 1H), 7.80 (s, 1H), 7.75 (d, *J* = 8.2 Hz, 2H), 7.61 – 7.54 (m, 3H), 7.38 (ddd, *J* = 8.3, 7.4, 1.7 Hz, 1H), 7.16 (dd, *J* = 8.3, 1.1 Hz, 1H), 7.08 (td, *J* = 7.4, 1.1 Hz, 1H), 4.02 (s, 2H), 3.86 (s, 3H), 3.42 (s, 4H), 3.11 (s, 4H), 2.92 (s, 3H) ppm. HRMS (APCI$^+$, m/z): calcd. for $C_{26}H_{29}N_4O$ [M+H$^+$]: 413.2341, found: 413.2337.

1-(3-(5-(4-((4-Methylpiperazin-1-yl)methyl)phenyl)-1H-pyrrolo[2,3-*b*]pyridin-3-yl)phenyl)-3-phenylurea (7au).

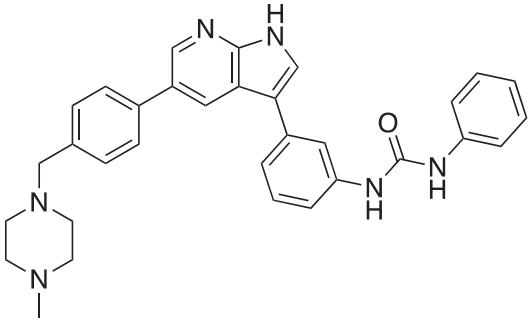

Compound **7au** was prepared according to the general procedure for the Suzuki coupling and *in situ* deprotection as described above using (3-(3-phenylureido)phenyl)boronic acid (**13e**, 19.2 mg, 0.075 mmol, 1.5 eq). The crude product was purified by preparatory HPLC purification to afford 1-(3-(5-(4-((4-methylpiperazin-1-yl)methyl)phenyl)-1*H*-pyrrolo[2,3-*b*]pyridin-3-yl)phenyl)-3-phenylurea (**7au**, 5.4 mg, 21% yield). ^{1}H NMR (400 MHz, Methanol-d_4) δ 8.61 (d, *J* = 2.0 Hz, 1H), 8.51 (d, *J* = 2.0 Hz, 1H), 8.08 (s, 1H), 7.78 – 7.71 (m, 3H), 7.60 (d, *J* = 6.9 Hz, 2H), 7.49 (d, *J* = 8.0 Hz, 2H), 7.46 – 7.40 (m, 1H), 7.41 – 7.36 (m, 2H), 7.36 – 7.27 (m, 2H), 7.24 – 7.17 (m, 1H), 3.76 (s, 2H), 3.13 (bs, 8H), 2.85 (s, 3H) ppm. HRMS (APCI$^+$, m/z): calcd. for $C_{32}H_{33}N_6O$ [M+H$^+$]: 517.2716, found: 517.2713.

2-Fluoro-N-(furan-2-ylmethyl)-5-(5-(4-((4-methylpiperazin-1-yl)methyl)phenyl)-1*H*-pyrrolo[2,3-*b*]pyridin-3-yl)benzamide (7av).

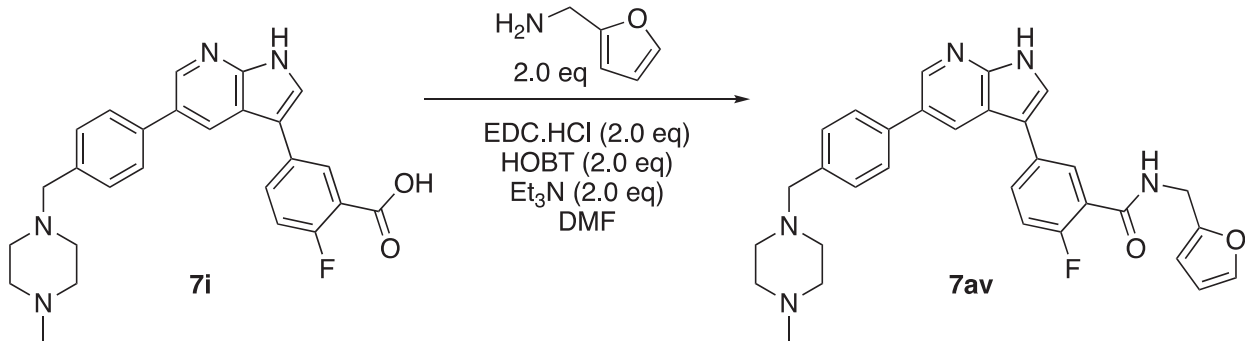

2-Fluoro-5-(5-(4-((4-methylpiperazin-1-yl)methyl)phenyl)-1*H*-pyrrolo[2,3-*b*]pyridin-3-yl)benzoic acid (**7i**, 3.3 mg, 7.4 μmol), EDC×HCl (2.8 mg, 14.8 μmol, 2.0 eq), and HOBT (2.0 mg, 14.8 μmol, 2.0 eq) were dissolved in DMF (1.0 mL). Furfurylamine (1.4 mg, 1.3 μL, 14.8 μmol, 2.0 eq) and Et_3N (1.5 mg, 2.0 μL, 14.8 μmol, 2.0 eq) were added and the reaction mixture was stirred at room temperature overnight. The solvent was evaporated and the crude mixture was purified by preparatory HPLC purification to afford 2-fluoro-*N*-(furan-2-ylmethyl)-5-(5-(4-((4-methylpiperazin-1-yl)methyl)phenyl)-1*H*-pyrrolo[2,3-*b*]pyridin-3-yl)benzamide (**7av**, 3.8 mg, 98% yield). ^{1}H NMR (400 MHz, Methanol-d_4) δ 8.54 (d, *J* = 2.0 Hz, 1H), 8.52 (d, *J* = 2.0 Hz, 1H), 8.08 (dd, *J* = 6.9, 2.4 Hz, 1H), 7.88 (ddd, *J* = 8.6, 4.8, 2.4 Hz, 1H), 7.78 (s, 1H), 7.73 (d, *J* = 8.2 Hz, 2H), 7.52 (d, *J* = 8.2 Hz, 2H), 7.44 (dd, *J* = 1.9, 0.9 Hz, 1H), 7.32 (dd, *J* = 10.7, 8.6 Hz, 1H), 6.37 (dd, *J* = 3.2, 1.9 Hz, 1H), 6.33 (dd, *J* = 3.2, 0.9 Hz, 1H), 4.61 (s, 2H), 3.84 (s, 2H), 2.97 – 2.84 (m, 8H), 2.88 (s, 3H) ppm. HRMS (APCI$^+$, m/z): calcd. for $C_{31}H_{31}FN_5O_2$ [M+H$^+$]: 524.2462, found: 524.2452.

1-Cyclohexyl-3-(4-(5-(4-((4-methylpiperazin-1-yl)methyl)phenyl)-1H-pyrrolo[2,3-*b*]pyridin-3-yl)phenyl)urea (7aw).

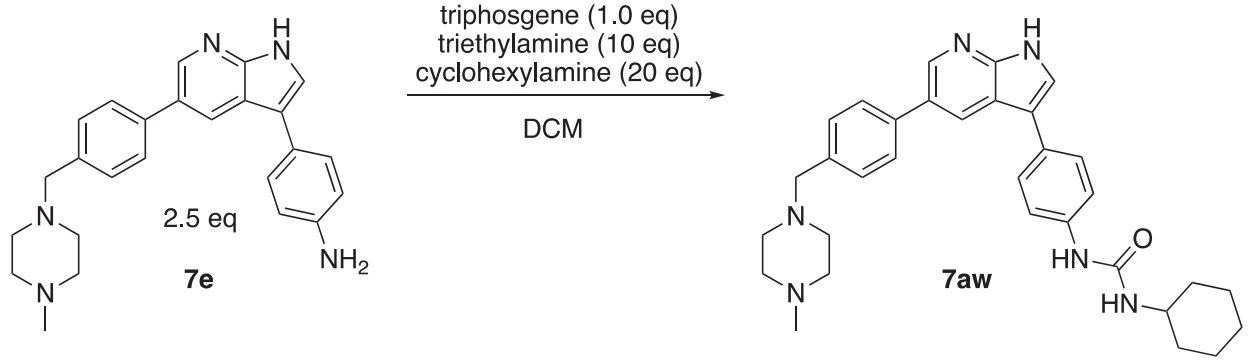

4-(5-(4-((4-methylpiperazin-1-yl)methyl)phenyl)-1*H*-pyrrolo[2,3-*b*]pyridin-3-yl)aniline (**7e**, 10 mg, 0.025 mmol, 2.5 eq) was dissolved in DCM (0.5 mL) and triethylamine (10 mg, 14 μL, 0.1 mmol, 10 eq) was added. The solution was added dropwise to a solution of triphosgene (3.0 mg, 0.01 mmol, 1.0 eq) in DCM (0.5 mL) and stirred for 5 min at room temperature. The reaction mixture was added to a solution of cyclohexylamine (19.8 mg, 23 μL, 0.2 mmol, 20.0 eq) in DCM (0.5 mL) and stirred overnight. The solvent was evaporated and the crude mixture was purified by preparatory HPLC purification to afford 1-cyclohexyl-3-(4-(5-(4-((4-methylpiperazin-1-yl)methyl)phenyl)-1*H*-pyrrolo[2,3-*b*]pyridin-3-yl)phenyl)urea (**7aw**, 2.8 mg, 54% yield). ^{1}H NMR (400 MHz, Methanol-d_4) δ 8.53 (m, 2H), 7.72 (d, *J* = 8.2 Hz, 2H), 7.68 (s, 1H), 7.64 – 7.59 (m, 2H), 7.52 (d, *J* = 8.2 Hz, 2H), 7.49 – 7.44 (m, 2H), 3.82 (s, 2H), 3.65 – 3.54 (m, 1H), 3.00 – 2.74 (bs, 8H), 2.88 (s, 3H), 2.00 – 1.90 (m, 2H), 1.84 – 1.71 (m, 2H), 1.65 (d, *J* = 12.9 Hz, 1H), 1.48 – 1.34 (m, 2H), 1.36 – 1.16 (m, 3H) ppm. HRMS (APCI$^+$, m/z): calcd. for $C_{32}H_{39}N_6O$ [M+H$^+$]: 523.3185, found: 523.3182.

(R)-1-(3-(5-(4-((4-methylpiperazin-1-yl)methyl)phenyl)-1*H*-pyrrolo[2,3-*b*]pyridin-3-yl)phenyl)-3-(1-phenylethyl)urea (7ax).

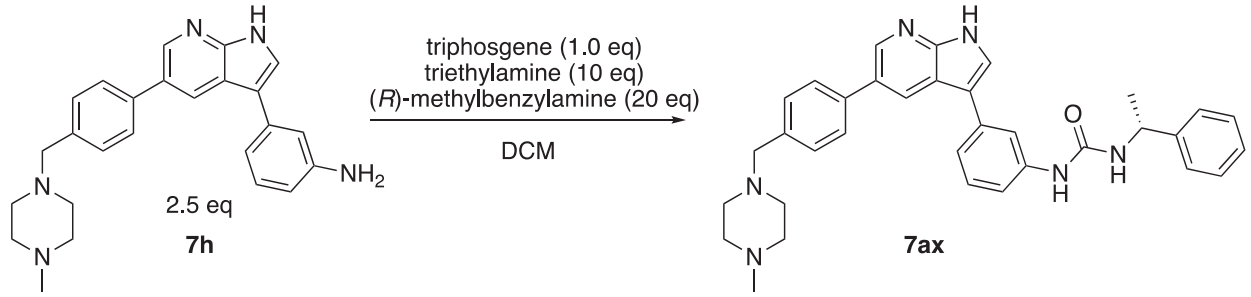

3-(5-(4-((4-Methylpiperazin-1-yl)methyl)phenyl)-1*H*-pyrrolo[2,3-*b*]pyridin-3-yl)aniline (**7h**, 16 mg, 0.04 mmol, 2.5 eq) was dissolved in DCM (1.0 mL) and triethylamine (16.2 mg, 22 μL, 0.16 mmol, 10 eq) was added. The solution was added dropwise to a solution of triphosgene (4.75 mg, 0.016 mmol, 1.0 eq) in DCM (1.0 mL) and stirred for 5 min at room temperature. The reaction mixture was added to a solution of (*R*)-(+)-α-methylbenzylamine (38.8 mg, 41 μL, 0.32 mmol, 20.0 eq) in DCM (1.0 mL) and stirred overnight. The solvent was evaporated and the crude mixture was purified by preparatory HPLC purification to afford (*R*)-1-(3-(5-(4-((4-methylpiperazin-1-yl)methyl)phenyl)-1*H*-pyrrolo[2,3-*b*]pyridin-3-yl)phenyl)-3-(1-phenylethyl)urea (**7ax**, 6.7 mg, 31% yield). ^{1}H NMR (400 MHz, Methanol-d_4) δ 8.65 (d, *J* = 2.0 Hz, 1H), 8.54 (d, *J* = 2.1 Hz, 1H), 7.94 (s, 1H), 7.78 – 7.72 (m, 3H), 7.51 (d, *J* = 8.0 Hz, 2H), 7.42 – 7.28 (m, 6H), 7.23 (t, *J* = 7.0 Hz, 1H), 7.18 – 7.11 (m, 1H), 4.95 (q, *J* = 7.0 Hz, 1H), 3.83 (s, 2H), 3.14 – 2.50 (bs, 8H), 2.88 (s, 3H), 1.50 (d, *J* = 7.0 Hz, 3H) ppm. HRMS (APCI$^+$, m/z): calcd. for $C_{34}H_{37}N_6O$ [M+H$^+$]: 545.3029, found: 545.3027.

1-(Furan-2-ylmethyl)-3-(3-(5-(4-((4-methylpiperazin-1-yl)methyl)phenyl)-1H-pyrrolo[2,3-*b*]pyridin-3-yl)phenyl)urea (7ay).

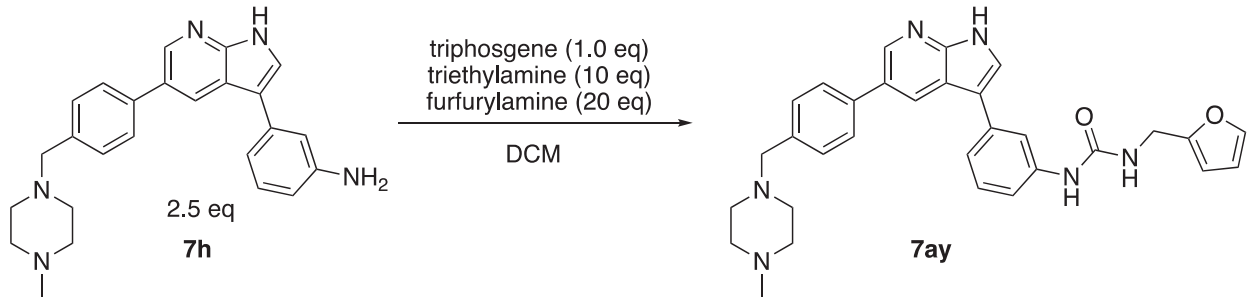

3-(5-(4-((4-Methylpiperazin-1-yl)methyl)phenyl)-1*H*-pyrrolo[2,3-*b*]pyridin-3-yl)aniline (**7h**, 16 mg, 0.04 mmol, 2.5 eq) was dissolved in DCM (1.0 mL) and triethylamine (16.2 mg, 22 μL, 0.16 mmol, 10 eq) was added. The solution was added dropwise to a solution of triphosgene (4.75 mg, 0.016 mmol, 1.0 eq) in DCM (1.0 mL) and stirred for 5 min at room temperature. The reaction mixture was added to a solution of furfurylamine (31.1 mg, 28.3 μL, 0.32 mmol, 20.0 eq) in DCM (1.0 mL) and stirred overnight. The solvent was evaporated and the crude mixture was purified by preparatory HPLC purification to afford 1-(furan-2-ylmethyl)-3-(3-(5-(4-((4-methylpiperazin-1-yl)methyl)phenyl)-1*H*-pyrrolo[2,3-*b*]pyridin-3-yl)phenyl)urea (**7ay**, 8.6 mg, 41% yield). ^{1}H NMR (400 MHz, Methanol-d_4) δ 8.74 (d, *J* = 2.0 Hz, 1H), 8.69 – 8.66 (m, 2H), 7.82 – 7.78 (m, 2H), 7.74 (s, 1H), 7.65 (d, *J* = 7.9 Hz, 2H), 7.41 – 7.34 (m, 4H), 6.35 (dd, *J* = 3.2, 1.9 Hz, 1H), 6.28 (dd, *J* = 3.2, 0.8 Hz, 1H), 4.41 (s, 2H), 3.89 (s, 2H), 3.21 (bs, 4H), 3.11 (bs, 4H), 2.89 (s, 3H) ppm. HRMS (APCI$^+$, m/z): calcd. for $C_{31}H_{33}N_6O_2$ [M+H$^+$]: 521.2665, found: 521.2670.

1-(2-Methoxyethyl)-3-(3-(5-(4-((4-methylpiperazin-1-yl)methyl)phenyl)-1H-pyrrolo[2,3-*b*]pyridin-3-yl)phenyl)urea (7az).

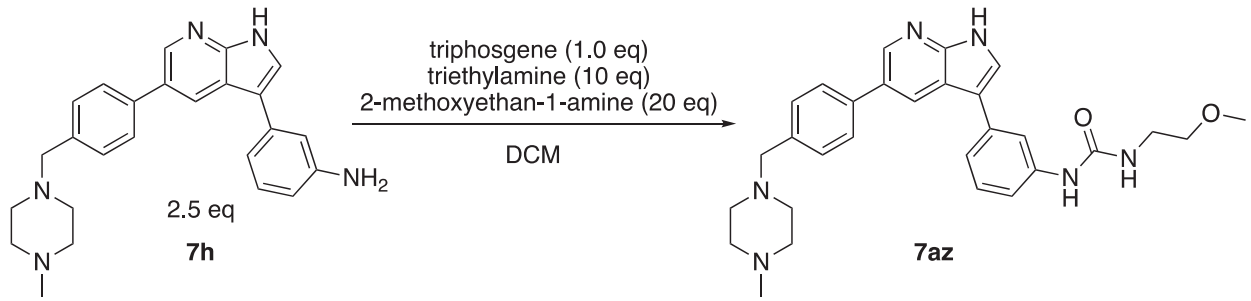

3-(5-(4-((4-Methylpiperazin-1-yl)methyl)phenyl)-1*H*-pyrrolo[2,3-*b*]pyridin-3-yl)aniline (**7h**, 16 mg, 0.04 mmol, 2.5 eq) was dissolved in DCM (1.0 mL) and triethylamine (16.2 mg, 22 μL, 0.16 mmol, 10 eq) was added. The solution was added dropwise to a solution of

triphosgene (4.75 mg, 0.016 mmol, 1.0 eq) in DCM (1.0 mL) and stirred for 5 min at room temperature. The reaction mixture was added to a solution of 2-methoxyethan-1-amine (24.0 mg, 27.8 μL, 0.32 mmol, 20.0 eq) in DCM (1.0 mL) and stirred overnight. The solvent was evaporated and the crude mixture was purified by preparatory HPLC purification to afford 1-(2-methoxyethyl)-3-(3-(5-(4-((4-methylpiperazin-1-yl)methyl)phenyl)-1*H*-pyrrolo[2,3-*b*]pyridin-3-yl)phenyl)urea (**7az**, 4.0 mg, 20% yield). ^{1}H NMR (400 MHz, Methanol-d_4) δ 8.78 (d, *J* = 2.0 Hz, 1H), 8.60 (d, *J* = 2.0 Hz, 1H), 8.48 (d, *J* = 2.0 Hz, 1H), 7.81 (s, 1H), 7.76 (s, 1H), 7.61 – 7.53 (m, 4H), 7.45 – 7.25 (m, 4H), 3.54 (s, 2H), 3.50 (s, 2H), 3.47 (s, 3H), 3.27 – 3.12(bs, 8H), 2.87 (s, 3H) ppm. HRMS (APCI$^+$, m/z): calcd. for $C_{29}H_{35}N_6O_2$ [M+H$^+$]: 499.2821, found: 499.2827.

General Procedure for the Synthesis of 9a, 9b, and 9c

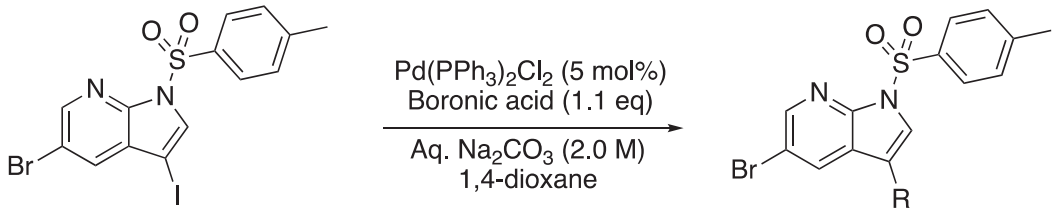

5-Bromo-3-iodo-1-tosyl-1*H*-pyrrolo[2,3-*b*]pyridine[1] (**8**, 1.0 g, 2.1 mmol, 1.0 eq) was dissolved in 1,4-dioxane (20 mL). The boronic acid (2.3 mmol, 1.1 eq) was added, followed by $Pd(PPh_3)_2Cl_2$ (70 mg, 0.1 mmol, 5 mol%). The reaction mixture was degassed by sonication under argon. Aqueous Na_2CO_3 was added and the reaction mixture was stirred at 45 °C until full completion (typically 8h). The reaction mixture was partitioned between EtOAc and brine, the layers separated, and the aqueous layer extracted with EtOAc (2x). The combined organic layers were dried with Na_2SO_4, filtered, and the solvent evaporated. The crude material was purified by column chromatography on silica (0 – 50% EtOAc in hexanes) to yield the desired product (**9a-c**).

4-(5-Bromo-1-tosyl-1H-pyrrolo[2,3-*b*]pyridin-3-yl)-1*H*-indazole (9a).

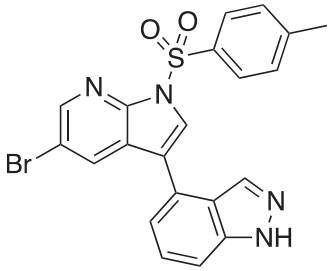

Following the general procedure described above, 4-(5-bromo-1-tosyl-1*H*-pyrrolo[2,3-*b*]pyridin-3-yl)-1*H*-indazole (**9a**) was isolated as a tan-colored solid (461 mg, 47% yield). ^{1}H NMR (400 MHz, Chloroform-*d*) δ 10.29 (bs, 1H), 8.53 (d, *J* = 2.2 Hz, 1H), 8.19 – 8.13 (m, 2H), 8.13 – 8.10 (m, 2H), 8.05 (s, 1H), 7.55 (d, *J* = 8.4 Hz, 1H), 7.49 (dd, *J* = 8.4, 6.9 Hz, 1H), 7.37 – 7.31 (m, 2H), 7.29 (dd, *J* = 6.9, 1.0 Hz, 1H), 2.41 (s, 3H) ppm. HRMS (APCI$^+$, m/z): calcd. for $C_{21}H_{16}N_4O_2SBr$ [M+H$^+$]: 467.0177, found: 467.0176.

5-Bromo-3-(3-fluorophenyl)-1-tosyl-1H-pyrrolo[2,3-*b*]pyridine (9b).

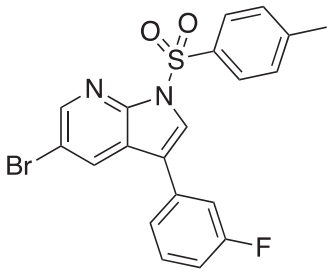

Following the general procedure described above, 5-bromo-3-(3-fluorophenyl)-1-tosyl-1*H*-pyrrolo[2,3-*b*]pyridine (**9b**) was isolated as a colorless solid (617 mg, 67% yield). ^{1}H NMR (400 MHz, Chloroform-*d*) δ 8.50 (d, *J* = 2.1 Hz, 1H), 8.19 (d, *J* = 2.1 Hz, 1H), 8.09 (d, *J* = 8.4 Hz, 2H), 7.90 (s, 1H), 7.44 (td, *J* = 8.0, 5.9 Hz, 1H), 7.36 – 7.28 (m, 3H), 7.27 – 7.21 (m, 1H), 7.08 (tdd, *J* = 8.4, 2.6, 1.0 Hz, 1H), 2.39 (s, 3H) ppm. HRMS (APCI$^+$, m/z): calcd. for $C_{20}H_{15}N_2O_2FSBr$ [M+H$^+$]: 445.0022, found: 445.0020.

5-Bromo-3-(3-chlorophenyl)-1-tosyl-1H-pyrrolo[2,3-*b*]pyridine (9c).

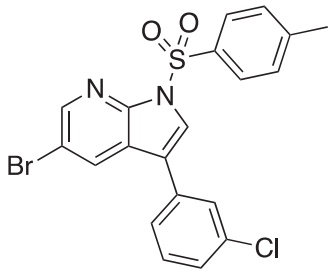

Following the general procedure described above, 5-bromo-3-(3-chlorophenyl)-1-tosyl-1*H*-pyrrolo[2,3-*b*]pyridine (**9c**) was isolated as a colorless solid (850 mg, 88% yield). ^{1}H NMR (400 MHz, Chloroform-*d*) δ 8.50 (d, *J* = 2.1 Hz, 1H), 8.18 (d, *J* = 2.1 Hz, 1H), 8.09 (d, *J* = 8.4 Hz, 2H), 7.89 (s, 1H), 7.56 – 7.50 (m, 1H), 7.46 – 7.40 (m, 2H), 7.40 – 7.34 (m, 1H), 7.31 (d, *J* = 7.8 Hz, 2H), 2.39 (s, 3H) ppm. HRMS (APCI$^+$, m/z): calcd. for $C_{20}H_{15}N_2O_2SBrCl$ [M+H$^+$]: 460.9726, found: 460.9715.

General Procedure for the Synthesis of 10a, 10b, and 10c

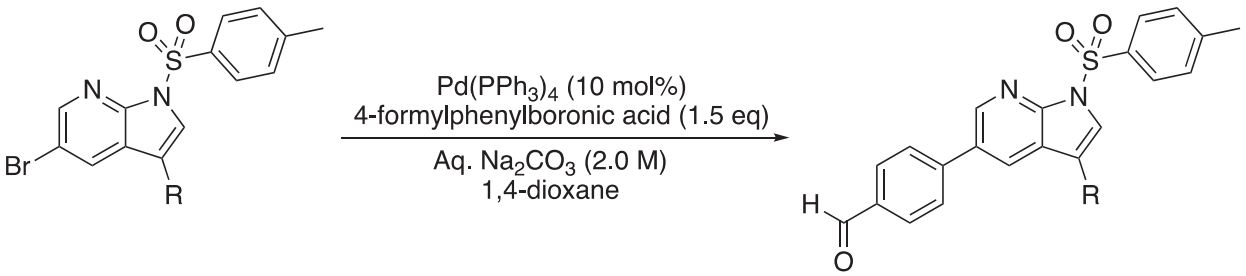

The substrate (**9a-c**, 1.0 mmol, 1.0 eq) was dissolved in 1,4-dioxane (40 mL) in a pressure tube, and 4-formylphenylboronic acid (225 mg, 1.5 mmol, 1.5 eq) was added. The reaction mixture was degassed by sonication under argon, and $Pd(PPh_3)_4$ (116 mg, 0.1 mmol, 10 mol%) was added. After addition of aqueous Na_2CO_3 (12.5 mL, 2.0 M), the reaction mixture was stirred at 100°C overnight. The crude mixture was partitioned between EtOAc and brine, the layers separated and the aqueous layer extracted with EtOAc (3x). The combined organic layers were dried with Na_2SO_4, and filtered over Celite. The solvent was evaporated and the crude material purified by column chromatography on silica (0 – 100% EtOAc in hexanes) to afford the desired product (**10a-c**).

4-(3-(1H-Indazol-4-yl)-1-tosyl-1*H*-pyrrolo[2,3-*b*]pyridin-5-yl)benzaldehyde (10a).

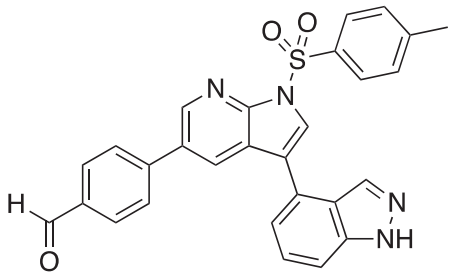

Following the general procedure described above, 4-(3-(1*H*-indazol-4-yl)-1-tosyl-1*H*-pyrrolo[2,3-*b*]pyridin-5-yl)benzaldehyde (**10a**) was isolated as a tan-colored solid (350 mg, 71% yield). ^{1}H NMR (400 MHz, Chloroform-*d*) δ 10.37 (bs, 1H), 10.06 (s, 1H), 8.78 (d, *J* = 2.2 Hz, 1H), 8.23 – 8.17 (m, 3H), 8.14 (d, *J* = 1.1 Hz, 1H), 8.10 (s, 1H), 7.96 (d, *J* = 8.3 Hz, 2H), 7.72 (d, *J* = 8.2 Hz, 2H), 7.59 – 7.51 (m, 2H), 7.40 – 7.32 (m, 3H), 2.41 (s, 3H) ppm. HRMS (APCI$^+$, m/z): calcd. for $C_{28}H_{21}N_4O_3S$ [M+H$^+$]: 493.1334, found: 493.1329.

4-(3-(3-Fluorophenyl)-1-tosyl-1H-pyrrolo[2,3-*b*]pyridin-5-yl)benzaldehyde (10b).

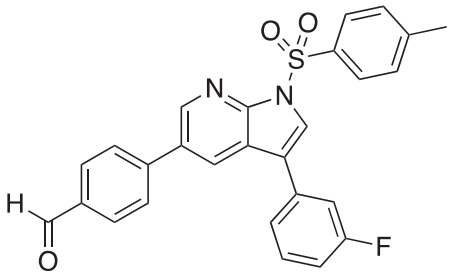

Following the general procedure described above, 4-(3-(3-fluorophenyl)-1-tosyl-1*H*-pyrrolo[2,3-*b*]pyridin-5-yl)benzaldehyde (**10b**) was isolated as a colorless solid (466 mg, 99% yield). ^{1}H NMR (400 MHz, Chloroform-*d*) δ 10.08 (s, 1H), 8.74 (d, *J* = 2.1 Hz, 1H), 8.26 (d, *J* = 2.1 Hz, 1H), 8.16 (d, *J* = 8.4 Hz, 2H), 7.99 (d, *J* = 8.4 Hz, 2H), 7.96 (s, 1H), 7.74 (d, *J* = 8.2 Hz, 2H), 7.47 (td, *J* = 7.9, 5.8 Hz, 1H), 7.40 (dt, *J* = 7.7, 1.3 Hz, 1H), 7.36 – 7.28 (m, 3H), 7.10 (tdd, *J* = 8.4, 2.6, 1.1 Hz, 1H), 2.40 (s, 3H) ppm. HRMS (APCI$^+$, m/z): calcd. for $C_{27}H_{20}N_2O_3FS$ [M+H$^+$]: 471.1179, found: 471.1185.

4-(3-(3-Chlorophenyl)-1-tosyl-1H-pyrrolo[2,3-*b*]pyridin-5-yl)benzaldehyde (10c).

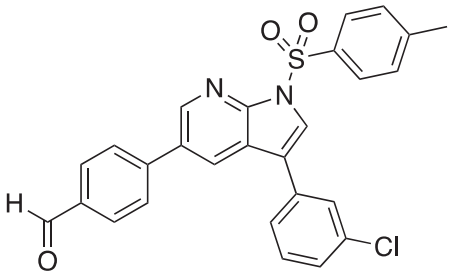

Following the general procedure described above, scaled up to 2.0 mmol starting material, 4-(3-(3-chlorophenyl)-1-tosyl-1*H*-pyrrolo[2,3-*b*]pyridin-5-yl)benzaldehyde (**10c**) was isolated as a colorless solid (730 mg, 87% yield). ^{1}H NMR (400 MHz, Chloroform-*d*) δ 10.08 (s, 1H), 8.74 (d, *J* = 2.1 Hz, 1H), 8.24 (d, *J* = 2.1 Hz, 1H), 8.16 (d, *J* = 8.4 Hz, 2H), 7.99 (d, *J* = 8.2 Hz, 2H), 7.95 (s, 1H), 7.74 (d, *J* = 8.2 Hz, 2H), 7.59 (t, *J* = 1.8 Hz, 1H), 7.50 (dt, *J* = 7.6, 1.5 Hz, 1H), 7.43 (t, *J* = 7.7 Hz, 1H), 7.38 (ddd, *J* = 7.9, 2.0, 1.3 Hz, 1H), 7.36 – 7.29 (m, 2H), 2.40 (s, 3H) ppm. HRMS (APCI$^+$, m/z): calcd. for $C_{27}H_{20}N_2O_3ClS$ [M+H$^+$]: 487.0883, found: 487.0878.

General Procedure for the Synthesis of 12a-l

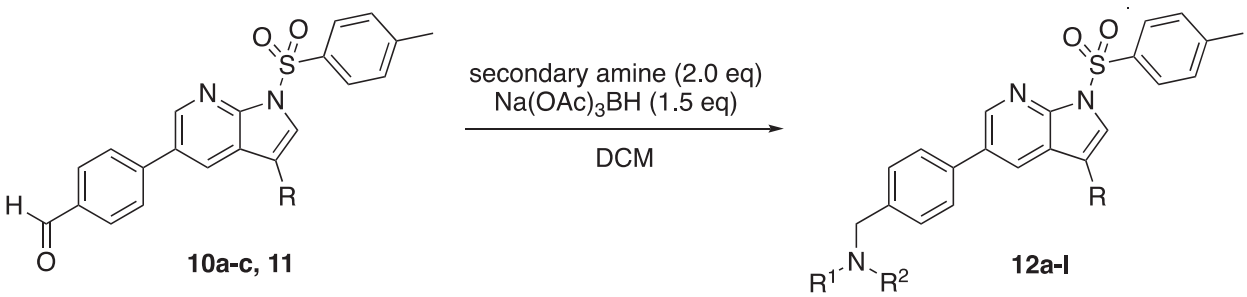

The aldehyde (**10a-c**, or **11** (Goodfellow et al., 2013)) (0.5 mmol, 1.0 eq) was dissolved in dichloromethane and the corresponding amine (1.0 mmol, 2.0 eq) and $Na(OAc)_3BH$ (159 mg, 0.75 mmol, 1.5 eq) were added. The reaction mixture was stirred at room temperature overnight, partitioned between dichloromethane and brine. The aqueous layer was extracted with dichloromethane (2x), the combined organic layers dried with Na_2SO_4, filtered, and the solvent evaporated. The crude product was used in the deprotection step without further purification.

The intermediate was dissolved in a mixture of acetone (20 mL), methanol (30 mL) and aqueous NaOH (2.0 M, 15 mL) and stirred at 65°C for 3 h. The reaction mixture was partitioned between ethyl acetate and aqueous NaOH (1.0 M). The layers were separated and the aqueous layer was extracted with ethyl acetate (2x). The combined organic layers were washed with brine, dried with Na_2SO_4, filtered and the solvent evaporated. The crude material was purified by preparatory HPLC purification to afford the product (**12a-l**).

3-(4-(3-(1H-Indol-5-yl)-1*H*-pyrrolo[2,3-*b*]pyridin-5-yl)benzyl)-8-oxa-3-azabicyclo[3.2.1]octane (12a).

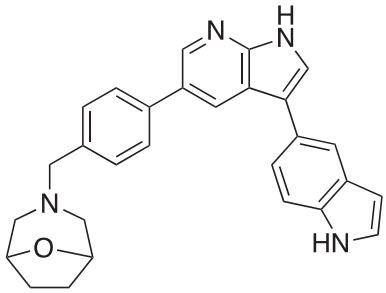

Following the general procedure described above, with 4-(3-(1*H*-Indol-5-yl)-1-tosyl-1*H*-pyrrolo[2,3-*b*]pyridin-5-yl)benzaldehyde (**11** (Goodfellow et al., 2013), 100 mg, 0.2 mmol) and 8-oxa-3-azabicyclo[3.2.1]octane (45 mg, 0.4 mmol, 2.0 eq) as the starting materials, 3-(4-(3-(1*H*-indol-5-yl)-1*H*-pyrrolo[2,3-*b*]pyridin-5-yl)benzyl)-8-oxa-3-azabicyclo[3.2.1]octane (**12a**) was isolated as a light-brown solid (37.2 mg, 43% yield over two steps). ^{1}H NMR (500 MHz, Methanol-d_4) δ 8.42 (d, *J* = 2.1 Hz, 1H), 8.40 (d, *J* = 2.1 Hz, 1H), 7.83 (d, *J* = 1.5 Hz, 1H), 7.55 (s, 1H), 7.52 (d, *J* = 8.1 Hz, 2H), 7.47 (d, *J* = 8.4 Hz, 1H), 7.46 – 7.39 (m, 1H), 7.33 (d, *J* = 7.9 Hz, 2H), 7.24 (d, *J* = 3.1 Hz, 1H), 6.49 (dd, *J* = 3.1, 0.8 Hz, 1H), 4.20 (dd, *J* = 4.7, 2.3 Hz, 2H), 3.41 (s, 2H), 2.52 (d, *J* = 11.5 Hz, 2H), 2.25 (dd, *J* = 11.4, 2.1 Hz, 2H), 2.00 – 1.90 (m, 3H), 1.86 – 1.73 (m, 2H) ppm. HRMS (APCI$^+$, m/z): calcd. for $C_{32}H_{33}N_6O$ [M+H$^+$]: 517.2716, found: 517.2713.

3-(1H-Indol-5-yl)-5-(4-((8-methyl-3,8-diazabicyclo[3.2.1]octan-3-yl)methyl)phenyl)-1*H*-pyrrolo[2,3-*b*]pyridine (12b).

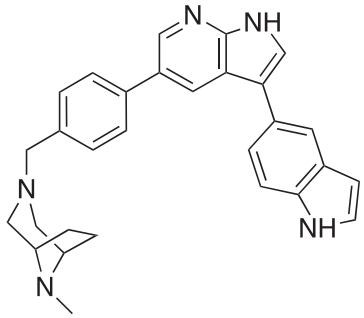

Following the general procedure described above, with 4-(3-(1*H*-Indol-5-yl)-1-tosyl-1*H*-pyrrolo[2,3-*b*]pyridin-5-yl)benzaldehyde (**11** (Goodfellow et al., 2013), 67.1 mg, 0.137 mmol) and 8-methyl-3,8-diazabicyclo[3.2.1]octane (**16b**, 55.5 mg, 0.44 mmol, 3.2 eq) as the starting materials, 3-(1*H*-indol-5-yl)-5-(4-((8-methyl-3,8-diazabicyclo[3.2.1]octan-3-yl)methyl)phenyl)-1*H*-pyrrolo[2,3-*b*]pyridine (**12b**) was isolated as a tan-colored solid (2.6 mg, 4% yield over two steps). ^{1}H NMR (400 MHz, Methanol-d_4) δ 8.57 (d, *J* = 2.0 Hz, 1H), 8.51 (d, *J* = 2.0 Hz, 1H), 7.87 (dd, *J* = 1.6, 0.7 Hz, 1H), 7.70 (d, *J* = 8.1 Hz, 2H), 7.65 (s, 1H), 7.56 – 7.38 (m, 5H), 7.27 (d, *J* = 3.2 Hz, 1H), 3.88 (s, 2H), 3.70 (s, 2H), 2.95 (d, *J* = 12.6 Hz, 2H), 2.80 (s, 3H), 2.57 (d, *J* = 13.0 Hz, 2H), 2.23 (s, 4H) ppm. HRMS (APCI$^+$, m/z): calcd. for $C_{29}H_{30}N_5$ [M+H$^+$]: 448.2501, found: 448.2505.

3-(1H-Indol-5-yl)-5-(4-((3-methyl-3,8-diazabicyclo[3.2.1]octan-8-yl)methyl)phenyl)-1*H*-pyrrolo[2,3-*b*]pyridine (12c).

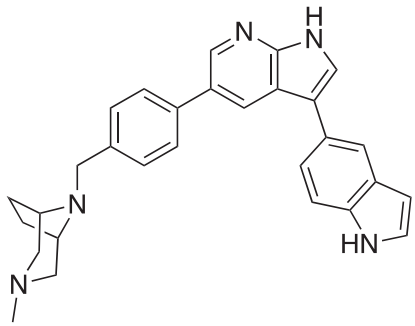

Following the general procedure described above, with 4-(3-(1*H*-Indol-5-yl)-1-tosyl-1*H*-pyrrolo[2,3-*b*]pyridin-5-yl)benzaldehyde (**11** (Goodfellow et al., 2013), 60.2 mg, 0.122 mmol) and 3-methyl-3,8-diazabicyclo[3.2.1]octane (**16a**, 36.6 mg, 0.29 mmol, 2.4 eq) as the starting materials, 3-(1*H*-indol-5-yl)-5-(4-((3-methyl-3,8-diazabicyclo[3.2.1]octan-8-yl)methyl)phenyl)-1*H*-pyrrolo[2,3-*b*]pyridine (**12c**) was isolated as a tan-colored solid (9.6 mg, 18% yield over two steps). ^{1}H NMR (400 MHz, Methanol-d_4) δ 8.74

(d, *J* = 2.0 Hz, 1H), 8.60 (d, *J* = 2.0 Hz, 1H), 7.88 (dd, *J* = 1.7, 0.8 Hz, 1H), 7.86 – 7.79 (m, 2H), 7.74 (s, 1H), 7.68 – 7.64 (m, 3H), 7.54 – 7.50 (m, 1H), 7.48 – 7.43 (m, 2H), 4.12 (s, 2H), 3.84 (bs, 4H), 3.29 (d, *J* = 2.7 Hz, 2H), 3.10 (bs, 4H), 2.69 (s, 3H) ppm. HRMS (APCI$^+$, m/z): calcd. for $C_{29}H_{30}N_5$ [M+H$^+$]: 448.2501, found: 448.2503.

4-(5-(4-((8-Methyl-3,8-diazabicyclo[3.2.1]octan-3-yl)methyl)phenyl)-1H-pyrrolo[2,3-*b*]pyridin-3-yl)-1*H*-indazole (12d).

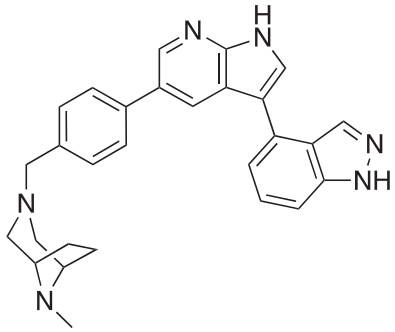

Following the general procedure described above, with 4-(3-(1*H*-indazol-4-yl)-1-tosyl-1*H*-pyrrolo[2,3-*b*]pyridin-5-yl)benzaldehyde (**10a**, 49.2 mg, 0.1 mmol) and 8-methyl-3,8-diazabicyclo[3.2.1]octane (**16b**, 39.1 mg, 0.31 mmol, 3.1 eq) as the starting materials, 4-(5-(4-((8-methyl-3,8-diazabicyclo[3.2.1]octan-3-yl)methyl)phenyl)-1*H*-pyrrolo[2,3-*b*]pyridin-3-yl)-1*H*-indazole (**12d**) was isolated as a light-brown solid (11.7 mg, 26% yield over two steps). ^{1}H NMR (400 MHz, Methanol-d_4) δ 8.61 (d, *J* = 2.0 Hz, 1H), 8.55 (d, *J* = 2.0 Hz, 1H), 8.18 (d, *J* = 0.9 Hz, 1H), 7.95 (s, 1H), 7.67 (d, *J* = 8.2 Hz, 2H), 7.55 – 7.50 (m, 2H), 7.47 (d, *J* = 8.2 Hz, 2H), 7.43 (dd, *J* = 6.5, 1.4 Hz, 1H), 3.88 (s, 2H), 3.70 (s, 2H), 2.94 (dd, *J* = 13.1, 2.8 Hz, 2H), 2.80 (s, 3H), 2.67 – 2.62 (m, 2H), 2.27 – 2.19 (bs, 4H) ppm. HRMS (APCI$^+$, m/z): calcd. for $C_{28}H_{29}N_6$ [M+H$^+$]: 449.2454, found: 449.2462.

4-(5-(4-((3-Methyl-3,8-diazabicyclo[3.2.1]octan-8-yl)methyl)phenyl)-1H-pyrrolo[2,3-*b*]pyridin-3-yl)-1*H*-indazole (12e).

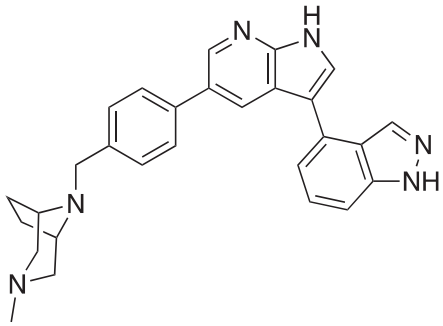

Following the general procedure described above, with 4-(3-(1*H*-indazol-4-yl)-1-tosyl-1*H*-pyrrolo[2,3-*b*]pyridin-5-yl)benzaldehyde (**10a**, 49.2 mg, 0.1 mmol) and 3-methyl-3,8-diazabicyclo[3.2.1]octane (**16a**, 34.0 mg, 0.27 mmol, 2.7 eq) as the starting materials, 4-(5-(4-((3-methyl-3,8-diazabicyclo[3.2.1]octan-8-yl)methyl)phenyl)-1*H*-pyrrolo[2,3-*b*]pyridin-3-yl)-1*H*-indazole (**12e**) was isolated as a light-brown solid (12.0 mg, 27% yield over two steps). ^{1}H NMR (400 MHz, Methanol-d_4) δ 8.60 (d, *J* = 2.1 Hz, 1H), 8.45 (d, *J* = 2.1 Hz, 1H), 8.18 (d, *J* = 0.7 Hz, 1H), 7.90 (s, 1H), 7.77 (d, *J* = 8.2 Hz, 2H), 7.62 (d, *J* = 8.2 Hz, 2H), 7.54 – 7.51 (m, 2H), 7.43 (dd, *J* = 5.6, 2.3 Hz, 1H), 4.09 (s, 2H), 3.80 (s, 2H), 3.18 (d, *J* = 11.9 Hz, 2H), 2.94 (d, *J* = 12.6 Hz, 2H), 2.61 (s, 3H), 2.45 – 2.36 (m, 2H), 2.14 (d, *J* = 8.6 Hz, 2H) ppm. HRMS (APCI$^+$, m/z): calcd. for $C_{28}H_{29}N_6$ [M+H$^+$]: 449.2454, found: 449.2455.

3-(3-Chlorophenyl)-5-(4-((3-methyl-3,8-diazabicyclo[3.2.1]octan-8-yl)methyl)phenyl)-1H-pyrrolo[2,3-*b*]pyridine (12f).

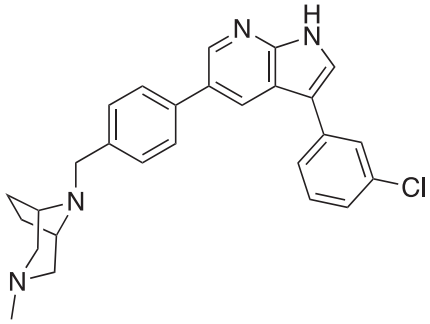

Following the general procedure described above, with 4-(3-(3-chlorophenyl)-1-tosyl-1*H*-pyrrolo[2,3-*b*]pyridin-5-yl)benzaldehyde (**10c**, 48.6 mg, 0.1 mmol) and 3-methyl-3,8-diazabicyclo[3.2.1]octane (**16a**, 25.2 mg, 0.2 mmol, 2.0 eq) as the starting materials, 3-(3-chlorophenyl)-5-(4-((3-methyl-3,8-diazabicyclo[3.2.1]octan-8-yl)methyl)phenyl)-1*H*-pyrrolo[2,3-*b*]pyridine (**12f**) was isolated as a pale-yellow solid (18.0 mg, 41% yield over two steps). ^{1}H NMR (400 MHz, Methanol-d_4) δ 8.54 (d, *J* = 2.1 Hz, 1H), 8.46 (d, *J* = 2.1 Hz, 1H), 7.81 – 7.75 (m, 3H), 7.70 (t, *J* = 1.9 Hz, 1H), 7.68 – 7.61 (m, 3H), 7.45 (t, *J* = 7.9 Hz, 1H), 7.30 (ddd, *J* = 8.0, 2.1, 1.0 Hz, 1H), 4.11 (s, 2H), 3.82 (s, 2H), 3.25 – 3.16 (m, 2H), 3.04 – 2.94 (m, 2H), 2.62 (s, 3H), 2.42 (dd, *J* = 9.6, 4.7 Hz, 2H), 2.17 (t, *J* = 7.3 Hz, 2H) ppm. HRMS (APCI$^+$, m/z): calcd. for $C_{27}H_{28}N_4Cl$ [M+H$^+$]: 443.2002, found: 443.2005.

5-(4-([1,4'-Bipiperidin]-1'-ylmethyl)phenyl)-3-(3-fluorophenyl)-1H-pyrrolo[2,3-*b*]pyridine (12g).

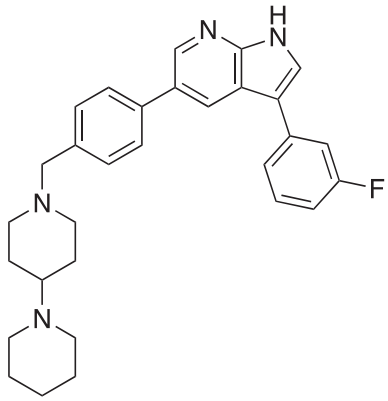

Following the general procedure described above, with 4-(3-(3-fluorophenyl)-1-tosyl-1*H*-pyrrolo[2,3-*b*]pyridin-5-yl)benzaldehyde (**10b**, 26.0 mg, 0.055 mmol) and 4-piperidinopiperidine (18.6 mg, 0.11 mmol, 2.0 eq) as the starting materials, 5-(4-([1,4'-bipiperidin]-1'-ylmethyl)phenyl)-3-(3-fluorophenyl)-1*H*-pyrrolo[2,3-*b*]pyridine (**12g**) was isolated as an off-white solid (6.2 mg, 24% yield over two steps). ^{1}H NMR (400 MHz, Methanol-d_4) δ 8.58 (d, *J* = 2.0 Hz, 1H), 8.56 (d, *J* = 2.1 Hz, 1H), 7.86 (d, *J* = 8.2 Hz, 2H), 7.82 (s, 1H), 7.66 (d, *J* = 8.2 Hz, 2H), 7.57 – 7.53 (m, 1H), 7.52 – 7.42 (m, 2H), 7.04 (tdd, *J* = 8.2, 2.6, 1.0 Hz, 1H), 4.43 (s, 2H), 3.72 (d, *J* = 12.9 Hz, 2H), 3.63 – 3.47 (m, 4H), 3.23 – 3.12 (m, 4H), 3.03 (t, *J* = 11.3 Hz, 2H), 2.41 (d, *J* = 13.5 Hz, 2H), 2.20 – 2.08 (m, 3H), 2.04 – 1.94 (m, 2H), 1.86 – 1.73 (m, 2H), 1.64 – 1.46 (m, 1H), 1.42 – 1.26 (m, 2H) ppm. HRMS (APCI$^+$, m/z): calcd. for $C_{30}H_{34}N_4F$ [M+H$^+$]: 469.2768, found: 469.2771.

2-(4-(4-(3-(3-Fluorophenyl)-1H-pyrrolo[2,3-*b*]pyridin-5-yl)benzyl)piperazin-1-yl)ethan-1-ol (12h).

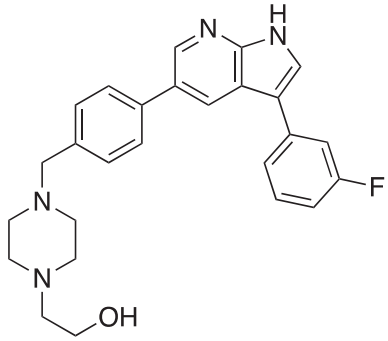

Following the general procedure described above, with 4-(3-(3-fluorophenyl)-1-tosyl-1*H*-pyrrolo[2,3-*b*]pyridin-5-yl)benzaldehyde (**10b**, 318 mg, 0.675 mmol) and 1-(2-hydroxyethyl)piperazine (176 mg, 166 μL, 1.35 mmol, 2.0 eq) as the starting materials, 2-(4-(4-(3-(3-fluorophenyl)-1*H*-pyrrolo[2,3-*b*]pyridin-5-yl)benzyl)piperazin-1-yl)ethan-1-ol (**12h**) was isolated as an off-white solid (153.7 mg, 53% yield over two steps). ^{1}H NMR (400 MHz, Methanol-d_4) δ 8.62 (d, *J* = 2.0 Hz, 1H), 8.60 (d, *J* = 2.0 Hz, 1H), 7.85 (s, 1H), 7.80 (d, *J* = 8.2 Hz, 2H), 7.62 (d, *J* = 8.2 Hz, 2H), 7.55 (dt, *J* = 7.8, 1.3 Hz, 1H), 7.51 – 7.42 (m, 2H), 7.05 (dddd, *J* = 9.0, 8.2, 2.6, 1.1 Hz, 1H), 4.22 (s, 2H), 3.95 – 3.85 (m, 2H), 3.58 (bs, 4H), 3.34 (bs, 6H) ppm. HRMS (APCI$^+$, m/z): calcd. for $C_{26}H_{28}N_4OF$ [M+H$^+$]: 431.2247, found: 431.2250.

(R)-1-(4-(3-(3-Fluorophenyl)-1*H*-pyrrolo[2,3-*b*]pyridin-5-yl)benzyl)pyrrolidin-3-ol (12i).

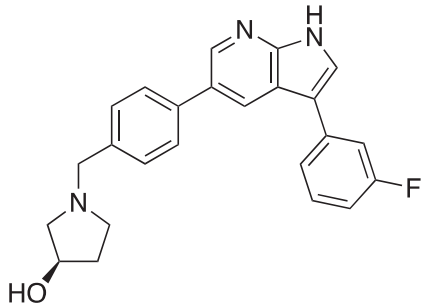

Following the general procedure described above, with 4-(3-(3-fluorophenyl)-1-tosyl-1*H*-pyrrolo[2,3-*b*]pyridin-5-yl)benzaldehyde (**10b**, 318 mg, 0.675 mmol) and (*R*)-3-pyrrolidinol (118 mg, 109 μL, 1.35 mmol, 2.0 eq) as the starting materials, (*R*)-1-(4-(3-(3-fluorophenyl)-1*H*-pyrrolo[2,3-*b*]pyridin-5-yl)benzyl)pyrrolidin-3-ol (**12i**) was isolated as an off-white solid (113 mg, 43% yield over two steps). ^{1}H NMR (400 MHz, Methanol-d_4) δ 8.56 (d, *J* = 2.0 Hz, 1H), 8.53 (d, *J* = 2.0 Hz, 1H), 7.84 – 7.77 (m, 3H), 7.68 – 7.61 (m, 2H), 7.52 (dt, *J* = 7.8, 1.3 Hz, 1H), 7.50 – 7.38 (m, 2H), 7.02 (dddd, *J* = 9.0, 8.2, 2.6, 1.1 Hz, 1H), 4.66 – 4.34 (m, 3H), 3.82 – 3.42 (m, 2H), 3.41 – 3.20 (m, 2H), 2.49 – 1.92 (m, 2H) ppm. HRMS (APCI$^+$, m/z): calcd. for $C_{24}H_{23}N_3OF$ [M+H$^+$]: 388.1825, found: 388.1824.

5-(4-((4-(tert-Butyl)piperazin-1-yl)methyl)phenyl)-3-(3-fluorophenyl)-1*H*-pyrrolo[2,3-*b*]pyridine (12j).

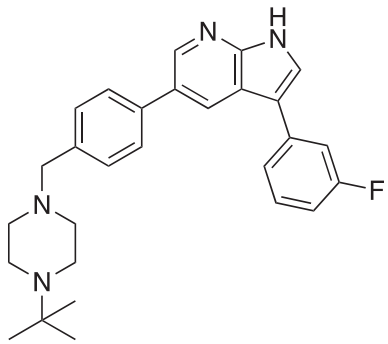

Following the general procedure described above, with 4-(3-(3-fluorophenyl)-1-tosyl-1*H*-pyrrolo[2,3-*b*]pyridin-5-yl)benzaldehyde (**10b**, 32.8 mg, 0.055 mmol) and 1-*tert*-butylpiperazine (15.7 mg, 0.11 mmol, 2.0 eq) as the starting materials, 5-(4-((4-(*tert*-butyl)piperazin-1-yl)methyl)phenyl)-3-(3-fluorophenyl)-1*H*-pyrrolo[2,3-*b*]pyridine (**12j**) was isolated as an off-white solid (9.8 mg, 40% yield over two steps). ^{1}H NMR (400 MHz, Methanol-d_4) δ 8.63 (d, *J* = 1.9 Hz, 1H), 8.60 (bs, 1H), 7.85 (s, 1H), 7.83 – 7.78 (m, 2H), 7.65 – 7.60 (m, 2H), 7.56 (dt, *J* = 7.8, 1.3 Hz, 1H), 7.52 – 7.42 (m, 2H), 7.05 (dddd, *J* = 9.0, 8.2, 2.6, 1.0 Hz, 1H), 4.22 (s, 2H), 3.89 – 3.04 (m, 8H), 1.44 (s, 9H) ppm. HRMS (APCI$^+$, m/z): calcd. for $C_{28}H_{32}N_4F$ [M+H$^+$]: 443.2611, found: 443.2610.

2-(4-(4-(3-(3-Chlorophenyl)-1H-pyrrolo[2,3-*b*]pyridin-5-yl)benzyl)piperazin-1-yl)ethan-1-ol (Protstetin/12k).

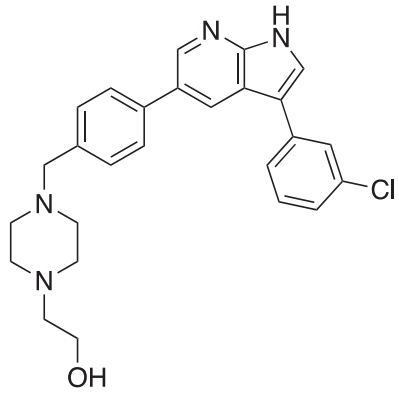

Following the general procedure described above, with 4-(3-(3-chlorophenyl)-1-tosyl-1*H*-pyrrolo[2,3-*b*]pyridin-5-yl) benzaldehyde (**10c**, 418 mg, 0.86 mmol) and 1-(2-hydroxyethyl)piperazine (224 mg, 211 μL, 1.72 mmol, 2.0 eq) as the starting materials, 2-(4-(4-(3-(3-chlorophenyl)-1*H*-pyrrolo[2,3-*b*]pyridin-5-yl)benzyl)piperazin-1-yl)ethan-1-ol (**Prostetin/12k**) was isolated as an off-white solid (139.9 mg, 36% yield over two steps). ^{1}H NMR (400 MHz, Methanol-d_4) δ 8.57 (d, *J* = 2.0 Hz, 1H), 8.54 (d, *J* = 2.0 Hz, 1H), 7.80 (s, 1H), 7.76 (d, *J* = 8.3 Hz, 2H), 7.65 (t, *J* = 1.9 Hz, 1H), 7.64 – 7.57 (m, 3H), 7.42 (t, *J* = 7.9 Hz, 1H), 7.29 (ddd, *J* = 8.0, 2.1, 1.0 Hz, 1H), 4.27 (s, 2H), 3.93 – 3.86 (m, 2H), 3.62 (s, 4H), 3.41 (s, 4H), 3.35 – 3.31 (m, 2H) ppm. HRMS (APCI$^+$, m/z): calcd. for $C_{26}H_{28}N_4OCl$ [M+H$^+$]: 447.1952, found: 447.1954.

(R)-1-(4-(3-(3-Chlorophenyl)-1*H*-pyrrolo[2,3-*b*]pyridin-5-yl)benzyl)pyrrolidin-3-ol (12l).

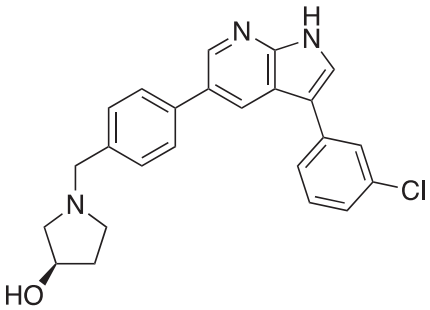

Following the general procedure described above, with 4-(3-(3-chlorophenyl)-1-tosyl-1*H*-pyrrolo[2,3-*b*]pyridin-5-yl)benzaldehyde (**10c**, 177 mg, 0.86 mmol) and (*R*)-3-pyrrolidinol (150 mg, 139 μL, 1.72 mmol, 2.0 eq) as the starting materials, (*R*)-1-(4-(3-(3-chlorophenyl)-1*H*-pyrrolo[2,3-*b*]pyridin-5-yl)benzyl)pyrrolidin-3-ol (**12l**) was isolated as an off-white solid (177 mg, 51% yield over two steps). ^{1}H NMR (400 MHz, Methanol-d_4) δ 8.52 (d, *J* = 2.0 Hz, 1H), 8.42 (d, *J* = 2.0 Hz, 1H), 7.78 – 7.71 (m, 3H), 7.64 – 7.60 (m, 3H), 7.58 (ddd, *J* = 7.7, 1.7, 1.1 Hz, 1H), 7.39 (t, *J* = 7.9 Hz, 1H), 7.25 (ddd, *J* = 8.0, 2.2, 1.0 Hz, 1H), 4.58 (s, 1H), 4.54 – 4.32 (m, 2H), 3.82 – 3.39 (m, 4H), 2.50 – 1.96 (m, 2H) ppm. HRMS (APCI$^+$, m/z): calcd. for $C_{24}H_{23}N_3OCl$ [M+H$^+$]: 404.1530, found: 404.1529.

General Procedure for the Synthesis of Boronic Acids 13a-e

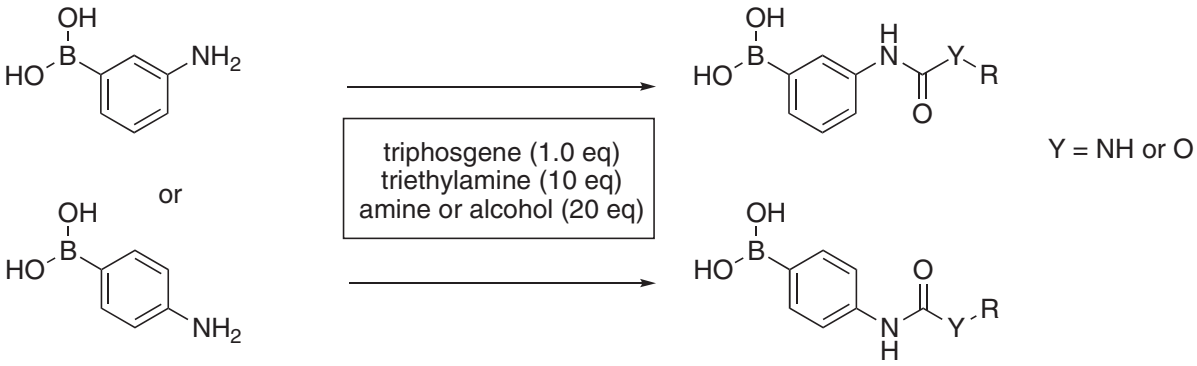

The boronic acid (3-aminophenylboronic acid or 4-aminophenylboronic acid, 87 mg, 0.5 mmol, 2.5 eq) was suspended in DCM (4 mL) and triethylamine (202 mg, 277 μL, 2.0 mmol, 10 eq) was added. The resulting solution was added dropwise to a solution triphosgene (59 mg, 0.2 mmol, 1.0 eq) in DCM (6 mL) and stirred for 5 min at room temperature. The amine (0.6 mmol, 3 eq) or alcohol (excess) was added dropwise and the mixture was stirred overnight at room temperature. The solvent was evaporated, toluene was added and the solvent was evaporated again. The crude material was analyzed by NMR and used in the next step without further purification.

(3-(3-Methylureido)phenyl)boronic acid (13a).

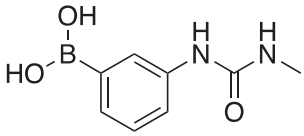

Following the general procedure described above, with 3-aminophenylboronic acid and methylamine, (3-(3-methylureido)phenyl) boronic acid (**13a**) was isolated as an off-white solid and used in the next step without further purification. ^{1}H NMR (400 MHz, Methanol-d_4) δ 7.49 (bs, 1H), 7.38 (bs, 1H), 7.22 (d, J = 5.3 Hz, 2H), 2.77 (s, 3H).

(3-((Methoxycarbonyl)amino)phenyl)boronic acid (13b).

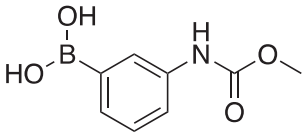

Following the general procedure described above, with 3-aminophenylboronic acid and methanol, (3-((methoxycarbonyl)amino) phenyl)boronic acid (**13b**) was isolated as an off-white solid and used in the next step without further purification. ^{1}H NMR (400 MHz, Methanol-d_4) δ 7.59 (bs, 1H), 7.48 (bs, 1H), 7.26 (d, J = 5.2 Hz, 2H), 3.73 (s, 3H).

(4-(3-Methylureido)phenyl)boronic acid (13c).

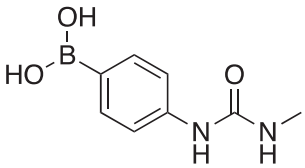

Following the general procedure described above, with 4-aminophenylboronic acid and methylamine, (4-(3-methylureido)phenyl) boronic acid (**13c**) was isolated as an off-white solid and used in the next step without further purification. ^{1}H NMR (400 MHz, Methanol-d_4) δ 7.62 (d, J = 8.5 Hz, 2H), 7.37 (d, J = 8.5 Hz, 2H), 2.77 (s, 3H).

(4-((Methoxycarbonyl)amino)phenyl)boronic acid (13d).

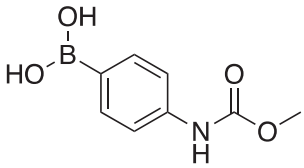

Following the general procedure described above, with 4-aminophenylboronic acid and methanol, (4-((methoxycarbonyl)amino) phenyl)boronic acid (**13d**) was isolated as an off-white solid and used in the next step without further purification. ^{1}H NMR (400 MHz, Methanol-d_4) δ 7.65 (d, J = 8.6 Hz, 1H), 7.43 (d, J = 8.6 Hz, 2H), 3.74 (s, 3H).

(3-(3-Phenylureido)phenyl)boronic acid (13e).

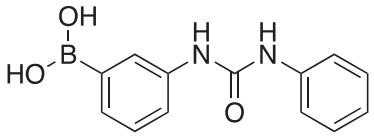

Following the general procedure described above, with 3-aminophenylboronic acid and aniline, (3-(3-phenylureido)phenyl)boronic acid (**13e**) was isolated as an off-white solid and used in the next step without further purification. ^{1}H NMR (400 MHz, Methanol-d_4) δ 7.62 (bs, 1H), 7.51 (d, J = 7.4 Hz, 1H), 7.34 – 7.23 (m, 2H), 7.08 (dd, J = 8.5, 7.4 Hz, 2H), 6.71 (dt, J = 7.7, 1.1 Hz, 2H), 6.67 (tt, J = 7.4, 1.1 Hz, 1H).

General Procedure for the Synthesis of Bicyclic Piperazines 16a-b

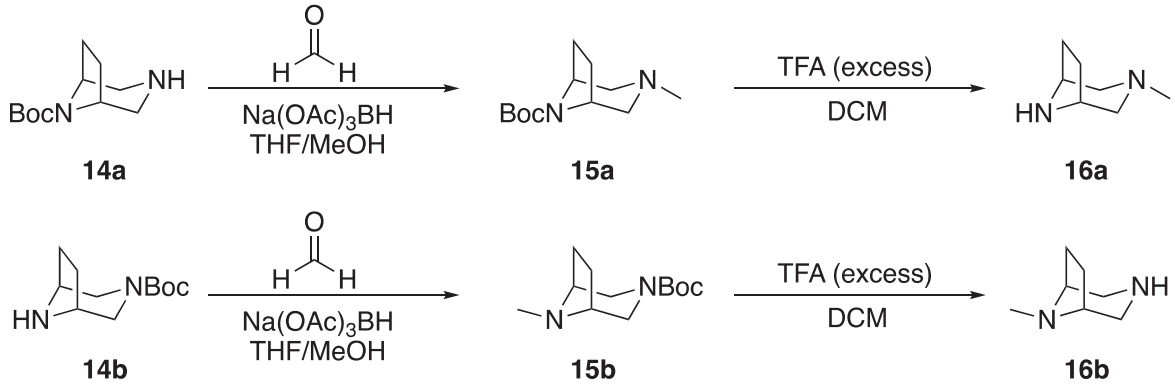

The Boc-protected bicyclic piperazine (**14a-b**; 250 mg, 1.18 mmol, 1.0 eq) was dissolved in a mixture of THF/MeOH (1:1). Formaldehyde (37% in H_2O, 287 μL, 3.53 mmol, 3.0 eq) was added, followed by addition of $Na(OAc)_3BH$ (274.5 mg, 1.30 mmol, 1.1 eq), and the reaction mixture was stirred overnight. The solvent was evaporated and the crude product purified by column chromatography on silica (0 – 20% MeOH in DCM). The product was visualized on the TLC plate using a $KMnO_4$ stain.

In order to remove the Boc-group, the product (**15a-b**) was dissolved in DCM, an excess of TFA was added, and the reaction mixture was stirred at room temperature overnight. The solvent was evaporated, toluene was added and the solvent was evaporated again. The crude products (**16a-b**) were used in the next step without further purification and the spectroscopic data matched those reported in literature (Paliulis et al., 2013).

In Vitro Microsomal Stability

The microsomal stability assay was performed in round-bottom 96-well plates (Perkin-Elmer). To each well was added phosphate buffer (182.2 μL, pH 7.4, 100 mM) followed by addition of NADPH regenerating system solution A (10 μL), and NADPH regenerating system solution B (2 μL) (Corning). A stock solution of the compound to be analyzed (0.8 μL. 5 mM) or ethoxycoumarin (positive control, 0.8 μL, 5 mM) was added and the mixture was warmed to 37°C for 5 min. The mouse microsomes (CD-1, 5 μL, thawed in a 37°C water bath before use, 20 mg/mL, Thermo Fisher) were added. At selected time points (0, 15, 30, 45, 60 and 120 min) aliquots (15 μL) were withdrawn from the plate and quenched upon addition to cold acetonitrile (60 μL), containing an internal standard (5 μM) in a 96-well plate. The samples were centrifuged at 13,000 rpm for 10 min at 4°C. The supernatant (40 μL) was withdrawn and transferred to a sample vial with insert. The samples were analyzed by LC-MS.

LC-MS analysis was performed on a platform comprising a Thermo Scientific Dionex Ultimate 3000 and a Bruker amaZon SL equipped with an electrospray ionization source controlled by Bruker Hystar 3.2. Chromatographic separation was performed by injecting 5 μL of the sample onto an Agilent Eclipse Plus C18 column (2.1 x 50 mm, 3.5 μm) maintained at 20°C. The flow rate was maintained at 400 μL/min. The initial flow conditions were 60% solvent A (water containing 0.1% acetic acid) and 40% solvent B (methanol containing 0.1% acetic acid). Solvent B was raised to 60% over 0.25 min and to 70% by 6.75 min. Solvent B was raised to 95% by 7.00 min and lowered back to initial conditions (40%) by 8.00 min with a total run time of 9.00 min.

In Vivo Pharmacokinetics

For *in vivo* administration, 40 mg/mL DMSO stocks of compound **1** and **Prostetin/12k** were further diluted to 2 mg/mL in a vehicle containing 40% PEG-400 (Sigma) and 55% of a (2-hydroxypropyl)-beta-cyclodextrin solution (20% in nanopure water, Sigma). Compounds were delivered at 10 mg/kg by intraperitoneal injection or oral gavage to 8-week old wild-type mice. After 15 min, 3 h, 8 h or 24 h, animals were decapitated to collect trunk blood and dissect fresh brain tissue. Blood samples were treated with EDTA solution (50 mM final concentration) to prevent coagulation and centrifuged for 10 min at 845 rcf at 4°C to separate plasma. Fresh brains were lysed in 5 volumes of ddH2O.

Plasma samples were transferred to Eppendorf tubes (50 μL per sample) and diluted with acetonitrile (200 μL). The samples were sonicated for 1 min followed by centrifugation at 16,000 rpm for 10 min. The supernatant was transferred to another Eppendorf tube and the solvent evaporated overnight. The samples were reconstituted in a mixture of 40 μL acetonitrile and 10 μL water transferred to a sample vial with insert, and analyzed by LC-MS.

Homogenized brain samples (250 μL) were transferred to Eppendorf tubes and diluted with acetonitrile (750 μL). The samples were sonicated for 1 min followed by centrifugation at 16,000 rpm for 10 min. The supernatant (900 μL) was transferred to another Eppendorf tube and the solvent evaporated overnight. The samples were reconstituted in a mixture of 80 μL acetonitrile and 20 μL water, transferred to a sample vial with insert, and analyzed by LC-MS.

LC-MS analysis was performed on a platform comprising a Thermo Scientific Dionex Ultimate 3000 and a Bruker amaZon SL equipped with an electrospray ionization source controlled by Bruker Hystar 3.2. The compound concentration in each plasma

sample was determined using a calibration curve. Chromatographic separation was performed by injecting 10 μL of the sample onto an Agilent Eclipse Plus C18 column (2.1 x 50 mm, 3.5 μm) maintained at 20°C. The flow rate was maintained at 400 μL/min. The initial flow conditions were 60% solvent A (water containing 0.1% acetic acid) and 40% solvent B (methanol containing 0.1% acetic acid). Solvent B was raised to 60% over 0.25 min and to 70% by 6.75 min. Solvent B was raised to 95% by 7.00 min and lowered back to initial conditions (40%) by 8.00 min with a total run time of 9.00 min.

Commercial In Vitro Kinase Inhibition Assays

Kinase inhibition assays were carried out by Reaction Biology Corp. using the "HotSpot" assay platform as described (Anastassiadis et al., 2011). In brief, recombinant kinases and their appropriate substrates were combined at 25°C with test compound and a mixture of ATP and ^{33}P ATP to a final concentration of 10 μM. For IC_{50} determination, 10 concentrations of each compound were tested for each kinase (0.0002 – 0.1 μM, 2-fold serial dilution for HGK and MINK1; 0.002 – 1 μM, 2-fold serial dilution for MLK1 and MLK3); otherwise, single compound concentrations were used, as indicated (Tables S3–S5 and S6). After 120 min, reactions were spotted onto P81 ion exchange filter paper, and unbound phosphate was removed through washing. Background signal was assessed from control reactions containing inactive enzymes. Kinase activity data were expressed as the percent remaining kinase activity in samples containing test compound vs. samples containing DMSO alone.

Microglia LPS Treatment and TNFα ELISAs

Immortalized N9 mouse microglia cells (Corradin et al., 1993) were plated at 8000 cells / well in gelatin-coated (0.1%, EMD Millipore) 96-well plates in DMEM containing FBS (10%, Fisher Scientific) and Glutamax (1%, Life Technologies). 24 h after plating, cells were treated with LPS from E. coli O111:B4 (Sigma) plus test compounds at the indicated concentrations. 24 h after the initiation of LPS treatment, 50 μL of cell culture media (25% of the final culture volume) were used to perform quantitative ELISAs for TNFα release according to the manufacturer's instructions (R&D Systems). Absorbance was assessed at 450 nm on a spectrophotometer (TECAM), and readings at 540 nm were used for wavelength correction. N9 cells remaining in the culture dishes were treated with AlamarBlue (Thermo Fisher) to assess viability. 5 μL AlamarBlue was added to each well (containing 50 μL culture media) and incubated for 4h at 37°C. Absorbance was assessed at 570 nm, and readings at 600 nm were used for wavelength correction.

QUANTIFICATION AND STATISTICAL ANALYSIS

Two-way hierarchical clustering analysis was performed using Spotfire software (version 2017, TIBCO) to rank the shared targets of hit compounds (Figure 1B). Strong inhibition of kinase activity was defined as <20% kinase activity remaining at 0.5 μM inhibitor concentrations. All statistical analyses were performed with Prism 8 (GraphPad Software). Data are represented as means ± SEM, and were assessed for normal distribution. Plots of means from motor neuron survival assays represent triplicate wells from single assays. Unpaired, two-tailed t-tests were used to compare the effects of treatment on motor neurons in western blot assays. Regression analyses (Pearson's r) were used to evaluate the degree to which the inhibition of the activity of a given kinase correlated with neuroprotection in the CPA assay for the listed compound **1** analogs (Table S2) at the indicated concentrations. In Figure 3D, kinases whose activity was poorly inhibited by all 10 of the analogs tested (>20% activity remaining) were excluded from analysis. Two-way ANOVAs were used to compare the effects of LPS vs. compound **1** analog treatment on N9 microglia. ANOVAs were supplemented with Dunnett's multiple comparisons tests to assess interactions between conditions.

DATA AND CODE AVAILABILITY

This study did not generate any datasets or code.